Assessing Transformation of Trace Metals and Crude Oil in Mississippi and Louisiana Coastal Wetlands in Response to the Deepwater Horizon Oil Spill

by

Jeffrey Paul Keevan

A thesis submitted to the Graduate Faculty of
Auburn University
in partial fulfillment of the
requirements for the Degree of
Master of Science

Auburn, Alabama
August 4, 2012

Approved by

Ming-Kuo Lee, Chair, Professor, Department of Geology and Geography
James A. Saunders, Professor, Department of Geology and Geography
Charles E. Savrda, Professor, Department of Geology and Geography

ABSTRACT

On April 20, 2010, the drilling rig Deepwater Horizon exploded in the Gulf of Mexico, resulting in the release of about 5 million barrels of crude oil into the environment. Coastal wetlands are particularly susceptible to oil contamination because they are composed largely of fine-grained sediments, which have a high capacity to adsorb oil and associated metals. Microbial activities may be enhanced by an increase in amounts of organic matter and subsequently influence the biogeochemical cycling of trace metals. This research assesses the levels of oil and trace metals, along with associated biogeochemical changes, in six coastal marshes in Mississippi and Louisiana.

Total digestion analysis of wetland sediments shows higher concentrations of certain trace metals (e.g., Ni, Cu, Pb, Zn, Co, V, Ba, Hg, As) in heavily-oiled Louisiana sites (e.g., Nay Jimmy and Bayou Dulac) compared to those at less-affected and pristine sites. Due to chemical complexation among organic compounds and metals, crude oils often contain elevated levels (up to hundreds of mg/kg) of trace metals. At the heavily-oiled Louisiana sites (e.g., Bay Jimmy and Bayou Dulac), elevated levels of metals and total organic carbon were found in sediments down to depths of about 30 cm. The contamination is not limited to shallow sediments; oil, along with various associated metals, may be invading into deeper (pre-industrial) portions of the marsh sediments. Pore waters extracted from contaminated sediments are characterized by very high levels of reduced sulfur (up to 80 mg/kg). Microbial analysis of oiled sediments indicates that the influx of oil into the wetlands might have provided the additional substrate and carbon source for stimulating sulfate-reducing bacteria. Moreover, pore-water pH values show a general increasing

trend (ranging from 6.6 to 8.0) with depth, possibly reflecting the combined effects of bacterial sulfate reduction and saltwater intrusion at depth. Despite high levels of trace metals in bulk sediments, concentrations of trace metals dissolved in pore waters are generally low. Pyrite-like iron-sulfides with distinct framboidal form are found in oiled sediments. Laser-ablation inductively coupled plasma mass spectrometer (LA-ICP-MS) analyses show that sulfide solids contain various levels of trace metals, including As, Hg, Pb, Cu, Zn, V, and Zn. Sulfide solids likely serve as local sinks for chalcophile ("sulfur-loving") trace metals under sulfate-reducing conditions. It appears that high organic matter content and bacterially-mediated sulfate reduction facilitate metal retention via sulfide formation in the oiled marsh sediments.

In addition to metals retention in sulfide solids, geochemical analyses show that residual oils remain in these wetlands up to months or possibly longer. High TOC and DOC levels (up to about 29% and 330 mg/kg, respectively), and low $\delta^{13}C$ values of affected sediments, confirm the persistence of oil in these salt marshes. Gas-chromatograph mass-spectrometer (GC-MS) analyses of extracted organic contaminants show that only lighter compounds of the Macondo-1 crude oil are quickly degraded, while the heavier components tend to remain in the environment months after the spill. The long-term biogeochemical effects of the remnant oil in the wetlands remains unclear, as does the possibility of re-oxidation of wetland sediments and metal sulfides. A potential effect would be the disaggregation of the solid sulfides and subsequent mobilization of sorbed trace metals. This possibility warrants further monitoring of affected wetlands.

ACKNOWLEDGMENTS

This project would not have been possible without research grants provided by the National Science Foundation and British Petroleum. I would like to extend my sincerest gratitude to my thesis advisor, Dr. Ming-Kuo Lee, for his patience, guidance, and support, for which this project would not have been possible. In addition, I would also like to thank my committee members, Dr. James Saunders and Dr. Charles Savrda, as well as the rest of the Auburn University Department of Geology and Geography faculty for their support over the last two years.

Many others contributed to various facets of research and analyses related to this study, and their efforts are greatly appreciated. They include Drs. Alison Keimowitz, Benedict Okeke, Randall Clark, Yonnie Wu, Michael Meadows, Ahjeong Son, Scott Phipps, Just Cebiran, Charlotte Brunner, Munir Humayan and Yang Wang. Field sampling and laboratory sample processing were made possible by contributions from various people, including Michael Shelton, Eric Sparks, Robin Governo, Ada Cotto, and Joel Abrahams. I am extremely appreciative to the Auburn University Department of Geology and Geography for granting me a full Teaching Assistantship and to Dr. Lee for a summer Research Assistantship.

I would like to thank my friends and family for their support and understanding for my numerous absences throughout the past two years. I also would like to extend my deepest gratitude to my research partner Mike Natter for the many long hours toiled in the field and laboratory. Finally, I dedicate this thesis to the memory of my father.

TABLE OF CONTENTS

LIST OF TABLES

LIST OF FIGURES

INTRODUCTION

On April 20, 2010, an explosion engulfed the oil rig Deepwater Horizon in the Gulf of Mexico, leading to an unprecedented environmental oil spill of approximately 5 million barrels (Cleveland et al., 2010; Crone and Tolstoy, 2010). The Macondo-1 oil spill is regarded as the worst marine oil spill in the history of petroleum exploration. This spilled oil inundated many Gulf coastal wetlands, and its presence has had detrimental effects on the aquatic zones and ecosystems of coastal marsh areas. This situation is particularly dire along the Gulf coastal wetlands because they are ecologically and economically important. Wetlands are well-known natural filters of debris and pollutants derived from rivers, streams, and the atmosphere. Many trace metals (such as arsenic and mercury) transported by the river systems are deposited and trapped in the wetlands, reducing their potential to enter the water column and food chain. Arsenic and mercury are of particular concern, because in excess they are extremely toxic to wildlife and humans (Guo et al., 1997; Wright and Welbourn, 2002).

Massive influxes of oil can increase microbial activity and enhance the mobilization and biotransformation of heavy metals such as arsenic and mercury. Arsenic can become mobilized through bacterial iron reduction (Islam et al., 2004; Saunders et al., 2008) of oxides, while bacterial sulfate reduction can cause methylation of mercury (Compeau and Bartha, 1984; Delaune et al., 2004). Methyl mercury (MeHg) and arsenic are bioaccumulated, and the risks associated with biotic accumulation underscore the necessity to understand their fate and transformation in coastal wetland sediments. The fate and transportation of toxic metals may

have an effect on aquatic and coastal ecosystems for many years, so a baseline assessment of metal concentrations is an important aspect of this study.

Also of concern is the long-term persistence of oil in the wetland environment after the arrival of spilled oil from the BP Macondo-1 well. Crude oils and associated compounds change in chemical composition after their release in natural environments due to microbial degradation and various physiochemical processes (i.e., evaporation, dispersion, oxidation, and mineral adsorption). Oudot and Chaillan (2010) showed that heavy fractions of oil remained in the wetland environment decades after the Amoco-Cadiz oil spill. Generally, natural microbes will quickly digest the lighter compounds of oil, leaving heavier components (e.g., asphaltenes, resins, and polycyclic aromatics) in contaminated sediments. Total organic carbon (TOC) content in sediments and dissolved organic carbon (DOC) content in sediment pore waters tend to increase as a result of massive oil spills. DOC and TOC contents may be measured as a non-specific indicator for the level of oil contamination and degradation.

To assess and quantify the impact of the Deepwater Horizon oil spill on wetland sediments, field sampling was conducted in ten different Gulf Coast wetlands (Figure 1). The ten sites selected are located up to three states apart and ranged in their degree of contamination from pristine to heavily-oiled. The varying degrees of contaminated wetlands allowed for a broad assessment of the impact of the oil both geographically and according to the amount od inundation. Sediment cores, near-surface sediments, surface water, and vegetation were collected from each site in order to assess changes induced by oil contamination. This study focuses on samples collected from 6 of the 10 sampling sites: Bayou Heron (BH); Point Aux Chenes Bay (PACB); Rigolets (RG); Bayou Dulac (BD); Bay Batiste (BB); and Bay Jimmy North (BJN). These sites are located along the coasts of Mississippi and Louisiana.

This study seeks to test two major hypotheses: 1) high inputs of spilled oil leads to increased bacterial activity and biotransformation of heavy metals; and 2) natural microbes digest lighter oils quickly (within months) while the heavy and less degradable oil persists longer in the environment. In order to test these hypotheses, geological, geochemical, and microbial analyses were performed to characterize the sediments and pore waters collected from sampling sites. The main objectives of this research are to (1) analyze mineralogy and grain-size distribution of wetland sediments, (2) compare organic carbon contents in sediments and pore waters extracted from oiled and unaffected marsh sites, (3) assess geochemical profiles of sediments and pore waters and changes in microbial communities with depth, and (4) conduct geochemical biomarker and stable carbon isotope analyses to correlate organic matter recovered from oiled marshes to their initial sources.

Since the sampling took place relatively soon (6 to 9 months) after the onset of the oil contamination, the results can provide baseline data for these sensitive wetlands that will be useful for developing long-term remediation and restoration strategies. The results of this study also will be of interest to communities that are located within the affected areas, as many of them could be directly affected by metal mobilization and oil incursion induced by the Deepwater Horizon explosion.

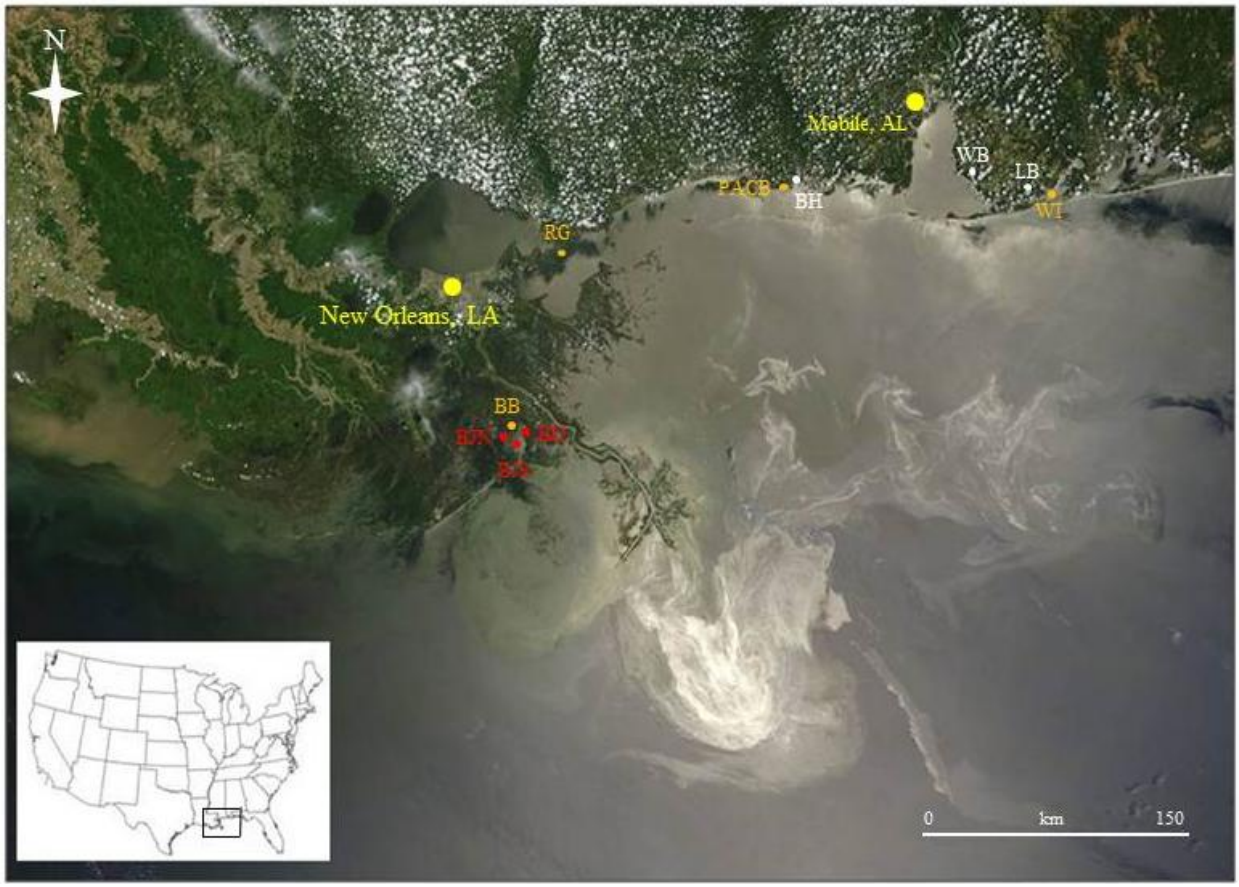

Figure 1. Sample location map showing ten wetland sampling sites along the coasts of Alabama, Mississippi, and Louisiana. White indicates no oil contamination, orange indicates moderate oil contamination, and red indicates heavy oil contamination. (http://www.tovima.gr/oldPhotos/Article%20Photos/20100528/334342.jpg)

BACKGROUND AND GEOLOGIC SETTING

The explosion of the oil rig Deepwater Horizon on April 20, 2010 led to an unprecedented environmental disaster in the Gulf of Mexico. Approximately 5 million barrels of oil were released into the Gulf waters (Cleveland et al., 2010; Crone and Tolstoy, 2010; Rosenbauer et al., 2010). Many coastal wetlands were inundated and contaminated with this oil. Of special interest is whether the influx of oil and organic matter may enhance the mobilization and biotransformation of heavy metals such as arsenic and mercury. This alteration may have a lasting effect on aquatic and coastal ecosystems (Kiemowitz et al., 2010). To determine whether coastal oil inundation has caused any localized detrimental effects, several coastal wetlands, representing affected and unaffected sites, were sampled and analyzed for geochemical and microbial changes.

Wetlands

The six sites sampled for this study (Bayou Heron, Point Aux Chenes Bay, Rigolets, Bay Batiste, Bayou Dulac, Bay Jimmy North) are typical coastal salt marsh wetlands located along the Gulf Coast (Figure 1). Wetland environments are well-documented as sinks for metals derived from natural and anthropogenic sources (Guo, 1997; Wright and Welbourn, 2002). Because their physical makeup is primarily organic-rich fine-grained sediments, wetlands have the ability to retain high concentrations of metals. When these estuarine environments undergo geochemical changes, such as oxidation or reduction events, metals can be transformed or mobilized, leading to potential toxicity hazards for wildlife, and potentially, humans.

Sample Sites

In all, ten marsh sites located along coastal wetlands of Alabama, Mississippi, and Louisiana were sampled for two separate theses research projects. The names and abbreviations of the sites, as well as their locations and sampling dates, are listed in Table 1. The sites range in their degree of contamination from pristine to completely oil immersed. Two sites from Mississippi (Bayou Heron and Point Aux Chenes Bay) and four sites from Louisiana (Rigolets, Bayou Dulac, Bay Batiste, and Bay Jimmy North) were ultimately chosen for this study to investigate biogeochemical changes within these distinct geographic areas. A parallel thesis project (Natter, 2012) focused on other coastal wetland sampling sites in Alabama and Louisiana. The sites chosen in this study represent some of the worst affected areas in Mississippi and Louisiana.

Table 1. Sample location information for Gulf marshes.

Sampling Sites	Sample ID	Latitude (degree)	Longitude (degree)	Date Sampled	Water Temp °C
Weeks Bay	WB	30.413	87.831	10/19/10	22.8
Longs Bayou	LB	30.308	87.623	10/20/10	22.6
Walker Island	WI	30.288	87.541	10/20/10	23.0
Bayou Heron	BH	30.396	88.401	10/22/10	21.6
Point Aux Chenes Bay	PACB	30.335	88.451	10/22/10	23.1
Rigolets	RG	30.172	89.690	01/10/11	8.8
Bayou Dulac	BD	29.456	89.808	01/11/11	11.5
Bay Batiste	BB	29.472	89.831	01/11/11	10.4
Bay Jimmy North	BJN	29.454	89.885	01/13/11	6.6
Bay Jimmy South	BJS	29.445	89.891	01/13/11	7.2

Geologic Setting

Grand Bay is located in the eastern portion of the Mississippi Sound. It receives its sediment inputs from nearby Mobile Bay. The drainage basin in this area is composed of small floodplains, swamps, and marshes (Greene et al., 2007). The geologic units surrounding Grand Bay are of Quaternary age and generally are made of loam, sand, gravel, and clay (Bicker, 1969).

Barataria Bay is located along the southeastern Louisiana shore and is part of the Mississippi River delta. The basin is characterized by four primary sedimentary facies of Quaternary age: (1) a proximal ebb-tidal delta facies, (2) a distal ebb-tidal delta facies, (3) a near-shore facies, and (4) an inner-shelf facies. Sediments deposited within these environments grade from sand to silt to silty clay. Sediments typically become finer upward and seaward. All of the facies include some mud (Fitzgerald et al., 2004). The presence of mud, or clay, is important, as heavy metals and organic matter tend to concentrate in fine-grained sediments that have high-surface areas, which are conducive to metal sorption. With higher levels of organic matter, potential for mercury methylation (Hammerschmidt et al., 2004) and arsenic mobilization increases (Burnol et al., 2010).

Bayou Heron (BH)

Bayou Heron (BH) is part of the larger Grand Bay area, located in eastern Mississippi. It is a part of the Mississippi Sound, which receives its sedimentation from nearby Mobile Bay. This site was sampled on October 22, 2010, at 20-cm water depth (Figure 2). The sampling site was located at latitude N 30° 23.732' and longitude W 88° 24.077' (Figure 3). Using a Google Earth layer which tracks all reports of locations of oil sightings post-Deepwater Horizon, Bayou Heron was determined to not have been affected by the oil spill and, on that basis, it stands as a control site for investigating the geochemical impacts in the Grand Bay area. Figure 3 shows the approximate geographic location of the sediment core/water sampling site.

Figure 2. Photograph of sediment coring and surface-water sampling at Bayou Heron (BH), Mississippi.

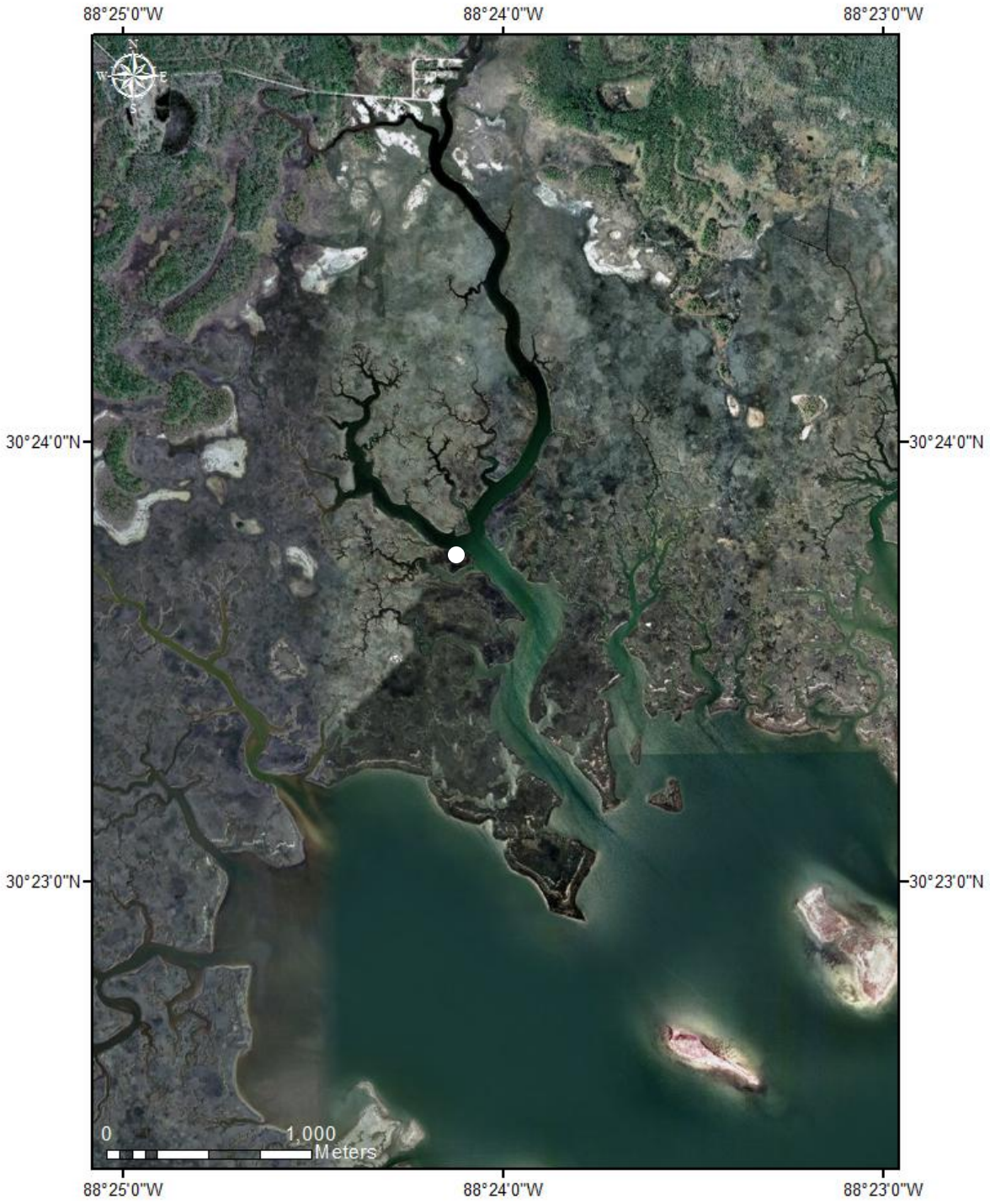

Figure 3. Map of sediment-coring and water-sampling site for Bayou Heron (BH).

Point Aux Chenes Bay (PACB)

Like Bayou Heron, Point Aux Chenes Bay (PACB) is located within Grand Bay, which is ultimately part of the Mississippi Sound. Sediment cores and surface-water samples were collected from PACB (Figure 4) on October 22, 2010 at latitude N 30° 20.08' and longitude W 88° 27.033' (Figure 5) at a water depth of 25 cm. In contrast to BH, PACB is open to the Gulf of Mexico. With no barriers protecting it, PACB was slightly contaminated with oil as tides carried oil toward shore. No visible oil was detected on the surface water at the time of sampling.

Figure 4. Photograph of sediment coring and surface-water sampling at Point Aux Chenes Bay (PACB), Mississippi.

Figure 5. Map of sediment-coring and water-sampling site at Point Aux Chenes Bay (PACB).

Rigolets (RG)

Rigolets (RG) is located in southeastern Louisiana, just outside (to the northeast) of the Barataria Bay Basin, where other Louisiana sampling was conducted. Rigolets is a narrow waterway situated between Lake Pontchartrain and the Gulf of Mexico. Its sediments consist largely of silt and clay, though some locations near barrier shorelines and deltaic progradations do host coarse-grained sediments (Flocks et al., 2009). The current natural sediment source for this area is derived from incoming rivers and shoreline erosion (Flocks et al., 2009). Sediment cores and surface-water samples were collected from RG (Figure 6) at latitude N 30° 10.346' and longitude W 89° 41.396' (Figure 7) at a water depth of 20 cm. This site was sampled on January 10, 2011. Geochemical analyses (see sections below) indicate that this site was only mildly contaminated with oil. As the results show that other Barataria Bay sites were heavily affected, RG serves as a control site for comparison.

Figure 6. Photograph of sediment coring and surface-water sampling at Rigolets (RG), Louisiana.

Figure 7. Map of sediment-coring and water-sampling site at Rigolets

Bayou Dulac (BD)

Bayou Dulac (BD) is situated within the Barataria Bay Basin near where a stream meets with tidal water from a larger water body of Bay Batiste. As part of the Mississippi River delta, Bayou Dulac receives its sediment loads from the Mississippi River. Sediment cores and surface-water samples were collected from BD (Figure 8) at latitude of N 29° 27.392' and longitude W 89° 48.469' (Figure 9) on January 11, 2011. Water depth at this location was 10 cm. Bayou Dulac was reported as one of the worst contaminated salt marsh sites in Louisiana. Visibly oiled marsh grass was present at the site at the time of sampling. Bulk surface sediments collected at this site had a strong, almost overpowering, odor of hydrogen sulfide during the collection process, indicating prevailing sulfate-reducing conditions. Since BD is part of a narrow water inlet from Bay Batiste, it is probable that any oil that washed up in this area would have been trapped, as this narrow inlet is a more stagnant water body than Bay Batiste and experiences limited seawater flushing.

Figure 8. Photograph of bulk sediment sampling in Bayou Dulac (BD), Louisiana. Slightly-oiled marsh grass can be seen in the background.

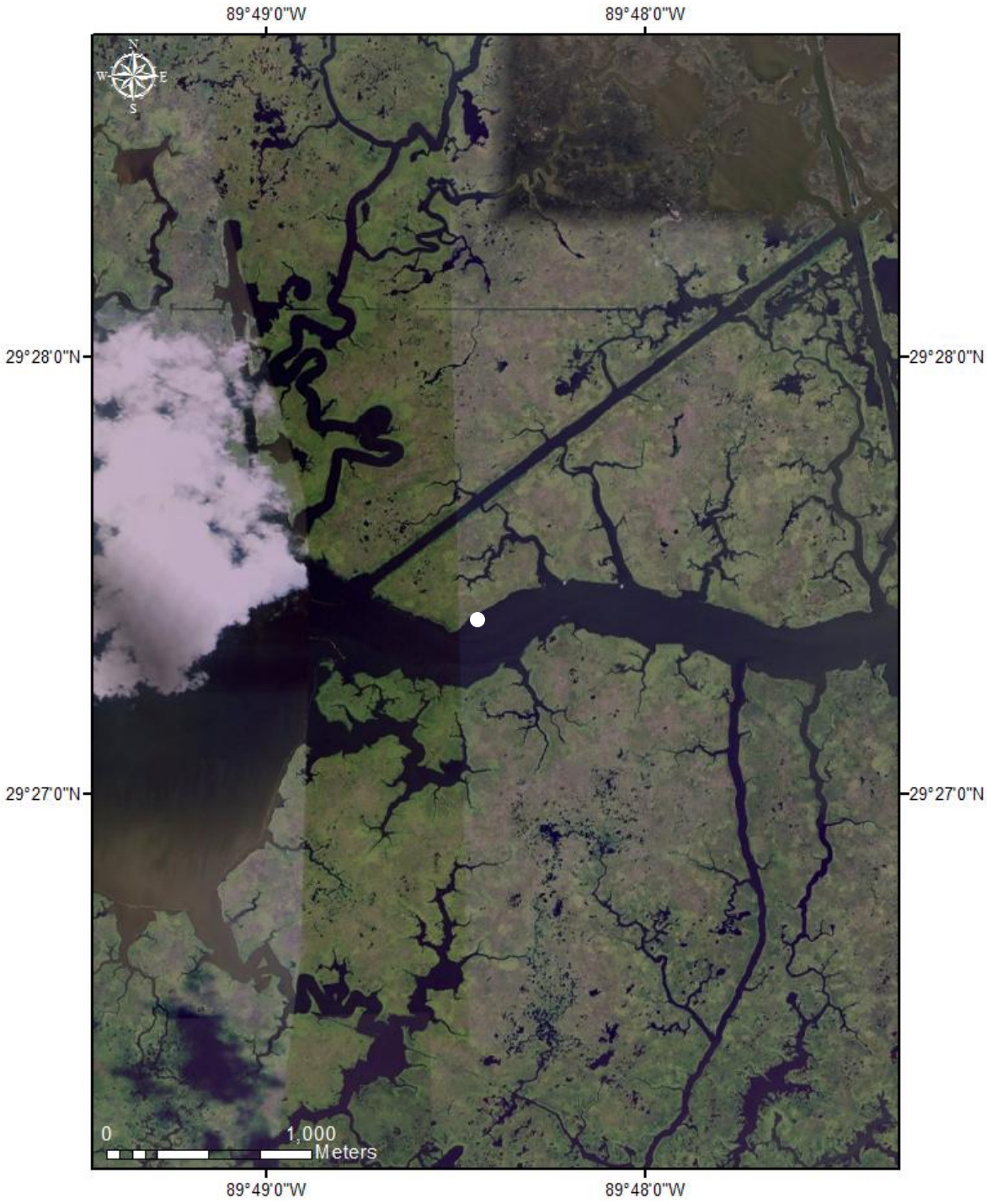

Figure 9. Map of sediment-coring and water-sampling site for Bayou Dulac (BD).

Bay Batiste (BB)

Bay Batiste (BB) is situated within the Barataria Bay Basin, just west of Bayou Dulac. As part of the Mississippi River delta, Bay Batiste receives its sediment load from the Mississippi River. BB is protected from the open Gulf by the larger Barataria Bay, but it is still open enough to experience considerable seawater flushing, which could aid in removing oil. Sediment cores and surface-water samples were collected from BB at latitude N 29° 28.340' and longitude W 89° 49.874' (Figure 11) on January 11, 2011. The samples were collected at 10-cm water depth. Though BB was reported as being heavily inundated with oil, only slight visible oil over dead marsh grass was seen at the time of sampling (Figure 10).

Figure 10. Photograph of light accumulations of oil covering dead marsh grass at Bay Batiste (BB), Louisiana. All grass that had been removed in the foreground is presumed to have been inundated with oil.

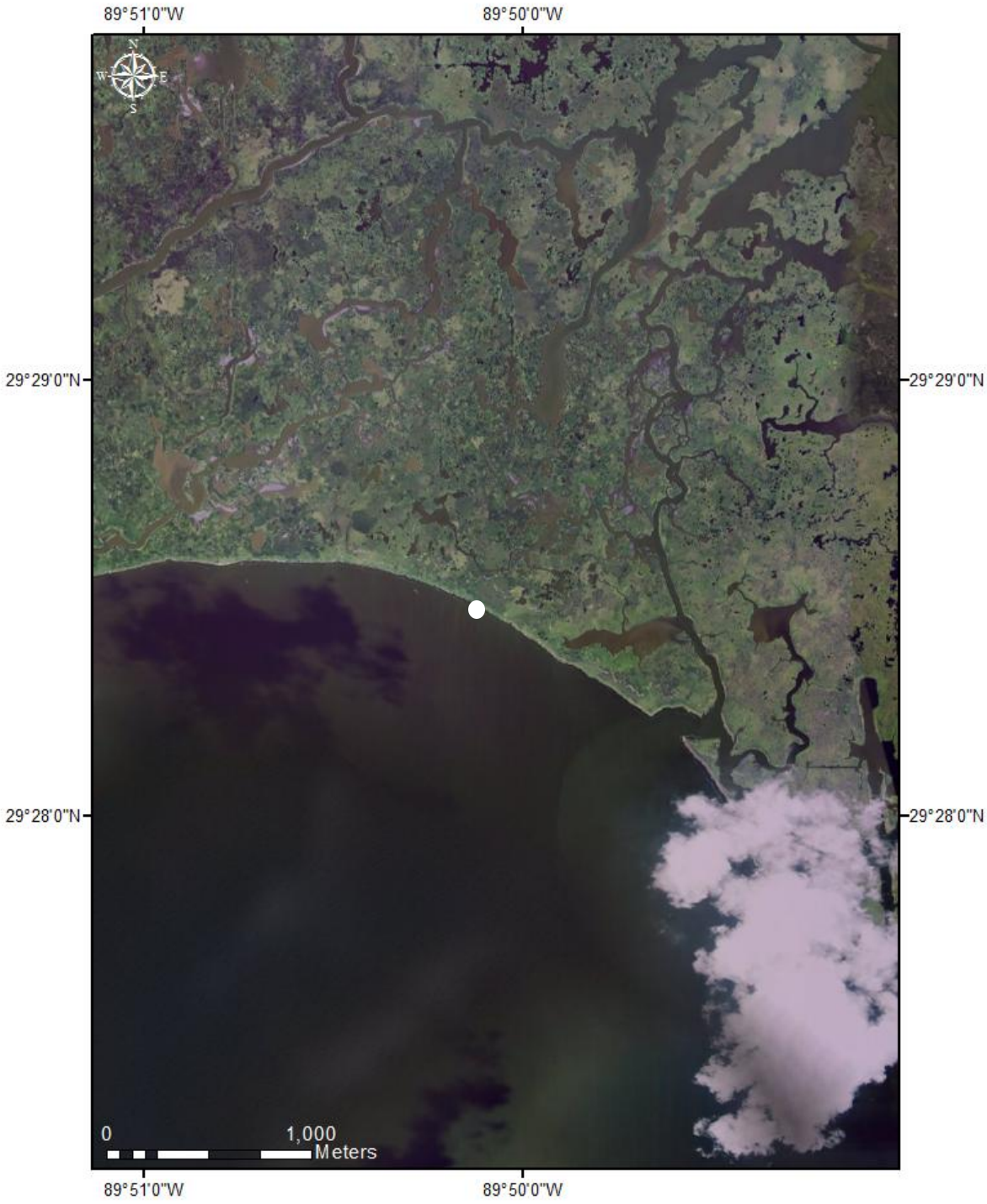

Figure 11. Map of sediment-coring and water-sampling site for Bay Batiste (BB), Louisiana.

Bay Jimmy North (BJN)

Bay Jimmy North (BJN) is located within the Barataria Bay Basin to the west of Bay Batiste and receives its sedimentation from the nearby Mississippi River. Sediment cores and surface water samples, in addition to bulk sediments and live and dead plants, were collected from BJN on January 13, 2011 at latitude N 29° 27.236' and longitude W 89° 53.512' (Figure 13). Samples were collected at a water depth of 10 cm. BJN was reported as having received a significant amount of oil from the BP oil spill – over 32,000 gallons of oil were removed during a 10-day period of cleaning (USA Today, 2010). Though BJN is open to Barataria Bay, a small island (BJS) bounds it to the south. Since oil was visibly present on the day of sampling (Figure 12), covering dead plants along the shoreline, it is probable that accumulations of oil in BJN are not as easily flushed. Or, perhaps there was enough oil inundation that flushing by ocean waves was not complete at time of sampling.

Figure 12. Photograph of heavily-oiled marsh grass and dead plants at Bay Jimmy North (BJN), Louisiana, extending several meters from the shoreline.

Figure 13. Map of sediment-coring and water-sampling site for Bay Jimmy North (BJN).

Geology and Biogeochemical Systems

The United States Gulf Coast region between Alabama to Louisiana is a unique area composed of Quaternary-aged alluvium deposited by numerous rivers distributing their sediment loads as they empty into the Gulf of Mexico. As these rivers aid in leveling much of the interior of the continent, they transform the coast into an area of natural complexity by transporting sediments, organic matter, and dissolved particles to the coastline. These sediments and dissolved loads interact with the environment to form unique and complex geologic, biologic, and geochemical systems. Many Gulf estuaries and coastal watersheds are highly susceptible to contamination by heavy metals, such as arsenic and mercury, that are extremely toxic to wildlife and humans (Guo, 1997; Wright and Welbourn, 2002). With increasing influx of organic matter from the oil spill, the complexities are amplified. Influx of high organic matter (OM) resulting from the oil spill may increase microbial activity, promote more strongly reducing conditions, and thereby affect the mobility and biogeochemical cycling of heavy metals in coastal wetlands (Keimowitz et al., 2005; Lee et al., 2005, 2007, 2010).

Knowledge of hydrogeology, geochemistry, and geobiology is essential to understand key reactions that result in geochemical changes of sediments and pore waters. It has been shown in previous studies that mobilization and biological transformation of arsenic and mercury occur in strongly reducing environments via bacterial iron- and sulfate-reduction (Keimowitz et al., 2005; Saunders et al., 2008; Merritt et al., 2009). The addition of oil can enhance these biogeochemical processes by providing organic carbon, which is the main energy source for bacteria.

Moreover, nutrients and bio-stimulants used to decompose oils in mitigation also may stimulate microbial activities that impact mobility and natural cycling of metals in Gulf waters.

Although most light compounds of oil are considered biodegradable, saturated heavy oils, which represent about 60% of initial crude, can persist in contaminated wetlands for decades (Oudot and Chiallan, 2010). Thus, it is important to monitor the evolution of oil and its impact on the concentration, speciation, and mobilization of metals in impacted wetlands. When living organisms are exposed to Hg and As in aqueous environments, these elements are taken up by the organisms and then transformed/accumulated throughout the food chain. The impacts of the current oil spill on Gulf coastal watersheds could last for many years, even after the degradable oil on the surface is cleaned up.

Bacterial Processes in Geological Environments

Bacterial activities can control the mobility and biogeochemical cycles of metals in various geological environments. Bacteria are unicellular organisms that are mostly invisible to the naked human eye. These microorganisms tend to form colonies referred to as microbial communities. These communities are found nearly everywhere in natural environments. They can be aerobic (require oxygen for respiration) or anaerobic (require substances other than oxygen for respiration). Bacteria aid greatly in the oxidation-reduction cycle by stripping electrons from an electron donor (oxidation) to derive energy for either substrate removal or cell synthesis. The redox cycle is completed by the free electron being paired up with an electron acceptor, resulting in that particular molecule being reduced. This process can be either assimilatory or dissimilatory; assimilatory microorganisms incorporate the metal for use in enzymes and cellular components, whereas dissimilatory microorganisms oxidize organic compounds and funnel the electrons to metals that are located outside of the organism (Liermann et al., 2007). Bacteria can utilize multiple other elements (e.g., Fe, Mn, S, etc) aside from oxygen

as their terminal electron acceptor for respiration under various redox conditions. In wetlands, bacteria can be found in both terrestrial and aqueous environments, and they play an important role in the biogeochemical cycles of carbon and metals. Two primary types of bacteria of interest for this study are dissimilatory iron-reducing bacteria (FeRB) and sulfate-reducing bacteria (SRB). Dissimilatory bacteria oxidize organic compounds and pass the electrons through the electron-transport chain to metals that are located outside of the organism (Liermann et al., 2007).

Iron-reducing bacteria are found in a multitude of environments, although in sulfate-rich marine environments they are outcompeted by sulfate-reducing bacteria (Madigan et al., 1997; Straub et al., 2000). One way they work is by oxidizing the electron donor (acetate or other short-chain fatty acids) to carbon dioxide, while utilizing ferric iron as the terminal electron acceptor (Champine and Goodwin, 1991; Lonergan et al., 1996). In this system, ferric iron (Fe(III)) is reduced to ferrous iron (Fe(II)) when iron accepts the electron. Since iron is the fourth most abundant element in the Earth's crust (around 5.1%), this process is widespread in natural settings. In fact, ferric iron is one of the most important electron acceptors in non-marine sediments (Straub et al., 2000). Ferric iron is found in many different forms in the environment; common mineral forms are amorphous iron oxides, ferric oxyhydroxides, and hydrous ferric oxides, together referred to as iron oxyhydroxides (Straub et al., 2000). As they age, iron oxyhydroxides transform and re-organize to hematite, limonite, and goethite with better-defined atomic structures.

A chief adverse effect of FeRB is that, through dissimilatory processes, oxidation of organic compounds can lead to the mobilization of certain adsorbed trace metals during iron reduction. As dissimilatory processes are occurring, electrons are funneled by FeRB from a

carbon source to ferric iron. Other elements near their terminal electron acceptor (i.e., elements sorbed into iron oxyhydroxides) will occasionally receive electrons, causing them to become reduced. Arsenic is a prominent metal involved in this cycle. Arsenic is introduced to the hydrosphere and atmosphere by natural weathering or human activities (e.g., burning of coal) and ultimately is transported by streams and rivers in suspended sediment loads (Drever, 1997; Saunders et al., 2008). Eventually, streams and rivers will empty their sediment loads into estuaries and bays, concentrating arsenic in wetland settings. In oxidizing conditions, arsenic is primarily immobilized by being co-precipitated and adsorbed onto iron or manganese oxy-hydroxides. During reduction, iron in these minerals is converted from Fe(III) (ferric iron) to Fe(II) (ferrous iron). This reduction has the tendency to disaggregate iron oxy-hydroxide minerals, thereby remobilizing arsenic. In addition to its release, arsenic is reduced from arsenate to arsenite when it receives electrons. Arsenite is the more adsorption-resistant and toxic form of arsenic.

Sulfate-reducing bacteria (SRB) are bacteria that respire by oxidizing organic compounds while utilizing sulfate as their terminal electron acceptor in a process known as anaerobic respiration. Important bacteria in subsurface, SRB are known to exist in a variety of terrestrial and aquatic environments. They tend to outcompete many other microbes in environments that are carbon-rich and oxygen-deficient (Chapelle, 1993). SRB are also considered to be one of the important microbes in driving carbon and sulfur cycles. Sulfur is found in three common oxidation states: -2 for monosulfides (-1 for disulfides), 0 for elemental sulfur, and +4 for sulfates. The sulfur cycle is very dependent on SRB for redistributing sulfur among the three oxidation states (Chapelle, 1993). SRB also utilize carbon produced by fermenters as a carbon source for their metabolism, thus playing a major role in carbon cycling.

If a carbon source is plentiful, SRB also tend to flourish in marine environments due to the abundance of sulfate in seawater. FeRB and SRB may, on occasion, also cohabitate in the same environment (Lovley and Chapelle, 1995). Like FeRB, many SRB species have the ability to utilize metals other than sulfate as their terminal electron acceptor (Lloyd et al., 2011). One adverse effect of SRB is their connection with mercury methylation. Methyl mercury is the most toxic and mobile form of mercury (Merritt et al., 2009; Acha' et al., 2011). Mercury methylation tends to occur in anoxic environments where SRB reside, and SRB are likely responsible for the methylation of mercury under favorable (i.e., acidic, warm, and low-salinity) geochemical conditions (Mason et al., 2005; Monreal, 2007). Under highly reducing conditions, SRB may reduce dissolved loads of many toxic metals by sequestering them in Fe-sulfides (Huerta-Diaz and Morse, 1992; Lee et al., 2005; Saunders et al., 2008).

Organic Carbon

Organic carbon in wetlands and salt marshes is introduced from both allochthonous and autochthonous sources (Bianchi et al., 2010). Organic carbon can be derived from terrigenous sources, such as the decaying of organic matter in soil and also from biological activity of organisms living in the water. Organic carbon is an important part of the carbon cycle, which is the process responsible for recycling and redistributing carbon throughout the biosphere.

By utilizing oxygen through the formation of carbon dioxide, bacterial degradation of organic carbon contributes to the development of anoxia in wetlands. Reducing bacteria, such as SRB, can further enhance this process through reduction of organic materials such as fulvic and humic acids. In low-temperature sedimentary environments, microbial processes are known to be

the primary oxidizers of organic material, resulting in the formation of carbon dioxide and reducing geochemical environments (Freeze and Cherry, 1979; Lovley and Chapelle, 1995).

Petroleum, or crude oil, is comprised of many components, including various hydrocarbons such as paraffins (alkanes), naphthenes (cycloalkanes), asphaltics (asphaltenes), and aromatics, trace metals and various other compounds. The mixture of these compounds defines the characteristics of crude oil. Aromatic hydrocarbons, which have alternating single and double carbon atom bonds, have been known to be both carcinogenic and mutagenic.

The chemical fingerprinting of oil is a relatively new procedure that has shown great promise in hydrocarbon exploration and also linking oil spills with their source. The primary factors controlling the individual geochemical characteristics of oil are: 1) the state of the source strata; 2) the thermal history of the source strata; 3) any chemical changes (e.g., degradation) resulting from the oil's migration from the source strata to its reservoir; and 4) the weathering of the oil after release into the environment (Wang and Stout, 2007). Weathering of the oil will continuously degrade it, although typically it affects just the lighter compounds. Primary degradation of oil occurs through evaporation, dissolution, emulsification, photo-oxidation, biodegradation, and sedimentation/oil-mineral aggregation.

Although weathering does result in a chemical change in the oil, certain compounds within the oil are resistant to degradation, even in severe weathering cases (Overton et al., 2004; Morrison and Murphy, 2006). These compounds, called biological markers (or biomarkers), are compounds that really have not changed much (if at all) from their original structure in living organisms (Wang and Stout, 2007). In fact, these compounds actually become concentrated (relative to degraded portions) during the weathering process due to their resistant nature (Wang and Fingas, 2003). Due to the lack of degradation of biomarkers and the geologic uniqueness of

reservoirs, spilled oil can be linked to its petrographic source on the basis of its biomarkers (Overton et al., 2004; Morrison and Murphy, 2006; Wang and Stout, 2007). It should be mentioned, however, that in certain climate conditions over long periods of time, even the usually degradation-resistant biomarkers can experience alteration (Wang et al., 2001). Biomarkers also can help characterize a particular oil's thermal history and depositional environment, as well as the type of organic matter in the source rock (Wang and Stout, 2007; Ventura et al., 2010).

Oil fingerprinting traditionally has been difficult, as crude oils consist of a wide range of organic compounds with different molecular weights and properties, though advancements in technology and analytical methods has made the practice more reliable and accessible (Wang and Fingas, 2003). Although biomarkers' concentrations are often low in oil (Wang and Stout, 2007), biomarkers are still easily detectable, given the sensitivity of modern analytical instruments. According to Wang and Stout (2007), gas-chromatograph mass spectrometer (GC-MS) is generally the best instrument to use for biomarker detection and quantification. The GC-MS can be run in full scan mode, which will analyze up to hundreds of ions at a lower sensitivity. A selected ion mode (SIM) also can be run; under this mode, a few diagnostic ions are analyzed under a narrow scan under much higher sensitivity. Steranes, terpanes, and hopanes are most often used in fingerprinting because of their resistance to degradation (Barakat et al., 2002). The GC-MS analysis measures the mass-to-charge (m/z) ratio, which is unique for each ion. For example, terpanes have an m/z ratio of 191.

Sedimentary/Framboidal Pyrite

Sedimentary, or biogenic, pyrite can form in wetland environments due to the reduction of ferric iron and sulfate by dissimilatory FeRB and SRB, and it is a prevalent authigenic component of sediments and sedimentary rocks (Berner, 1970). The free products of the reduction, ferrous iron and sulfide, can bind together and produce pyrite-like solids. The main limiting factors that limit the amount of sedimentary pyrite formed are the amounts of organic material, sulfate, and reactive iron in the system (Berner, 1970; Canfield et al., 1992; Morse, 1999). In marine systems, the amount of iron is often the limiting factor for these reactions (Canfield et al., 1992; Morse, 1999). There also must be enough reactive organic material to initiate and sustain the bacterial sulfate-reduction process (Berner, 1983). The formation of sedimentary pyrite tends to occur within muds, as coarser-grained sediments do not normally contain the requisite amount of reactive iron or organic matter necessary for pyrite formation (Morse, 1999). However, poorly sorted, coarser-grained sediments may contain sufficient amounts of fines to accommodate pyrite formation.

Pyrite is thought to initially form in sediments as iron monsulfides, and possibly disordered mackinawite and greigite, but then in early stages of sedimentary diagenesis converts to iron bisulfide, or pyrite (Berner, 1970; Morse, 1998). The initial monosulfide phase can lead to another form of pyrite called framboidal pyrite (Wilkin and Barnes, 1996). Framboidal pyrite has a raspberry-like appearance and, in fact, takes its name from the French word for raspberry (framboid). The formation of framboidal pyrite is not wholly understood; it is thought by some to be an authigenic process (Berner, 1970; Wilkin and Barnes, 1996; Wilkin et al., 1996) and by others a biogenic process (Donald and Southam, 1999; Folk, 2005). Wilkins and Barnes (1996) propose that a likely scenario for framboidal pyrite formation is that the initial sulfide formed is

actually greigite (Fe_3S_4). Greigite has shown ferrimagnetic tendencies, so a possible model would be that greigite grains attach to each other through magnetic attraction, form spheroidal textures. Because greigite has been shown to be thermodynamically unstable in marine environments, it would likely be replaced by pyrite (Wilkin and Barnes, 1996; Wilkin et al., 1996). Berner (1969) describes a process by which synthetic framboidal pyrite was formed in a laboratory setting, indicating that microorganisms were not necessary for the process. Conversely, Folk (2005) cites several studies where framboidal pyrite was found in conjunction with decaying organic matter, and, in his own study, he found that the spherical components that make up the framboids are actually nannobacterial cells. The typical model for pyrite formation in aqueous solutions, described by Rickard and Luther (2006), is as follows:

$$FeS + H_2S \longrightarrow FeS_2 + H_2$$

It seems plausible that both authigenic and biogenic processes result in the formation of framboidal pyrite. Donald and Southam (1999) performed laboratory experiments in which iron monosulfides was produced. In the setup with no bacteria, excess H_2S in the system was a catalyst in converting the product into pyrite, while in the biogenic system bacteria were able to catalyze the iron-monsulfide conversion to pyrite. Although the exact mechanism for the formation of sedimentary pyrite is not well understood, the ability of pyrite to co-precipitate with and adsorb trace metals is well documented (Huerta-Diaz and Morse, 1992; Lee et al., 2005; Saunders et al., 2008).

Trace Metals

Trace metals are found in minute quantities in the cells and tissues of organisms. The metals are an integral part of proper nutrition for plants and animals, but can be toxic when accumulated in high levels. Wetlands are important because they have been recognized as both sinks and sources of trace metals, depending on climate variability and geochemical conditions. Inland wetlands at times may be sinks for trace metals. However, with seasonal and geochemical changes, metals in these settings may become mobilized (Olivie-Lauquet et al., 2000). Coastal wetlands are the final terrestrial sink for metals. Any metals mobilized within this realm may be released into the water column and ingested by organisms.

Trace metals in wetlands have been known to concentrate in both authigenic (Huerta-Diaz and Morse, 1992) and biogenic (Orberger et al., 2003) pyrite through co-precipitation and adsorption. Trace metals/metalloids typically associated with sedimentary pyrite include As, Cd, Co, Cr, Cu, Hg, Mn, Mo, Ni, Pb, and Zn (Huerta-Diaz and Morse, 1992). In addition to the trace metals already captured naturally by wetlands, additional trace metals may be added during organic incursions such as those associated with oil spills (Karchmer and Gunn, 1952; Ball et al., 1960; Barwise, 1990). Metals found in varying concentrations in oil include Ni, V, Fe, Ba, Al, Cr, Cu, and U (Karchmer and Gunn, 1952; Ball et al., 1960; Barwise, 1990; Kennicutt et al., 1991).

METHODOLOGY

Field Methods

In order to understand the biogeochemical effects of the Gulf oil spill on coastal salt marshes, field sampling was conducted at both pristine and contaminated sites, with various laboratory analyses being conducted afterwards. Surface-water, sediments, and pore-water samples collected at these sites were subjected to a variety of analyses in order to characterize their geological, geochemical, and microbiologic profiles.

Field sampling for this study was conducted in six coastal marshes in Mississippi and Louisiana, two of the states most affected by the oil spill. The sites were selected based on the degree of inundation with oil (sites range from pristine to heavily inundated), and their sedimentologic characteristics, mainly sediment texture. Finer-grained sediments were the primary focus because they host more organic matter, adsorb more heavy metals, and have higher porosities, which would yield more pore water for geochemical analyses. Each site was accessible by boat.

Upon arrival at each site, surface water was sampled using a Van-Dorn water sampler. After collection, water samples were subjected to measurements of temperature, pH, dissolved oxygen (DO), conductivity, and oxidation-reduction potential (ORP) by portable meters. At certain collection sites, water-quality parameters were measured using an *in situ* multi-parameter monitor TROLL 9000. All surface-water samples were filtered using a 0.45-μm nylon filter. Samples for trace element and cation analyses were acidified with trace-metal grade HNO_3 and

stored in polyethylene bottles that were pre-leached by 3% HNO_3 to ensure trace-metal cleanliness.

Following surface-water sampling, 7 to 8 cores, separated from each other by 1 to 2 meters, were collected at each site using a Wildco push-type corer. Each corer provided a minimum of 30 cm of *in situ* sediments. The metal corer was equipped with a plastic nose and a plastic liner (cab tube) to avoid metal contamination. Once core samples were taken, the cab tubes were removed and immediately capped to seal off oxygen. Each cab tube containing sediment was then packed with ice or dry ice for preservation purposes. All core samples were quickly transported back to the laboratory to be prepared for various sedimentological, geochemical, and microbial analyses. Plant samples also were collected at all sites for carbon isotope analysis and comparison with marsh sediment and BP crude oil isotope signatures. Weathered oils were scraped off from plants at heavily oil sites to characterize the source of oil and its degree of degradation.

Laboratory Methods

Due to the necessity of processing redox-sensitive samples in a timely fashion, temporary laboratories were set up in convenient locations near the sampling sites. Wet chemistry laboratories in the Stennis Space Center and Dauphin Island Sea Laboratories were utilized for the initial processing of core samples collected from Louisiana and Mississippi salt marshes, respectively.

In the laboratory, sediment cores were processed in a sealed glove bag that was flushed with nitrogen and sealed to ensure an anoxic environment. Inside the glove bag, cores were sectioned into 3-cm segments and placed into 50-ml centrifuge tubes, which were labeled for

each specific range of depth. Some of these 3-cm sections were centrifuged to separate pore waters and sediments. Pore waters were filtered through a 0.45-μm filter in the glove bag for various geochemical analyses listed in Table 2. Water samples were acidified by trace-grade HNO_3 for trace-element and cation analyses. Water samples for total and organic mercury analyses were stored in VWR trace clean vials for later analysis.

Table 2. Geochemical analyses performed on pore-water and sediment samples.

Core	Analysis	Instrument	Location of Analysis	Analytical/ Preservation
A	Major Ions	Ion Chromatography (IC)	Vassar College	Flash Frozen
	As Speciation	IC-Atomic Fluorescence Spectrometer	Vassar College	Flash Frozen
	Trace Elements	ICP-MS	Vassar College	Acidified
B	Hg Speciation	Tekran 2500	Woods Hole	EPA method 1631
	Fe(II)	HACH spectrophotometer	Field	EPA method 8146
	Sulfide	HACH spectrophotometer	Field	EPA method 8131
C	Dissolved Organic Carbon (DOC)	TOC-V Combustion Analyzer	Auburn	Filtered
	Sediment Total Organic Carbon	LECO Carbon Analyzer	Auburn	Inorganic C removed by HCl
D	Grain Size Analysis	Sieve/Pipette	Auburn	Ice
E	Sediment Bulk Elemental Composition	ICP-MS	ACTLAB	Total digestion
	Sediment $^{13}C/^{12}C$	Finnigan IRMS	Florida State	EA-IRMS
F	Microbial Analysis	Eppendorf thermal cycler	AUM	MPN/PCR
G	Organic compounds (crude oil/PAHs)	GCMS	Auburn	Biomarker Analysis EPA method 3570
H	Extra			Cold room (5°C)

Cores were designated letters A through H (in no specific order) so that they could be separated and grouped on the basis of the analyses to be performed. Depending on the varying needs for preserving oxidation states for various analyses, cores were either processed in or out of the glove bag.

Core A was sectioned into 3-cm segments within a nitrogen glove bag. Each segment was placed into a 50-ml centrifuge tube and labeled with the corresponding depth. After separation, the tubes were sealed to prevent oxidation and then centrifuged. The tubes were subsequently placed back into the nitrogen glove bag. Pore waters were then extracted and placed into pre-labeled sterile 2-ml vials. Pore-water subsamples were analyzed for 1) major ions using ion chromatography (IC), 2) arsenic speciation using an ion chromatography atomic fluorescence spectrometer (IC AFS), and 3) trace elements using inductively coupled plasma mass spectrometry (ICP-MS). All analyses for this core were performed at Vassar College. Sediments from this core were retained for future testing.

Core B was processed in a similar manner as Core A. The pore waters were extracted, placed into 2-ml vials, and split for three different analyses. One subsample set was sent to the Woods Hole Laboratory, MA, where it was analyzed for mercury speciation using a Tekran model 2500 Cold Vapor Atomic Fluorescence Spectrophotometer (CVAFS). The other two sets of pore-water subsamples were analyzed on site using a Hach spectrophotometer for ferrous iron using EPA method 8146 and reduced sulfur by EPA method 8131. These 2 analyses were performed immediately to minimize oxidation, which can alter speciation ratios.

Core C was sectioned without a nitrogen glove bag and subsequently placed into 50-ml tubes. The tubes were then centrifuged. Afterwards, pore waters were placed into 2-ml vials for

storage. The pore waters were later analyzed for dissolved organic carbon (DOC) at the Auburn University Forestry Department using a TOC-V Combustion Analyzer. The sediments from Core C were later dried and pulverized to pass through a 230-mesh sieve. A portion of this powder was analyzed for total organic carbon using a LECO carbon analyzer in the sedimentology laboratory at Auburn University.

Core D was sectioned outside of the nitrogen glove bag. It was divided into ten 3-cm segments, and placed into bags labeled with corresponding depth. The samples were brought back to Auburn University and analyzed for grain size. In the interest of time, only 3 samples from each site were analyzed. The surface (0-3 cm), the middle (12-15 cm), and the bottom (27-30 cm) intervals were analyzed for each site in order to characterize the sediment column and grain-size distribution. The samples were separated into sand and silt/clay fractions by washing the samples with distilled water through a 230-mesh sieve. All sediments retained on the sieve were in the range of sand. Any obvious organics were picked out to reduce their impact on the weight of the sand fractions. Sand percentages were visually estimated, and if it was (qualitatively) determined that there was less than 5% sand, then the sand portion was thrown out and the sample recorded as consisting of less than 5% sand. If there was more than 5% sand, then the sample was retained, dried, and ultimately dry-sieved at 1-phi intervals from >-1 to 4 phi. Separate sand fractions were weighed and used to determine grain size distribution within coarse sediments. Sediments passing through the 4-phi sieve were flushed into a 1000-ml graduated cylinder. A 30-ml of sodium hexametaphosphate solution was added as a deflocculant, the container was filled to the 1000-ml mark, and the silt and clay fractions of the sample were determined by standard pipette techniques.

Core E was processed without the use of a nitrogen glove bag. This core was broken into ten 3-cm segments. Each segment was placed into a sample bag pre-labeled with a corresponding depth. The samples were brought back to Auburn University and dried at a temperature of approximately 100°C in order to achieve consistent drying. Once dried, the samples were powdered by mortar and pestle, and then they were passed through a 230-mesh sieve. Approximately 2 to 3 grams of the sample that passed through the sieve was placed in small sample bag pre-labeled with the corresponding depth. All ten samples from each core were then sent to ACME Labs in Vancouver, British Colombia, and analyzed for bulk chemical composition by inductively coupled plasma mass spectrometry (ICP-MS). Approximately 5 grams of the remaining material was sent to the National High Magnetic Field Laboratory at Florida State University, where it was subjected to bulk sediment carbon isotopic analysis using a Finnigan mass spectrometer. Pristine plants, plants covered in oil, and initial BP crude oil from the Macondo-1 well also were subjected to the $^{13}C/^{12}C$ analysis at the High Magnetic Field Laboratory.

The remaining powdered material from core E samples was bagged. Some of these samples were later used for x-ray diffraction analysis using a Rigaku Miniflex in the Chemistry Department at Auburn University. No attempts to remove organics from the samples were made, other than hand-picking large organic substances out prior to sieving. The surface (0-3 cm), middle (12-15 cm), and bottom (27-30 cm) sections were analyzed to characterize the mineralogy at each site. The samples were prepared for XRD analysis by first spreading a small amount of sample onto a zero-background disc. A few drops of hexane were then added to the samples to randomly orient the grains. The samples were then placed into the X-ray diffractometer with a start angle of 3° and a stop angle of 60°. After all of the samples were

analyzed, the raw files generated by the X-ray diffractometer were collected and analyzed with the program Crystal Match.

Some of the other dried and bagged samples also were used for scanning electron microscopy (SEM) and energy dispersive X-ray (EDAX) analysis. In all, sediments from 2 sites (Bayou Dulac and Bay Jimmy North) were utilized in SEM/EDAX analysis in order to identify sulfides and any trace metals adsorbed on them. Sulfides were extracted by immersing samples in a centrifuge tube containing high-density tetrabromoethane. Samples were centrifuged at 3000 rpm for 10 minutes. Next, the cake of lighter elements that was floating on top of the tetrabromoethane was removed, and the samples were centrifuged again at 3000 rpm for 10 minutes. The cake was again removed, and the tetrabromoethane was poured off. Samples were then washed with acetone, placed in a filter paper, and vented in the fume hood for several hours. Residues were then dried in an oven overnight. After drying, the samples were removed from the filter paper and placed in a pre-cleaned 2-ml autosampler vial for storage. Some of the sample was then mounted on a glass slide with epoxy. The epoxy was ground down and smoothed to expose the powdered sample at the surface. Sulfides were identified with a reflecting light microscope. Photos were taken, and areas of interest were marked. Next, samples were gold-coated and taken for SEM and EDAX analysis. After SEM/EDAX analysis, the epoxy-mounted grains on glass slides were analyzed for specific trace metal content via laser ablation-inductively coupled plasma/mass spectrometry (LA-ICP/MS) at the National High Magnetic Field Laboratory at Florida State University in Tallahassee, FL. Equipment used included a UP 193 FXArF (193 nm) excimer laser ablation system (New Wave Research, Fremont, CA, USA) coupled to a Thermo Finnigan Element XR ICP-MS. Since Fe and S are the two primary constituents of these samples, results generated were normalized to Fe and S.

Core F was processed as soon as possible after collection for preservation purposes. This core was processed inside a nitrogen glove bag in order to provide an anoxic environment. This sample was divided into ten 3-cm segments. Each segment was placed into a 50-ml centrifuge tube pre-labeled with the corresponding depths. The surface (0-3 cm), middle (12-15 cm), and bottom (27-30 cm) segments were collected from each site and heat sealed within a Mylar bag to reduce oxidation. The Mylar bags were labeled for each site and then sent to Dr. Benedict Okeke at Auburn University at Montgomery. Dr. Okeke performed microbial analysis using an Eppendorf thermo cycler and most probable number (MPN) and polymerase chain-reaction techniques. Extra samples were brought back to Auburn University and placed in storage for potential future analyses.

Core G for each site was brought back to Auburn University as a whole core. The cores were heat sealed in Mylar bags and stored in a 5°C cold room located in Auburn University's Funchess Hall. It was later determined that a couple of different analyses were necessary, and core G was selected for these. Polycyclic aromatic hydrocarbon (PAH) fingerprinting was employed to trace oils from contaminated sites back to those from the Macondo-1 well. PAH fingerprinting involves the extraction of PAHs from oiled sediment samples and subsequent analysis by a Waters orthogonal acceleration time-of-flight mass spectrometer (GC-TOF/MS). PAH extraction was performed at Auburn University utilizing a modification of EPA Method 3570. The first step in this process was to break the core into ten 3-cm segments without the use of a nitrogen glove bag. The segments were placed in sample bags pre-labeled with corresponding depths. The surface (0-3 cm), middle (12-15 cm), and bottom (27-30 cm) segments were selected for analysis. In all, 5 of the 6 study sites were analyzed for PAH fingerprinting (lacking evidence of contamination, the Bayou Heron site was not utilized). Once

the cores were broken into segments, and the three segments from each site were selected, the PAH extraction process began.

The PAH extraction process started by adding 5 g of anhydrous sodium sulfate to a pre-cleaned PTFE extraction tube. Next, approximately 3 g of the sediment of interest were added to the tube. After that, 10 g of dichloromethane (DCM) were added to the tube, and the tube was sealed with a PTFE screw cap. The outside of the tube was then wrapped with parafilm, which allowed for easy detection of leaks. Samples were shaken for approximately 2 minutes to produce a slurry, and then rotated on a rotating incubator for approximately 24 hours. Next, the samples were centrifuged at 3000 rpm for 10 minutes. The liquid was then pipetted over to a 16x100 glass extraction vial. This liquid was then filtered and placed into a new 16x100 glass extraction vial. The extraction vial was then placed under a fume hood and blown with nitrogen gas for at least 30 minutes. Once the DCM was volatilized, the PAHs were extracted from the glass vial by adding a final solution of hexane and methyl tert-butyl ether (1:1 ratio). The final solution was then extracted by a glass syringe, and 1.5 ml of the solution was added to a 2-ml autosampler vial. The vials containing the solutions were stored in the freezer until analysis by the GC/MS.

Results show that GC-TOF/MS analyses in full-scan mode were not specific enough for fingerprinting petroleum compounds. Hence, a more sensitive method of gas chromatography-selected ion mode/mass spectrometer (GC-SIM/MS) was used to generate gas fragmentograms (of selected organic molecule fragments) using a Agilent 5975C GC-MS, where specific mass-to-charge (m/z ratios) could be identified for fingerprinting. Gas chromatographs were used to trace the weathering and biotransformation of oils in coastal wetlands with respect to the initial BP oil. Identifications of key organic compounds were achieved by comparison with special oil

biomarkers such as terpanes (m/z 191), steranes (m/z 217), and seco-hopanes (m/z 218). The degree of similarity in biomarkers was used to assess whether extracted oils were originated from the Macondo-1 well, or from other Gulf oil sources.

RESULTS AND DISCUSSION

Surface Water

Water quality parameters of surface waters (Table 3) can change for a variety of reasons and at a variety of time scale: they may vary on a daily basis due to the effects of tides, and they also may vary seasonally; mixing between seawater and freshwater also affects the water quality. Shallow surface-water samples show varying ranges of temperature that correlate with sampling time. Mississippi sites, sampled in October, show higher temperatures than those recorded at Louisiana sites in January. Dissolved oxygen (DO) concentrations are also higher in colder water. Electrical conductivity and pH values show lower values than what is typically found in seawater, indicating that there is varying amounts of freshwater and seawater mixing within the estuaries. Positive ORP (65-230 mV) and relatively high DO values (6.9-12.32 mg/kg) indicate that surface waters were under oxidized conditions months after the oil spill. This shows that the majority of the oil in surface waters had evaporated, dispersed, or degraded by microbial activity. The dissolved organic carbon contents are slightly higher at oiled Louisiana sites (>40 mg/kg) with respect to those measured at Mississippi sites (< 30 mg/kg), suggesting the presence of very small quantities of residual oil in Louisiana surface waters. The pH values ranged from 7.54 to 7.88 and 7.63 to 7.90 in the Mississippi and Louisiana sites, respectively. Processes such as biodegradation of oil, bacterial sulfate reduction, and seawater intrusion all can affect the pH of water, which in turn can affect the sorption and desorption of trace metals and methylation of mercury.

Table 3. Surface-water data collected via *in situ* meters of TROLL 9000.

Sample ID	Water Depth (cm)	Temp. (°C)	pH	ORP (mV)	DO (mg/kg)	Cond (mg/kg)	DOC (mg/kg)
WB	85	22.8	8.3	189	8	>2000	17.3
LB	40	25.3	7.03	196	6.98	>2000	26.6
WI	30	25.3	7.53	160	8.09	>2000	33.0
BH	20	21.6	7.54	134	6.9	>2000	32.4
PACB	25	23.1	7.88	135	7.7	>2000	31.3
RG	20	8.8	7.63	230	10.80	16990	23.4
BD	10	11.5	7.73	102	9.73	20000	40.0
BB	10	10.4	7.81	65	10.72	18000	43.4
BJN	5	6.6	7.90	220	12.32	15360	41.8
BJS	5	7.2	8.08	180	11.65	13950	41.9

Pore-water Geochemistry

Porewaters were measured directly in the field laboratories for reduced (solubilized) iron and sulfur content using a HACH spectrophotometer. Other pore-water subsamples also have been analyzed for major and trace element contents, as well as DOC. Porewaters extracted from one sediment core in each oiled Louisiana site were also measured for pH values at 3-cm depth intervals.

Reduced iron concentrations are typically low in seawater, and the measured reduced iron levels (Figure 14, Appendix 1) at the Mississippi (0.01 to 0.04 mg/kg) and Louisiana (0.01 to 0.03 mg/kg) sites fall within this scenario. With very low concentrations, there is not a clear relationship between reduced iron at pristine and contaminated sites. Contaminated sites generally contain slightly less solubilized iron, indicating some dissolved iron has been removed during formation of iron-sulfide solids (see Petrographic section).

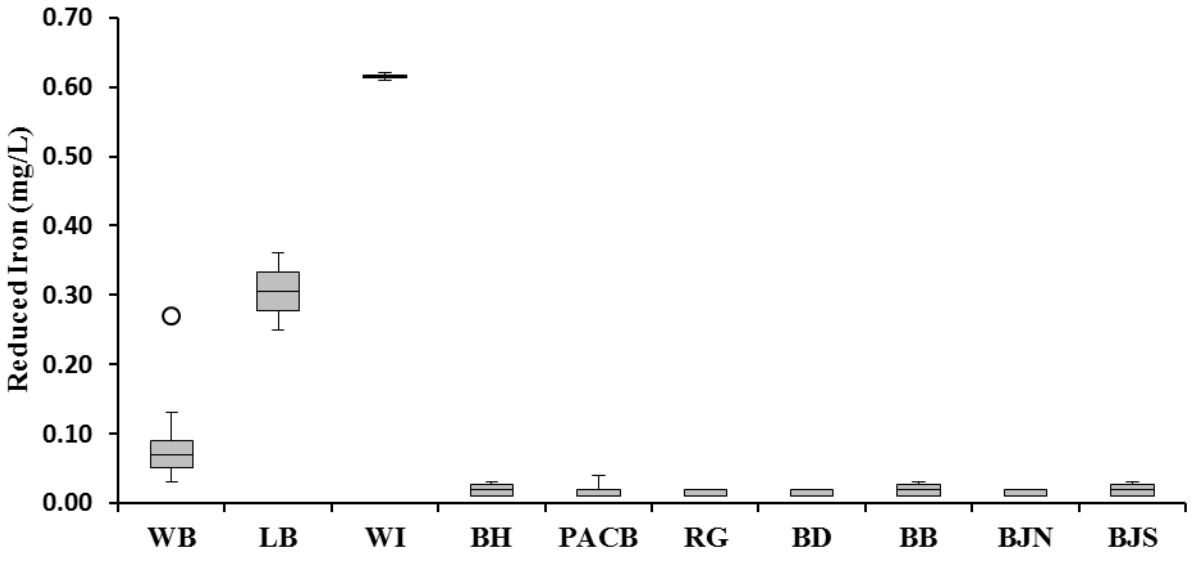

Figure 14. Box and whisker plot showing spatial variability of reduced iron. Ferrous iron concentrations are very low at many contaminated sites, indicating that most of the dissolved iron is removed by the formation of iron sulfides. Open circles represent outliers with distance from the box > 1.5 times the difference between the third and the first quarter.

The level of reduced sulfur in porewater is an important indicator of redox conditions. Reduced sulfur concentrations were very low (<1 mg/kg) at unaffected salt marsh sites in Alabama (Natter, 2012). In contrast, reduced sulfur contents are very high at contaminated Louisiana sites (Figure 15, Appendix 1). RG, the control site, had an average of approximately 8 mg/kg. The heavily-oiled sites all showed extremely high levels of reduced sulfur: BD showed a range of 4 to 59 mg/kg; BB showed a range of 4 to 49 mg/kg; and BJN showed a range of 5 to 83 mg/kg. Very high reduced sulfur and low reduced iron contents suggest that iron-reducing bacteria (FeRB) are being outcompeted by sulfate-reducing bacteria (see Microbial section) in oiled marsh environments. Influx of oil in muddy sediments probably provided additional substrate and carbon sources for sulfate-reducing bacteria.

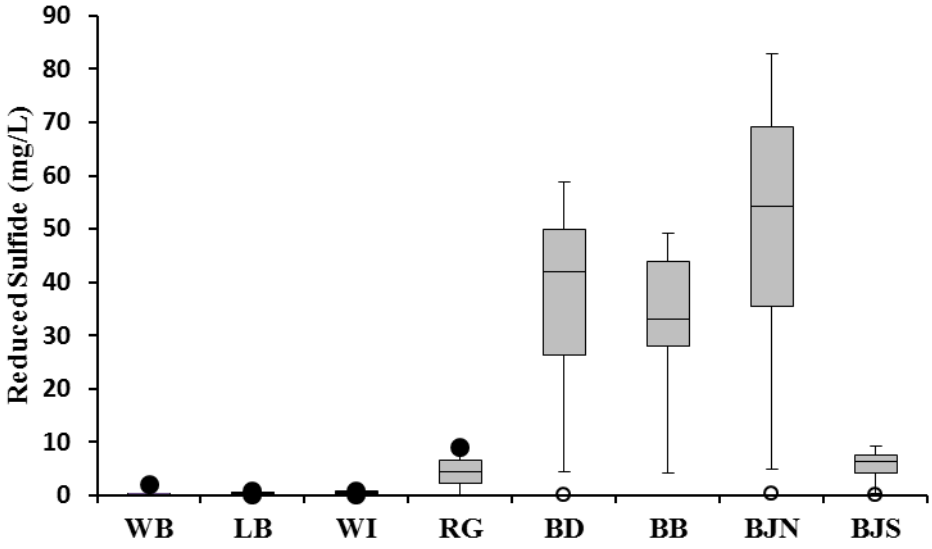

Figure 15. Box and whisker plot showing spatial variability of reduced sulfur in pore waters. Reduced sulfur was found to be highest at contaminated sites.

Reduced sulfide concentrations (Figure 16) show marked increases with respect to depth in the sediment column. Given that seawater contains copious amounts of sulfate (approximately 2,000 ppm), it is likely that seawater is invading the deeper parts of the sediment column, where sulfate is being utilized as an electron acceptor by sulfate-reducing bacteria. Influx of oil fuels activities of sulfate-reducing bacteria, which convert sulfate to hydrogen sulfide and consume protons in porewater:

$$SO_4^{-2} + 2CH_2O + 2H^+ \rightarrow 2CO_2 + H_2S + 2H_2O$$

This reaction could explain the elevated pH levels with depth (Figure 17) in porewaters measured at the oiled Barataria Bay sites, as hydrogen ions are being consumed during the reaction, effectively making the water more basic. Any oil (i.e., organic material) present can invade into sediments along with the seawater, providing the substrate to allow for such a

reaction to occur. Thus, the concurrent increases in pore-water, pH, and sulfide concentrations with depth indicates the combined effects of seawater intrusion and possibly enhanced bacterial sulfate reduction induced by spilled oil. The low reduced iron concentrations (< 0.02 mg/kg) and very high levels of sulfide at highly contaminated Louisiana sites indicate that bacterial sulfate reduction has fixed most reduced Fe and other trace metals by forming iron sulfide solids (see Petrographic section).

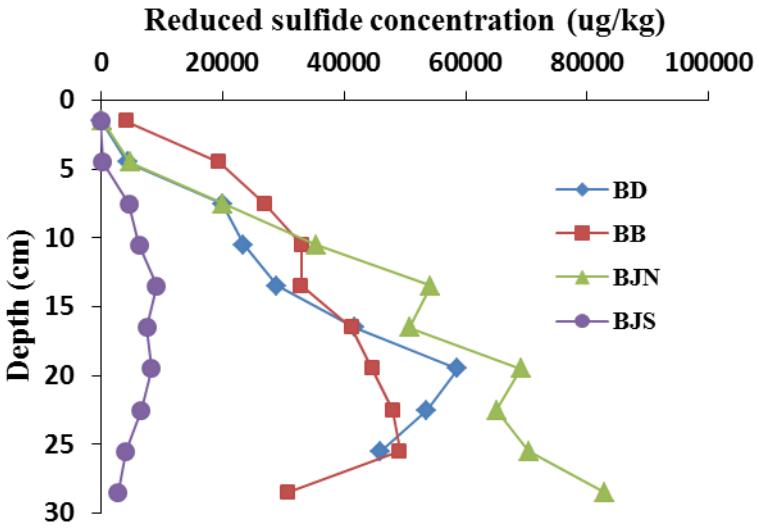

Figure 16. Profile showing reduced sulfur concentration with depth at several oiled marsh sites in Louisiana. The general trend shows significant increases in sulfide concentration with depth.

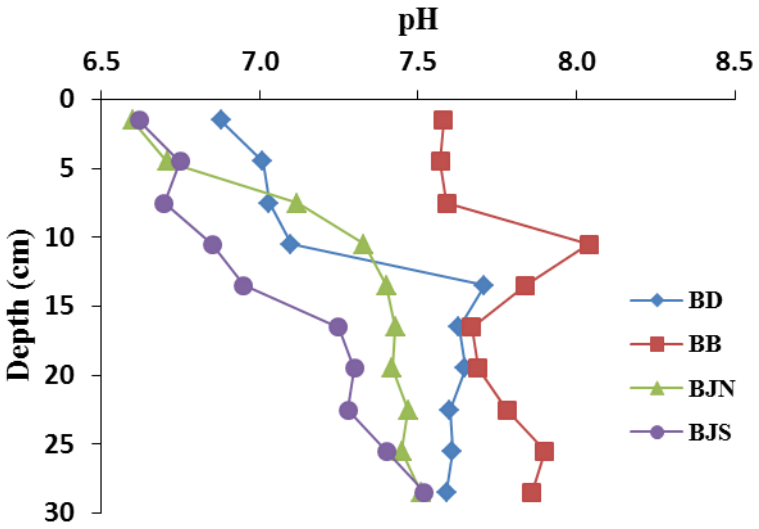

Figure 17. Profile illustrating pH trends with depth at heavily oiled marsh sites in Louisiana. The general trend shows significant increases in pH with depth.

Figure 18 shows depth profiles and spatial variation of DOC concentrations in porewaters among the sites. At Mississippi sites, BH contains an average of twice as much DOC as PACB at depths > 15 cm. By contrast, PACB shows slightly higher DOC values (approximately 27-38 ppm) than those at BH (approximately 12-32 ppm) in the upper 10 cm of the sediments. This contrast with depth suggests a possibility that residual oil remains in porewaters within the uppermost sediment column of PACB. This higher amount of DOC near the water-sediment interface of PACB could explain why measured ORP levels (Table 3) are about the same at PACB and BH sites (135 vs. 134 mV, respectively), even though PACB was expected to be much more oxygenated in its high-energy, ocean-front environment.

DOC concentrations of porewaters at BD, BB, and BJN sites averaged 227, 267, and 269 mg/kg, respectively, compared with an average value of 96 mg/kg at the RG site. The DOC contents of porewater at these Louisiana oiled sites are much higher than those measured at less

affected BH and PACB sites in Mississippi (generally < 50 mg/kg). DOC levels also are much higher in porewaters than in surface water (Table 3) at heavily oiled sites. These results indicate that elevated DOC levels could persist in sediment porewater for months or longer even after a significant portion of the oil in the surface water has evaporated, dispersed, or been degraded by microorganisms. Porewaters with very high DOC were noticeably discolored; some with a yellowish hue, and some were dark brown to black. These distinct colors may be caused by oil components and/or increased organic substances released by microbial activities fueled by the spilled oil.

BH contains an average of twice as much DOC as PACB, reflecting its high TOC contents in sediments. However, PACB shows higher amounts of DOC through the upper 10 cm of the sediment column. This finding suggests that residual oil remains in porewaters within the uppermost sediment column of PACB. At the Louisiana sites, DOC levels tend to increase with depth. The DOC contents in near-surface sediments may be reduced by freshwater recharge from rainfall or shallow groundwater. A positive relationship between DOC and TOC ($r = 0.47$) is observed, although the cause of correlation is not clear. This positive correlation suggests that either DOC or TOC may be used as an indicator of oil-contamination levels. Quantitative assessment of oil contamination also may be achieved by the stable carbon isotopic analysis of bulk sediments (see Carbon Isotope section).

The concurrent increase of DOC, TOC, pH and sulfide concentrations (see Figures 18, 42, 17, and 16, respectively) with sediment depth suggests that oil could be intruding into the deeper portions along with seawater. This suggests, in turn, that not all of the spilled oil rose to the surface, and a fraction of oil plumes might spread in the water column and contaminate the underlying sediments. Moreover, the DOC levels are also much higher in porewaters than in

surface water (ranging from 23 to 43 mg/kg at heavily oiled Louisiana sites). This is also indicative that despite microbial degradation, evaporation, and dispersion processes, remnants of the oil are still remaining in the environment. These remnants could continue to persist in marsh sediments for many years (Oudot and Chaillan, 2010).

It is important to note that the DOC levels of surface water at heavily oiled sites (range from 23 to 43 mg/kg) are similar in magnitude to those of surface water and porewater at unaffected sites (Table 3). This indicates that oils in the water column had evaporated or dispersed within about six to eight months after the spill. At the oiled Louisiana sites, DOC levels of porewater tend to increase with depth. The DOC contents in near-surface sediments may be reduced by freshwater recharge from rainfall or shallow groundwater.

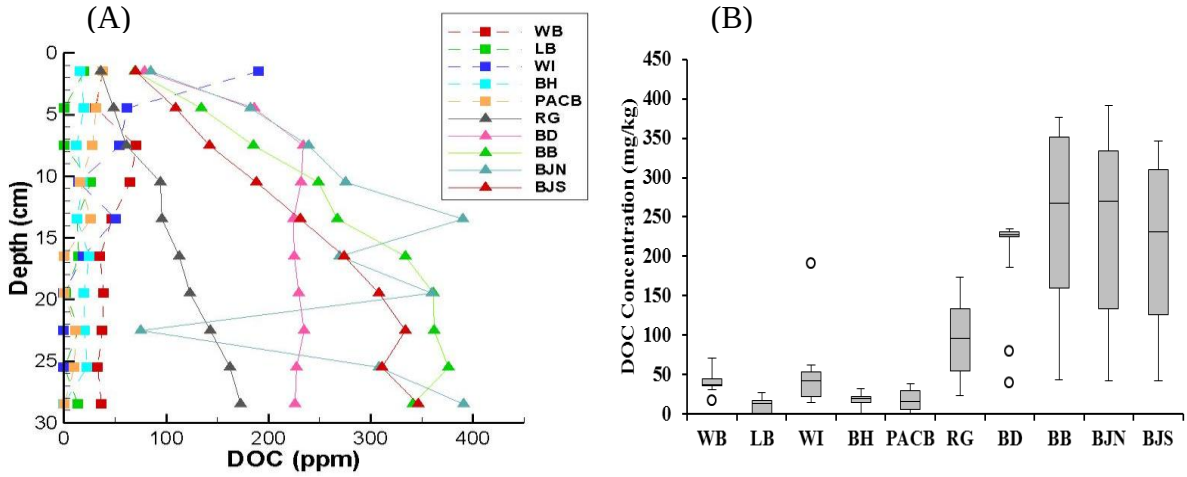

Figure 18. (A) Depth profile and (B) box and whisker-plot showing depth and spatial variability of DOC in pore waters. Contaminated sites show much higher DOC levels compared to those at non-contaminated sites.

Sediment Characteristics (Grain Size and Mineralogy)

In order to characterize each site on the basis of the sediment texture, grain-size analyses were performed on sediment cores from 0-3 cm, 12-15 cm, and 27-30 cm intervals. Grain size can significantly affect the fate and mobility of trace metals in sediments. Fine-grained sediments (as well as organics) have a higher capacity to adsorb trace metals than coarse-grained sediments (Horowitz and Elrick, 1987).

Ultimately, samples were classified based on their phi values on the modified Udden-Wentworth scale. Phi values of -1 to 4, 4 to 8, and greater than 8 were designated as sand, silt, and clay, respectively. Using these designations, sand (when applicable), silt, and clay percentages from all sites were calculated and graphed in a ternary diagram (Figures 19-21). In addition, sediment mean phi size, mode, and textural group are listed in Tables 4-6. More detailed information is shown in Appendix 2.

The two Mississippi sites, BH and PACB, are relatively coarse-grained. BH contains approximately 30-35% sand in the upper (0-3 cm) and lower (27-30 cm) portions of the sediment core, while the middle portion (12-15 cm) grades to approximately 50% sand, perhaps due to inputs of tidal surge from a storm event. Overall, PACB is generally coarser than BH. BH is located in an inlet setting, while PACB is in a location that is more open to the Gulf and therefore more likely to receive coarse-grained sediments from higher-energy processes. PACB graded from 64% sand at the top to 74% sand at the bottom. BH is classified as a sandy silt throughout the entirety of the 30-cm core. PACB sediments grade from a muddy sand in the upper portion, through silty sand in the middle portion, and to silty sand to sandy silt in the lowest depth.

The four Louisiana sites, RG, BD, BB, and BJN, showed variance in their grain size but are generally finer-grained relative to the two Mississippi sites. RG, the control site for the sampled Louisiana wetlands, is characterized by the coarsest-grained sediments. Sediments in RG were composed of approximately 50% sand in the upper (0-3 cm) and middle (12-15 cm) portion of the core, and graded to muds (silt and clay) in the lowest portion (27-30 cm) of the core. BD was dominated by fine-grained sediments, containing no sand. BD sediments become finer with depth, grading from about 70% silt and 30% clay in the upper part (0-3 cm) to about 57% silt and 43% clay in the bottom (27-30 cm) portion. BB was also sand free, and sediments become finer with depth as well. BB sediments are composed of approximately 75% silt and 25% clay in the upper portion (0-3 cm), and about 56% silt and 44% clay in the lower portion (27-30 cm). BJN also contained no sand; sediments are relatively coarser in the upper and lower parts (67% and 87% silt, respectively), and somewhat finer (58% clay) in the middle (12-15 cm) portion. The dominance of fine-grained sediments at these sites reflects the low energy environments within the Barataria Bay.

Sediment grain size is important because of its effect on metal and oil retention in wetland sediments. Finer-grained sediments (i.e., clay minerals, oxides, sulfides, and organic matter) are the primary adsorptive surface for metals (Figure 22) and oils in marsh environments (Dzombak and Luthy, 1984). Conversely, coarser-grained sediments, such as quartzose and feldspathic sand, show limited ability to adsorb oil or metals (Ciccioli et al., 1980; Rogers et al., 1980).

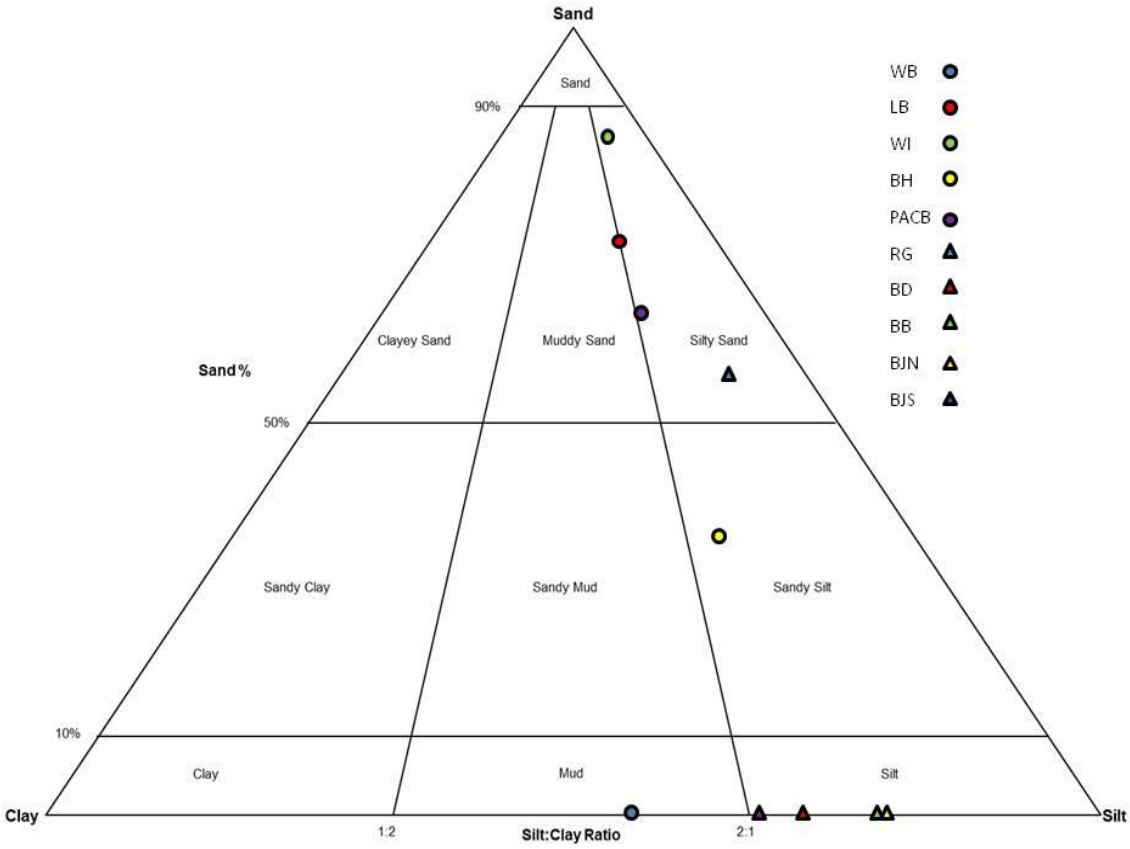

Figure 19. Folk classification ternary diagram showing sand, silt, and clay percent at 0-3 cm depth of ten different salt-marsh sites.

Table 4. Textural parameters and classification of sediments in upper parts of cores from the 10 study sites.

Sample ID	Sand %	Silt %	Clay %	Sediment Name	Textural Group
WB	0.00	54.03	45.97	Mud	Mud
LB	75.25	15.87	8.88	Muddy very fine sand	Muddy sand
WI	88.46	7.93	3.61	Fine silty medium sand	Silty sand
BH	35.87	45.13	19.01	Very fine sandy coarse silt	Sandy silt
PACB	63.68	23.88	12.44	Muddy fine sand	Muddy sand
RG	56.69	34.83	8.47	Very coarse silty very fine sand	Silty sand
BD	0.00	70.31	29.69	Medium silt	Silt
BB	0.00	75.97	24.03	Medium silt	Silt
BJN	0.00	67.34	32.66	Very coarse silt	Silt
BJS	0.00	77.33	22.67	Very coarse silt	Mud

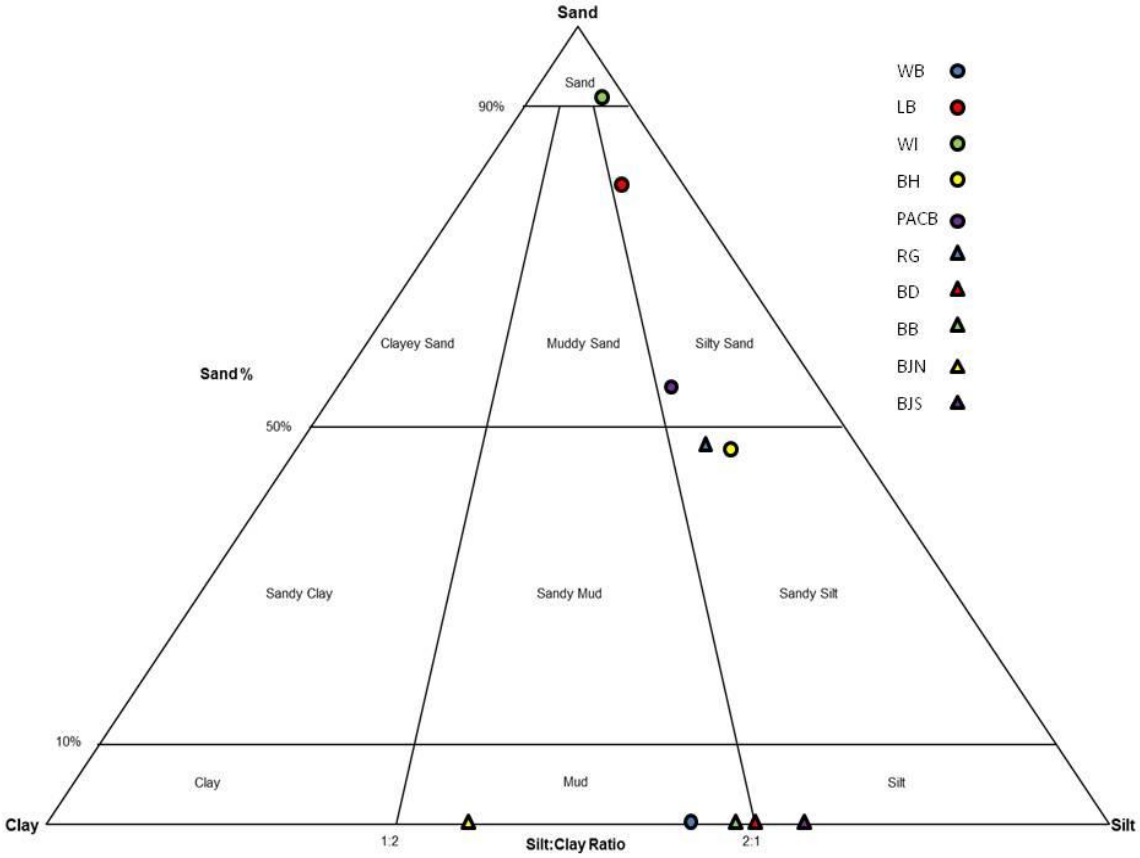

Figure 20. Folk classification ternary diagram showing sand, silt, and clay percent at 12-15 cm depth of ten different salt-marsh sites.

Table 5. Textural parameters and classification of sediments in middle parts of cores from the 10 study sites.

Sample ID	Sand %	Silt %	Clay %	Sediment Name	Textural Group
WB	0.00	60.78	39.22	Mud	Mud
LB	83.45	11.48	5.07	Very coarse silty very fine sand	Silty sand
WI	93.30	4.00	2.70	Medium sand	Sand
BH	50.63	37.07	12.30	Fine sandy very coarse silt	Sandy silt
PACB	56.02	29.63	14.35	Very coarse silty fine sand	Silty sand
RG	47.49	37.20	15.31	Very fine sandy very coarse silt	Sandy silt
BD	0.00	65.55	34.45	Mud	Mud
BB	0.00	62.09	37.91	Mud	Mud
BJN	0.00	41.37	58.63	Mud	Mud
BJS	0.00	73.57	26.43	Coarse silt	Silt

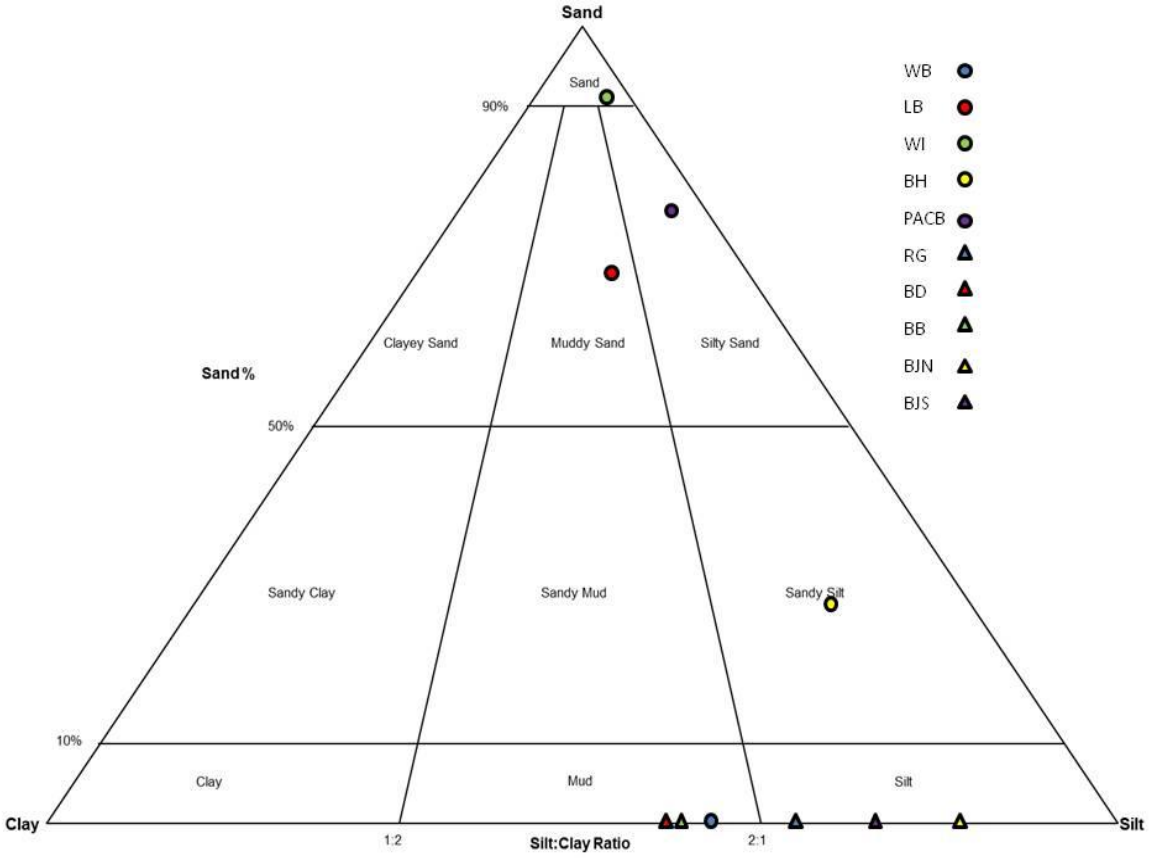

Figure 21. Folk classification ternary diagram showing sand, silt, and clay percent at 27-30 cm depth of ten different salt-marsh sites.

Table 6. Textural parameters and classification of sediments in middle parts of cores from the 10 study sites.

Sample ID	Sand %	Silt %	Clay %	Sediment Name	Textural Group
WB	0.00	61.73	38.27	Mud	Mud
LB	69.08	17.81	13.11	Muddy fine sand	Muddy sand
WI	92.66	4.66	2.68	Medium sand	Sand
BH	29.04	59.48	11.47	Very fine sandy coarse silt	Sandy silt
PACB	74.08	21.85	4.07	Coarse silty fine sand	Silty sand
RG	0.00	68.05	31.95	Medium silt	Silt
BD	0.00	57.52	42.48	Mud	Mud
BB	0.00	56.71	43.29	Mud	Mud
BJN	0.00	87.16	12.84	Medium silt	Silt
BJS	0.00	73.49	26.51	Coarse silt	Silt

Mineralogy of sediments in the upper, middle, and lower sections of the cores was determined utilizing the XRD analyses described in the Methods section. Mineral contents in these sections are summarized in Tables 7-9. The percentages defined for the minerals are weight percent. Throughout all three sections of the sediment core, quartz and various clays are the primary minerals detected, reflecting the grain-size data with silt- and clay-sized particles comprising the majority of the samples. In the upper portion of the core, only a very few sulfates and sulfides were detected the XRD analysis. In the middle section of the sediment core, sulfide minerals show a marked increase, especially at oiled the Louisiana sites. In the lower section of the sediment core, sulfides, especially non-iron sulfides, show a very marked increase.

Mineralogy of estuarine sediments is important because it reflects certain hydrological and geochemical changes taking place at depth. Formation of certain minerals can have profound effects on the pore-water chemistry in wetlands. For example, the formation of an evaporate mineral would reduce sulfate and other ion concentrations in porewaters. Clay minerals and sulfide solids have great sorbing capabilities to reduce metal concentrations in porewaters. At the Mississippi sites, more clay minerals are present in BH than in PACB, indicating possible higher metal adsorption capability in BH relative to PACB. However, the levels of certain trace metals are slightly higher in PACB sediments than those in BH (see Sediment Geochemistry section), indicating minor metal contamination derived from spilled oils or other sources. At Louisiana sites, all three of the heavily-oiled zones (BD, BB, and BJN) contain higher clay mineral contents than does the slightly contaminated RG site. This suggests a higher metal retention potential at BD, BB, and BJN sites.

Iron and non-iron sulfide minerals were common minerals present in the middle (12-15 cm) and deepest (27-30 cm) sections of the sediment cores, especially in the more heavily-oiled

Louisiana marshes. In contrast, the top sections of the sediment cores show little or no sulfide solids at all the sites. The top portion near the sediment-water interface is under less-reducing conditions. Sulfates are generally predominate in the uppermost section of the cores, while sulfide solids formed from bacterial sulfate reduction dominate at greater depths under strong reducing conditions (see Background section). The fact that very few sulfates are found in the middle and lower sections of the sediment cores suggests either that nearly all sulfate solids have been reduced to sulfide by SRB at depth, or that they never formed at all.

Table 7. Average mineral composition of sediment samples from XRD analyses for 0-3 cm interval.

Minerals 0-3 cm	WB %	LB %	WI %	BH %	PACB %	RG %	BD %	BB %	BJN %	BJS %
Quartz	46	63	75	73	83	53	57	43	57	65
Clays	48	37	15	27	9	41	27	50	43	15
Sulfates	0	0	10	0	8	6	0	7	0	20
Fe Sulfides	0	0	0	0	0	0	5	0	0	0
Non-Fe Sulfides	0	0	0	0	0	0	0	0	0	0
Other	6	0	0	0	0	0	11	0	0	0

Table 8. Average mineral composition of sediment samples from XRD analyses for 12-15 cm interval.

Minerals 12-15 cm	WB %	LB %	WI %	BH %	PACB %	RG %	BD %	BB %	BJN %	BJS %
Quartz	54	63	88	66	84	41	27	9	29	54
Clays	20	29	7	26	9	52	15	51	51	15
Sulfates	9	0	5	8	7	7	16	12	7	0
Fe Sulfides	8	0	0	0	0	0	15	9	13	6
Non-Fe Sulfides	9	8	0	0	0	0	27	19	0	25
Other	0	0	0	0	0	0	0	0	0	0

Table 9. Average mineral composition of sediment samples from XRD analyses for 27-30 cm interval.

Minerals 27-30 cm	WB %	LB %	WI %	BH %	PACB %	RG %	BD %	BB %	BJN %	BJS %
Quartz	26	79	82	49	63	56	18	58	49	54
Clays	42	16	12	23	24	23	41	29	15	19
Sulfates	4	0	0	4	8	0	9	0	0	7
Fe Sulfides	28	1	6	0	5	7	3	0	5	6
Non-Fe Sulfides	0	4	0	3	0	14	29	6	31	14
Other	0	0	0	21	0	0	0	7	0	0

Sediment Geochemistry

The determination of bulk sediment geochemistry is important to this study, as it allows for quantification of total organic carbon contents and trace-metal concentrations, as well as an assessment of geochemical impacts of the oil spill on marsh sediments. Analyses involve the total digestion analysis via ICP/MS, petrographic (image) and semi-quantitative elemental analyses using SEM and EDAX, high-resolution microanalysis of sulfide solids using Laser Ablation ICP/MS, and TOC analysis. Sediments also were analyzed for their stable carbon isotopic signatures for comparison with marsh plants and initial BP crude oil. In addition to geochemical analyses, oil compounds extracted from sediments were analyzed for their general geochemical characteristics via GC-MS in full scan mode. Certain samples were further analyzed via GC-MS under high sensitivity single ion mode (SIM), allowing for characterization of petroleum biomarkers with a specific mass-to-charge (m/z) ratio of 191.

Geochemical results from total digestion analysis show variations in concentrations of major and trace elements with depth (Figures 22 to 40, Appendices 3, 4). The results are also plotted as box plots to illustrate the spatial variability among sites (Figures 22 to 40). Seventeen metals were chosen for analysis because they represent common contaminants in salt marshes (Huerta-Diaz and Morse, 1992; Olivie-Lauquet et al., 2000; Davranche et al., 2011), in crude oil (Karchmer and Gunn, 1952; Ball et al., 1960; Barwise, 1990; Kennicutt et al., 1991), or both. The results show that concentrations of numerous elements (e.g., Ni, Cu, Pb, Zn, Sr, Co, V, Ba, Hg, As, S, Fe) are generally higher in heavily-oiled Louisiana zones compared to less-affected and pristine sites at Mississippi.

At the Mississippi sites, the concentrations of many metals in PACB sediments are typically 1 to 3 times higher than those associated with BH (Figures 22 to 40), despite the fact

that BH contains finer-sized sediments with greater metal sorption capabilities. PACB was slightly contaminated with the Macondo-1 oil spill, while BH was unaffected. Spilled oil, and perhaps higher terrestrial metal inputs, may account for the increased level of metals in PACB sediments. In addition, many metals (Fe, S, Pb, Co, As, Hg) show a trend of increasing concentration from the surface to the middle parts (12-15 cm) of cores. The majority of metals at both sites decrease from the middle section to the bottom section (27-30 cm) of the cores. The slight enrichment of trace metals in shallow (post-industrial) sediments may also be related to riverine inputs derived from anthropogenic sources, as low sedimentation rates in these areas (approximately 0.2 cm/year) (Corbett et al., 2004) suggest that approximately only the upper 20 cm of the sediment core is within the last 100 years, a period of time that would span the majority of the industrial age for this area of the United States.

Metal concentrations in oiled Louisiana marsh sediments are much higher (as much as one order of magnitude) than those in Mississippi marshes (Appendices 3, 4). The slightly-oiled RG site contains the highest average concentrations for a few metals (e.g., As, Th, Ba, Hg). Otherwise, sites BD and BB generally contain the highest average metal concentrations.

Because oil is known to carry numerous trace metals in its complex chemical make-up, it is likely that the oil that has inundated BD, BB, and BJN sites resulted in a high influx of trace metals. RG hosts the highest average concentrations of particular metals (As, Th, Ba, Hg) that are often anthropogenically concentrated. The RG site is located near the major outlet for Lake Pontchartrain in a highly-trafficked area. It is likely that RG receives metal inputs from Lake Pontchartrain discharge and heavy motor traffic. This can explain why the slightly-oiled RG site contains higher average metal levels than BJN, a site that was much more affected by the oil spill. BD and BB are located slightly further inland than BJN, yet they generally contained the

highest average metal concentrations. There are two possible interpretations for this: 1) BD and BB both have more metal sorption capabilities owing to their finer-grained sediments than BJN; and 2) BD and BB are less open to seawater flushing. Any oil that was washed into BB, and especially BD, likely became trapped while it slowly degraded instead of being flushed out. The Louisiana sites are similar to the Mississippi sites in that metal concentrations are generally higher in the upper and middle portions of the sediment columns while decreasing in the lower portions. A possible mechanism for this model is that metals are intruding down into the mid-portion of the sediment columns, and the decrease of metal concentrations towards the lower sections of the sediment core reflects pre-industrial metal concentration levels.

The level of certain metals/metalloids (e.g., arsenic) correlated well with (r = 0.47) the abundance of clay-sized particles (Figure 41). This confirms that the fine-grained sediments in salt marshes have high capacity to adsorb metals derived from terrestrial or marine sources. This correlation suggests that the retention of trace metals in salt marshes is strongly controlled by the geology and sediment characteristics of each individual site.

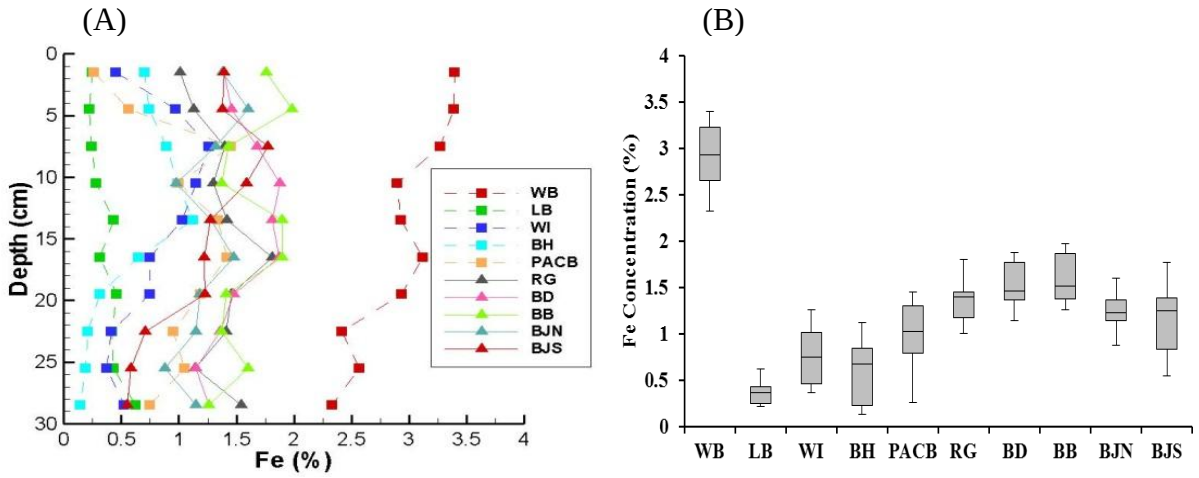

Figure 22. (A) Depth profile and (B) box and whisker plot showing depth- and spatial-variability of iron. Contaminated sites show much higher iron levels compared to those at non-contaminated sites.

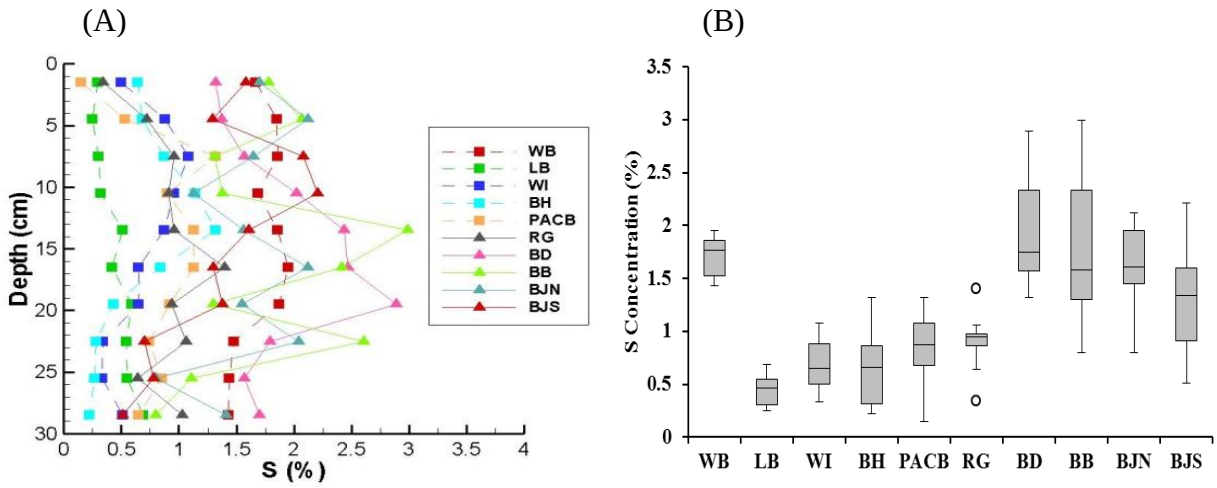

Figure 23. (A) Depth profile and (B) box and whisker plot showing depth- and spatial-variability of sulfur. Contaminated sites show much higher sulfur levels compared to those at non-contaminated sites.

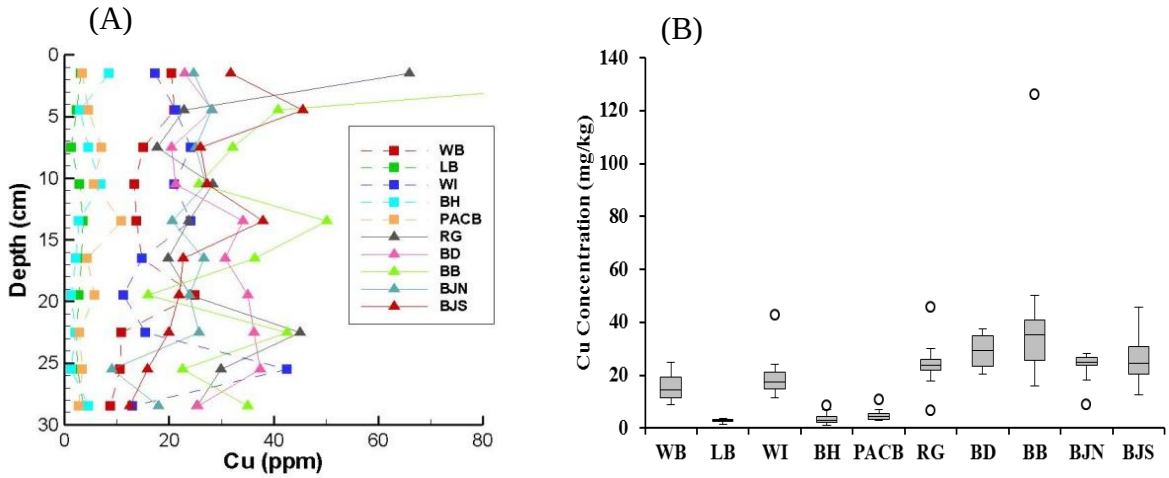

Figure 24. (A) Depth profile and (B) box and whisker plot showing depth- and spatial-variability of copper. Contaminated sites show much higher copper levels compared to those at non-contaminated sites.

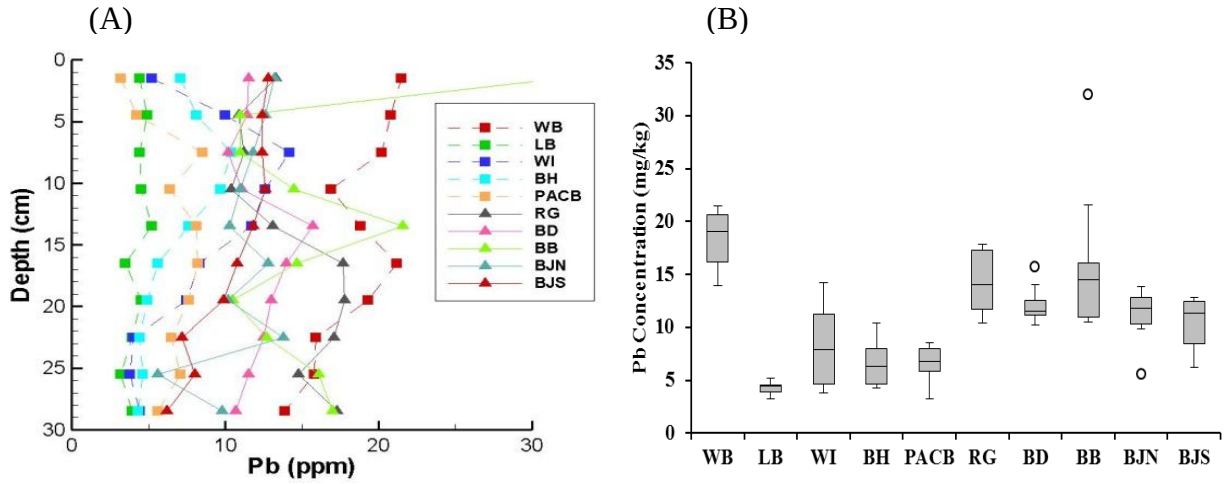

Figure 25. (A) Depth profile and (B) box and whisker plot showing depth- and spatial-variability of lead. Contaminated sites show much higher lead levels compared to those at non-contaminated sites.

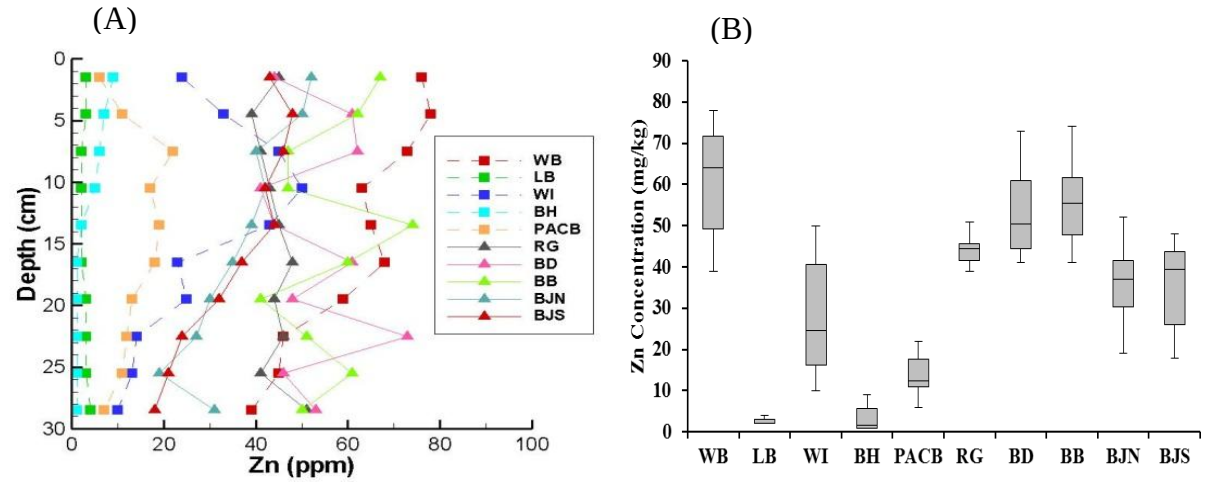

Figure 26. (A) Depth profile and (B) box and whisker plot showing depth- and spatial-variability of zinc. Contaminated sites show much higher zinc levels compared to those at non-contaminated sites.

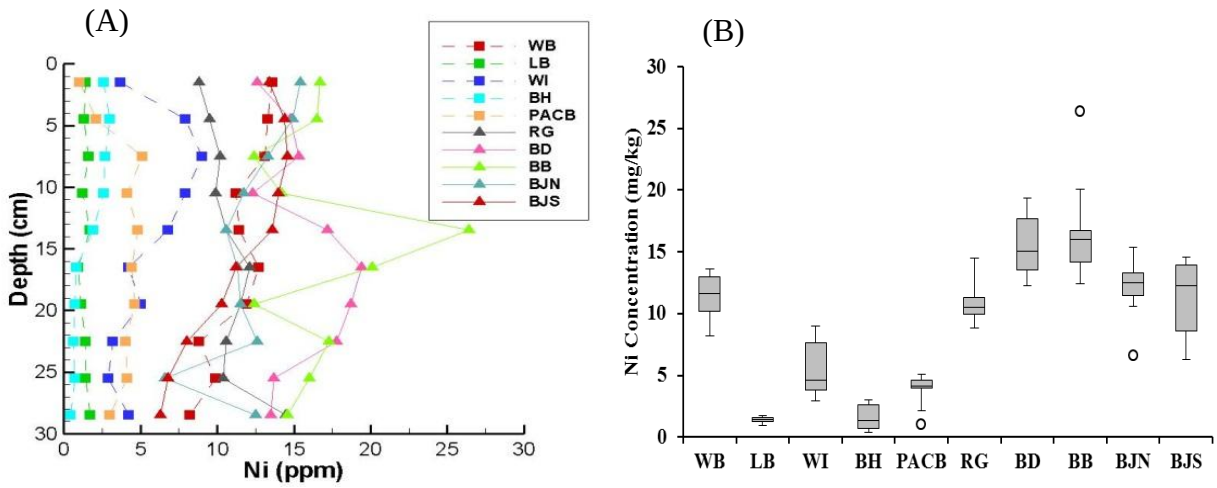

Figure 27. (A) Depth profile and (B) box and whisker plot showing depth- and spatial-variability of nickel. Contaminated sites show much higher nickel levels compared to those at non-contaminated sites.

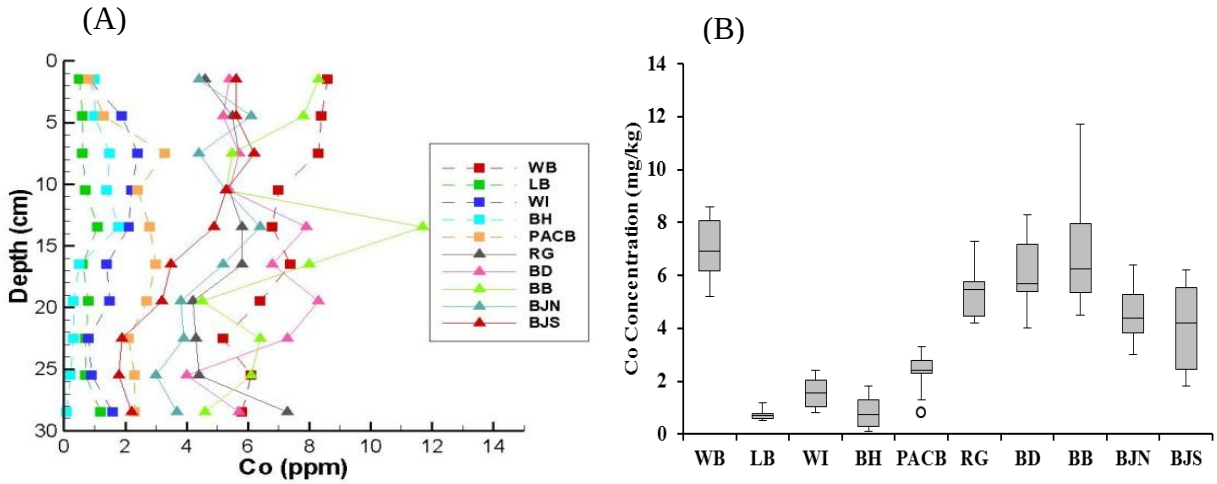

Figure 28. (A) Depth profile and (B) box and whisker plot showing depth- and spatial-variability of cobalt. Contaminated sites show much higher cobalt levels compared to those at non-contaminated sites.

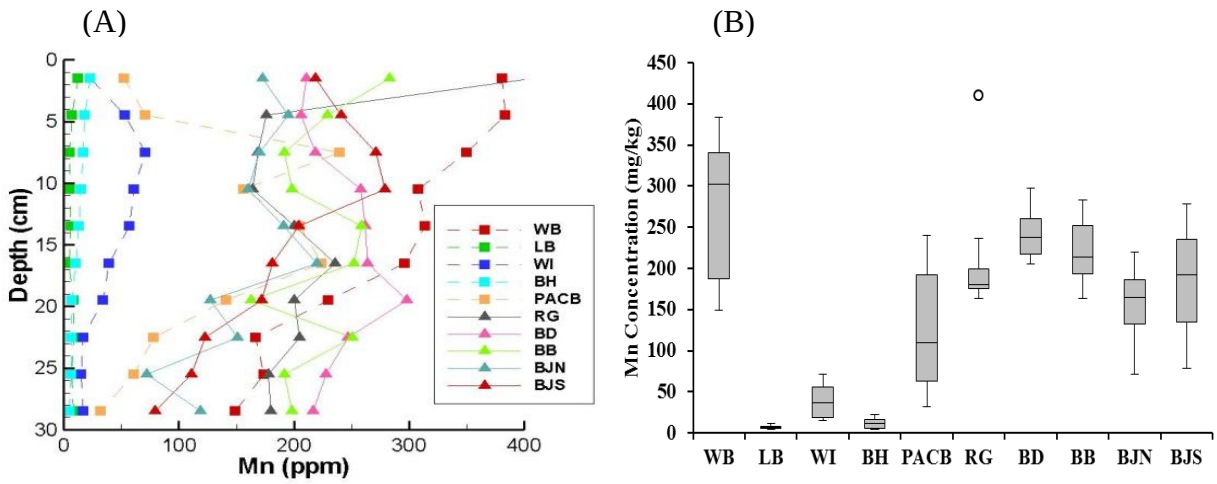

Figure 29. (A) Depth profile and (B) box and whisker plot showing depth- and spatial-variability of manganese. Contaminated sites show much higher manganese levels compared to those at non-contaminated sites.

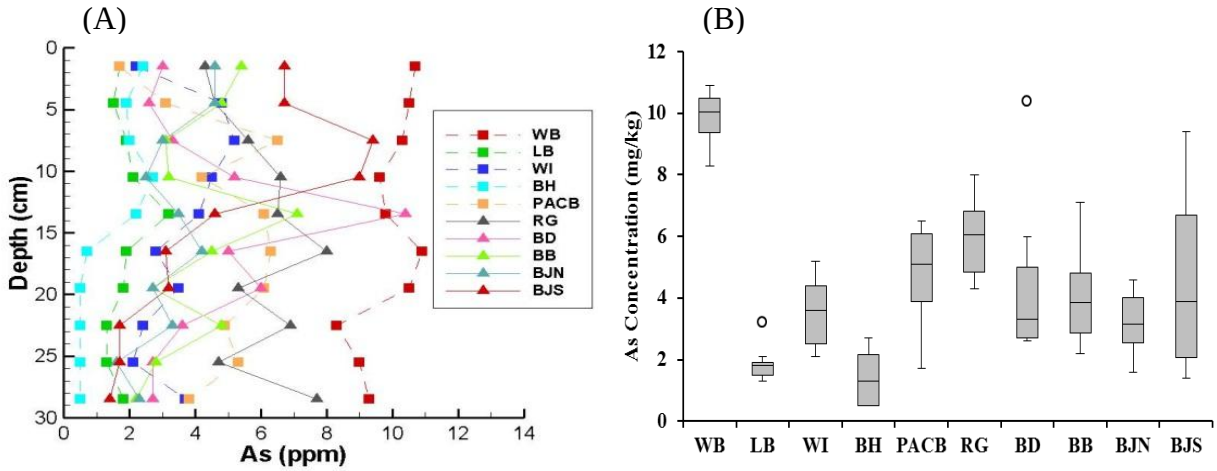

Figure 30. (A) Depth profile and (B) box and whisker plot showing depth- and spatial-variability of arsenic. Contaminated sites show much higher arsenic levels compared to those at non-contaminated sites.

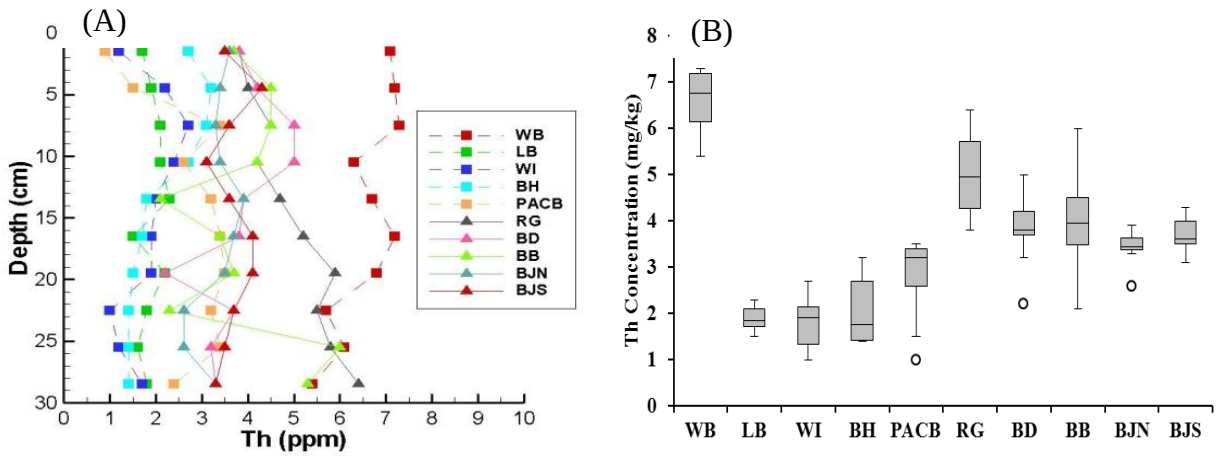

Figure 31. (A) Depth profile and (B) box and whisker plot showing depth- and spatial-variability of thorium. Contaminated sites show much higher thorium levels compared to those at non-contaminated sites.

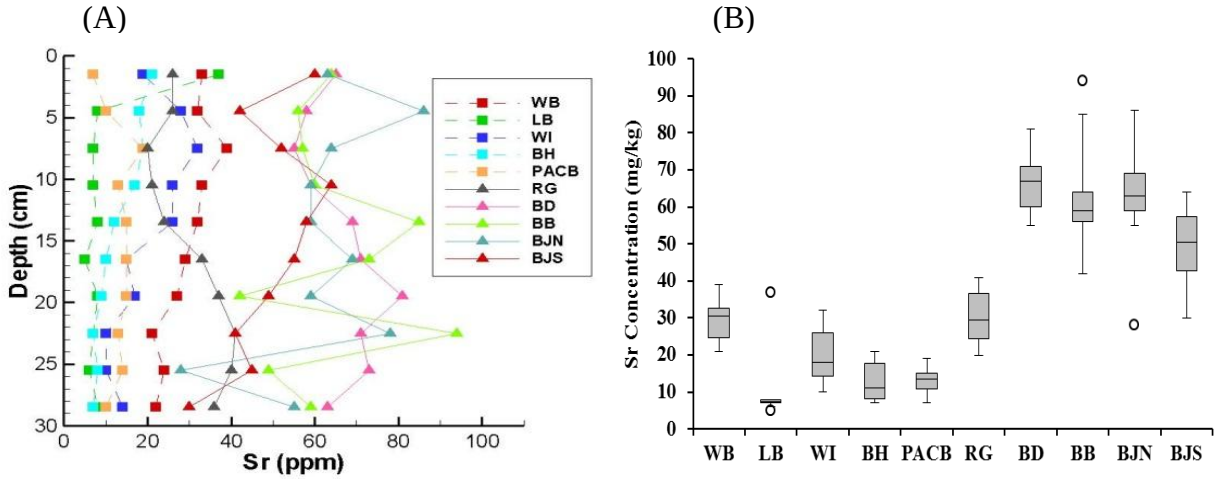

Figure 32. (A) Depth profile and (B) box and whisker plot showing depth- and spatial-variability of strontium. Contaminated sites show much higher strontium levels compared to those at non-contaminated sites.

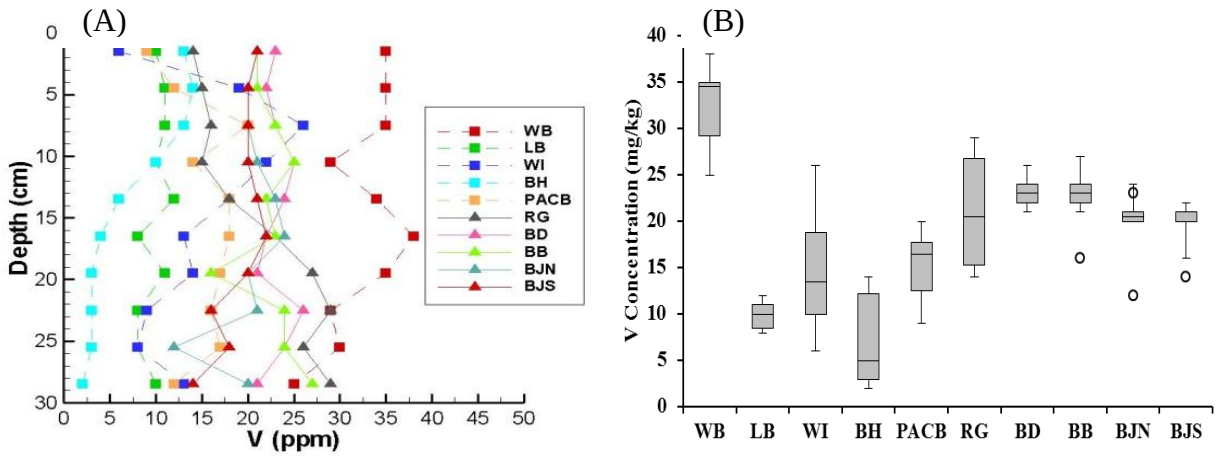

Figure 33. (A) Depth profile and (B) box and whisker plot showing depth- and spatial-variability of vanadium. Contaminated sites show much higher vanadium levels compared to those at non-contaminated sites.

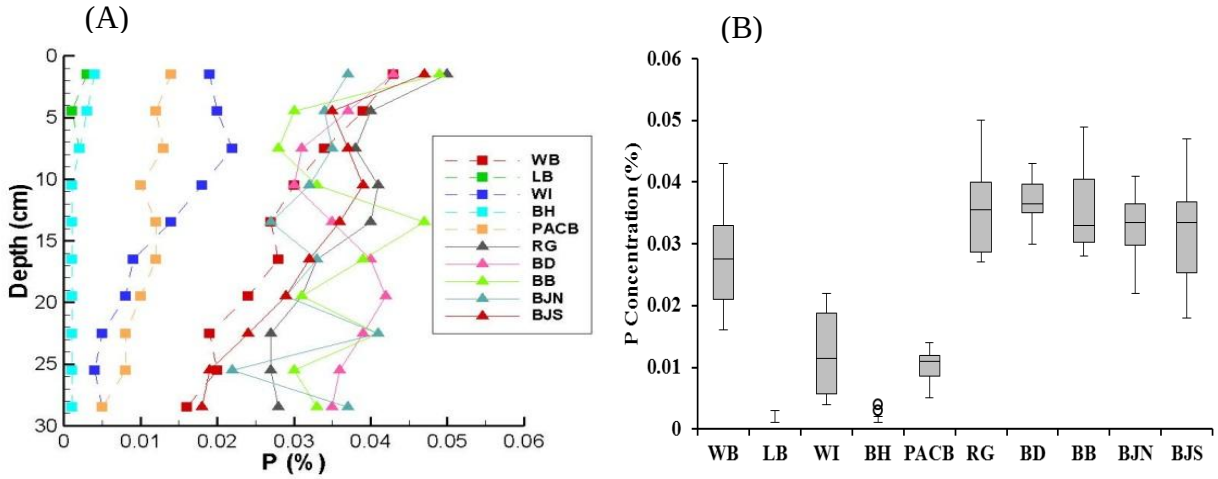

Figure 34. (A) Depth profile and (B) box and whisker plot showing depth- and spatial-variability of phosphorous. Contaminated sites show much higher phosphorous levels compared to those at non-contaminated sites.

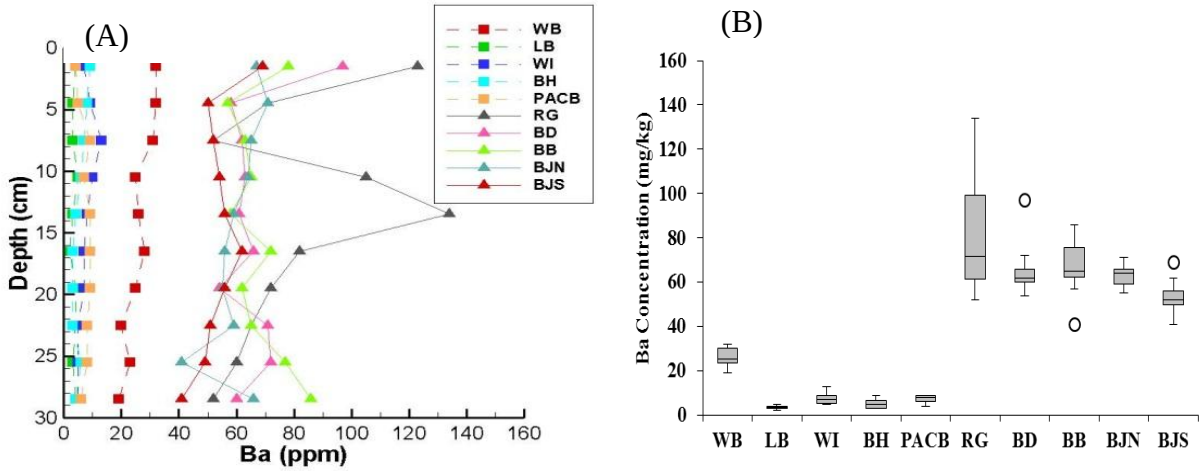

Figure 35. (A) Depth profile and (B) box and whisker plot showing depth- and spatial-variability of barium. Contaminated sites show much higher barium levels compared to those at non-contaminated sites.

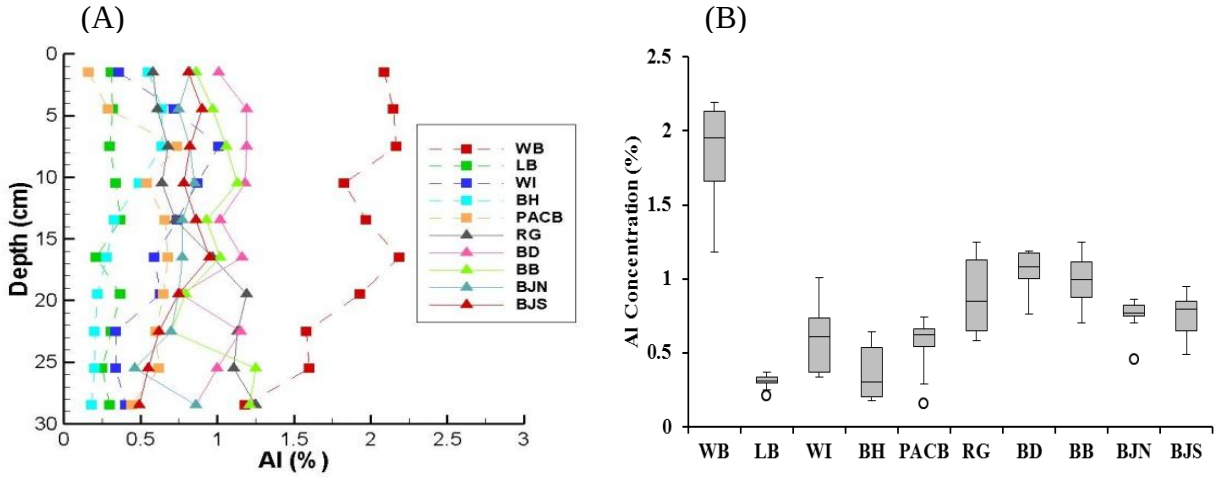

Figure 36. (A) Depth profile and (B) box and whisker plot showing depth- and spatial-variability of aluminum. Elevated aluminum levels likely reflect anthropogenic contamination.

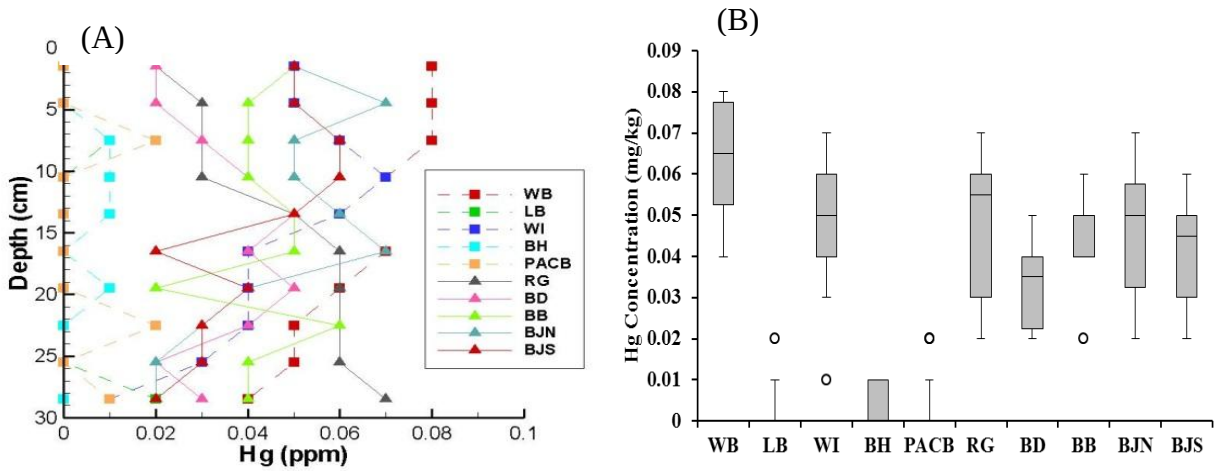

Figure 37. (A) Depth profile and (B) box and whisker plot showing depth- and spatial-variability of mercury. Contaminated sites generally show much higher mercury levels compared to those at non-contaminated sites.

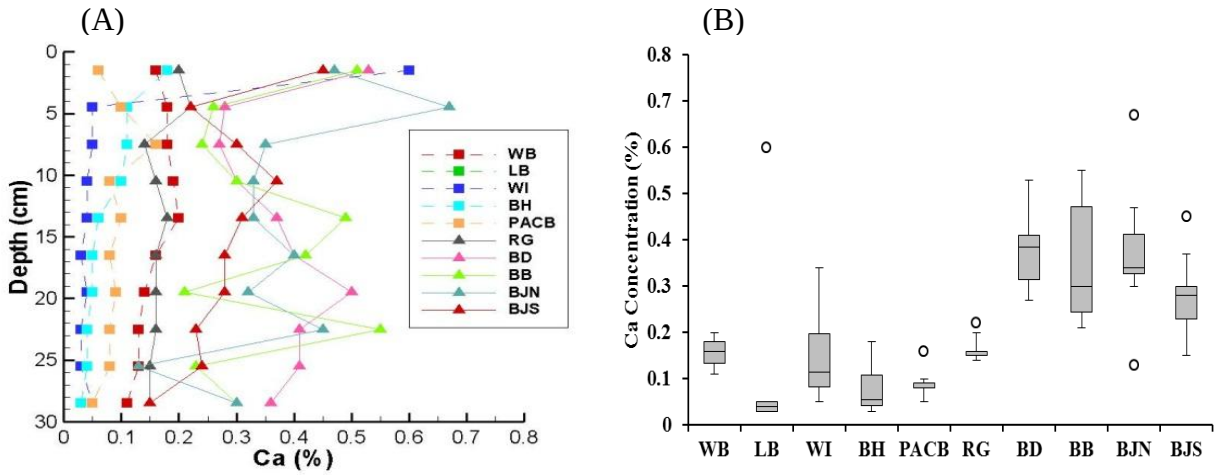

Figure 38. (A) Depth profile and (B) box and whisker plot showing depth- and spatial-variability of calcium. Elevated calcium levels likely reflect anthropogenic contamination.

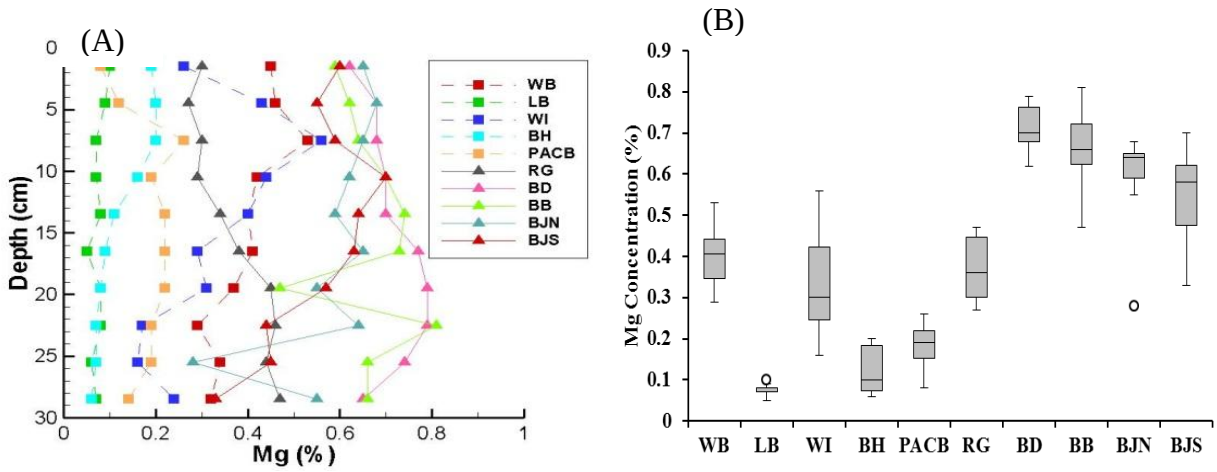

Figure 39. (A) Depth profile and (B) box and whisker plot showing depth- and spatial-variability of magnesium. Contaminated sites show much higher magnesium levels compared to those at non-contaminated sites.

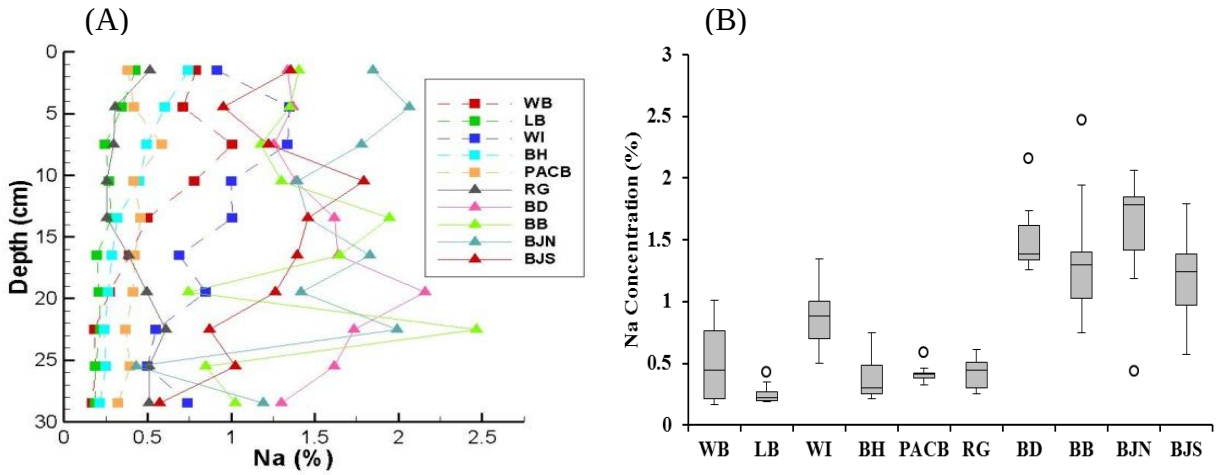

Figure 40. (A) Depth profile and (B) box and whisker plot showing depth- and spatial-variability of sodium. Contaminated sites show much higher sodium levels compared to those at non-contaminated sites.

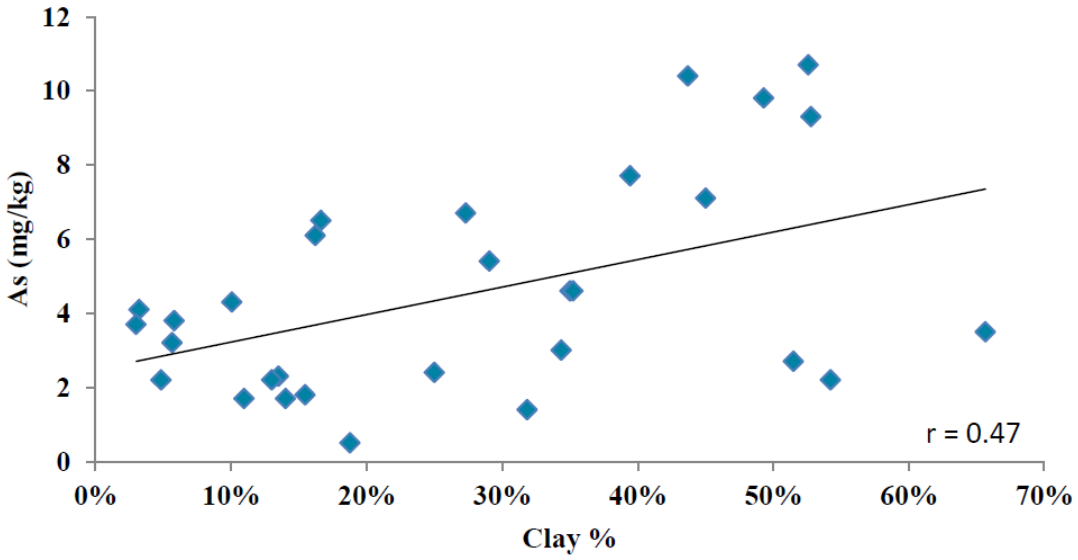

Figure 41. An increase in As concentration corresponds to increasing clay content.

Metal Enrichment in Wetland Sediments

Concentrations of elements derived from bulk sediment geochemical analysis were normalized to aluminum, the selected reference element (Table 10). The average normalized enrichment factor (ANEF)

$$\frac{Me_{sample} / Al_{sample}}{Me_{crust} / Al_{crust}} \quad (1)$$

evaluates the enrichment of elements relative to aluminum. Aluminum is the third most abundant element in the earth's crust (Wedepohl, 1995). Since there are no known anthropogenic sources of aluminum in marsh sediments, any metal with ANEF above 1 can be inferred as likely receiving anthropogenic inputs other than natural terrigenous sources.

Overall, ANEF values show enrichment of many metals at marsh sites beyond levels of terrestrial inputs, suggesting anthropogenic contamination from either industrial sources or from a marine source, such as an oil spill. In Mississippi, PACB has much higher ANEF values for As (mean = 35.28) in comparison to those at BH (mean = 13.62). In addition, sediments at PACB are enriched in many other metals (Ni, Co, V, Zn, Fe, Mn, etc.) with respect to those at BH. Ni and V are common metals found in crude oil, implying that PACB might be slightly contaminated by oil. BH is likely receiving anthropogenic inputs from nearby streams, leading to enriched metal concentrations. Although PACB also may receive some anthropogenic input, it is located farther from major stream sources than is BH. The higher enrichment levels observed at site PACB (those that are above levels at site BH) must be received from non-terrestrial sources. Spilled oil from the Macondo-1 well likely is responsible for elevated levels of certain metals (e.g., Zn, Mn, Fe, As, Ni, Co, V, Mg) at PACB.

The Louisiana sites are enriched in many metals. Although RG is a relatively unaffected site, it is more highly enriched in many metals than heavily oiled sites BD, BB, and BJN. RG is located in close proximity to Lake Pontchartrain and Interstate 10, and therefore is subject to many potential anthropogenic sources of contamination from human traffic (boats, cars, etc). Carbon isotope signatures of sediments (see section below) indicate that RG only received slight contamination from the Macondo-1 well oil. Highest ANEF values of common elements in crude oil (e.g., Ni, V, S) are observed at BD, BB, and BJN sites in the Barataria Bay, suggesting that much of metal contamination at these sites is derived directly from the BP Macondo-1 oil spill.

Table 10. Calculated average normalized enrichment factor (ANEF) of selected elements at various salt marsh sites.

Element	WB	LB	WI	BH	PACB	RG	BD	BB	BJN	BJS
Cu	4.40	4.95	21.91	5.68	5.68	20.68	15.49	24.89	16.27	18.43
Pb	4.53	6.32	6.04	8.92	5.87	7.61	5.39	7.64	6.70	6.28
Zn	4.85	1.34	6.79	1.14	3.95	7.98	7.62	8.65	7.15	6.89
Mn	2.12	0.34	0.90	0.47	3.44	3.93	3.46	3.42	3.06	3.59
Fe	3.97	3.04	3.16	3.95	4.59	4.07	3.70	4.17	4.17	3.80
Ba	0.16	0.13	0.15	0.18	0.17	1.22	0.74	0.82	0.93	0.85
Hg	4.71	1.76	10.94	1.55	1.15	7.17	4.63	6.24	8.38	7.52
As	20.97	23.48	23.78	13.62	35.28	27.73	16.92	16.79	16.58	23.34
S	75.51	120.86	92.14	153.08	122.59	85.22	153.72	155.79	173.73	141.57
Sr	0.38	0.81	0.82	0.88	0.64	0.85	1.60	1.66	2.01	1.63
Ni	2.55	1.88	3.83	1.64	2.87	5.34	6.30	7.25	6.63	6.15
Co	2.53	1.64	1.76	1.35	2.91	4.33	4.04	4.77	4.11	3.47
V	2.57	4.74	3.58	2.53	4.56	3.49	3.26	3.39	3.92	3.79
Th	2.69	4.67	2.37	4.54	3.89	4.38	2.71	2.98	3.36	3.80
Ca	0.22	0.82	0.61	0.53	0.49	0.55	1.00	0.99	1.30	0.99
Mg	1.23	1.40	3.14	1.92	2.04	2.45	3.97	3.95	4.43	4.21
Na	0.77	2.55	4.74	3.28	2.82	1.44	4.58	4.52	6.08	4.77
Al	1.00	1.00	1.00	1.00	1.00	1.00	1.00	1.00	1.00	1.00

Total Organic Carbon in Sediments

Total organic carbon contents of sediments are summarized in Appendix 5. Results (Figure 42) not only show variations of TOC with depth, but also substantial differences among various marsh sites. BH shows slightly higher levels of TOC (mean = 5.0 %) than PACB (mean = 2.4 %), despite receiving no oil contamination. This suggests that BH receives more terrigenous carbon influx than does the PACB site. Moreover, BH is better sheltered from strong ocean currents from the Gulf and thus contains more fine-grained sediments than PACB. Fine-grained sediments have greater potential to retain organic solids. In contrast, PACB is open to flushing of ocean waves; it is likely that much of the oil contamination that the PACB site received has been dispersed and washed by longshore currents. TOC levels at heavily oiled

Louisiana sites (BD, BB, and BJN) are much higher (6.8 to 29 %) than those at RG site (mean = 1.5%) and two Mississippi sites. The relatively low TOC and DOC contents at RG sites suggest that it was only slightly contaminated (compared to BD, BB, and BJN located in the Barataria Bay).

BD shows the highest TOC levels (up to 29%) among all marsh sites investigated in this study. BD is located in a narrow waterway landing into the large Batiste Bay; it is likely that oil plumes were funneled and concentrated through this narrow channel during high tides. Large areas of dead marsh plants covered with oil were clearly visible in and around the BD, BB, and BJN sampling sites. All these sites show significant increases in TOC concentrations from the surface to middle sections (around 15 cm) of the core. The TOC contents in uppermost sediments may be reduced by microbial degradation, water mixing, wave flushing form tides, and the use of dispersants. Many oiled sites in the Barataria Bay have been treated by surface dispersant applications after oil washed ashore. Dispersants tend to change the inherent chemical and physical properties of oil so that natural microbes could digest oil faster (Kujawinski et al., 2011). Higher levels of TOC in contaminated sediments can be positively correlated to higher metal concentrations (Figure 43, Appendices 3, 4), indicating that organic carbon and metal contaminants are likely derived from the same source. TOC and DOC depth profiles also indicate that the contamination is not limited to surface sediments. Spilled oil may have spread throughout water column and, in addition to contaminating surface sediments, may have contaminated deeper sediments via mixing and intruding with denser seawater.

A linear relationship between DOC and TOC ($r = 0.47$) is observed, although the cause of correlation is not clear. This positive correlation suggests that either DOC or TOC may be used as an indicator for the level of oil contamination. Quantitative assessment of oil contamination

also may be achieved by the stable carbon isotopic signatures of bulk sediments (see Carbon Isotope section).

Organic carbon is essential in wetlands, but too much of it can have a negative effect on wetlands. Elevated amounts of organic carbon can induce numerous detrimental effects: (1) organic carbon can be utilized as an electron donor by iron- and sulfate-reducing bacteria, thereby facilitating reducing conditions; (2) reducing conditions can lead to a subsequent mobilization of metals through disaggregation of host minerals; (3) organic matter can compete with metals for sorption onto mineral surfaces, further contributing to metal mobilization, and; (4) organic matter also can amplify the biological transformation of mercury into methylmercury.

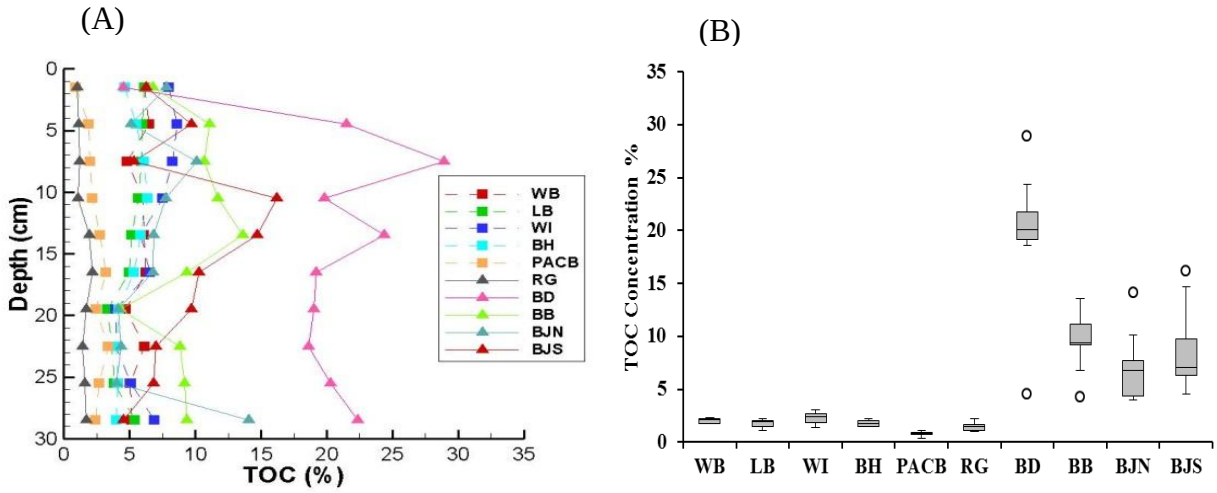

Figure 42. (A) Depth profile and (B) box and whisker plot showing depth- and spatial-variability of TOC. Contaminated sites show much higher TOC levels compared to those at non-contaminated sites.

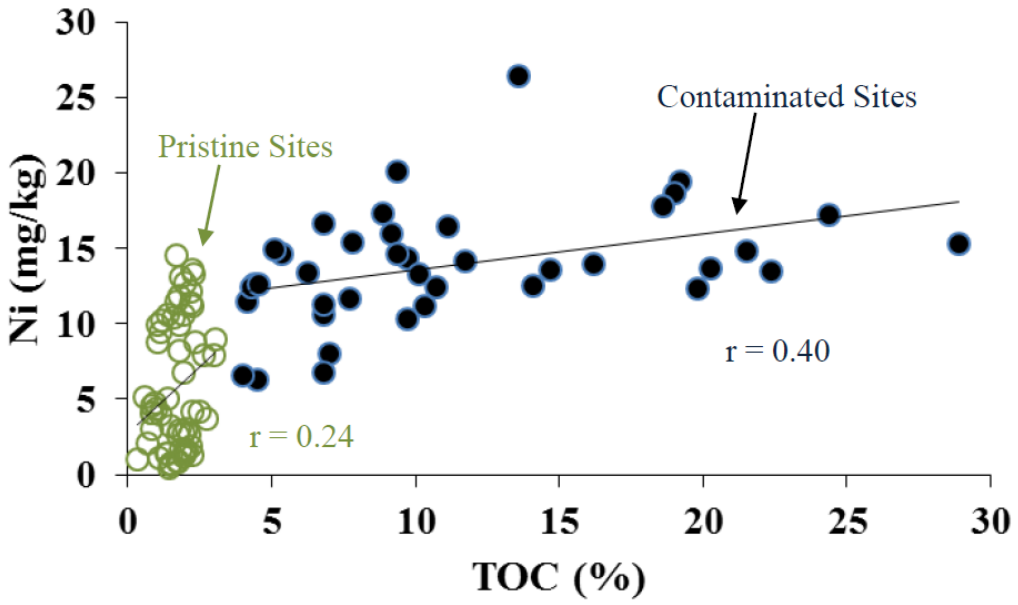

Figure 43. Plot of higher Ni levels correspond more strongly to high TOC levels.

Petrographic, SEM and LA-ICP-MS Analyses of Sulfide Solids

Pyritic minerals with distinct framboidal form occur in Louisiana oiled marsh sediments (Figure 44). Sedimentary pyrite that takes on a unique framboidal ("raspberry-like") form has been interpreted to have originated authigenically (Berner, 1970; Wilkin and Barnes, 1996; Wilkin et al., 1996), biogenically (Folk, 2005; Donald and Southam, 1999), or a combination of both (Donald and Southam, 1999). Framboidal pyrites were found primarily at three heavily contaminated sites: BD, BB, and BJN. These three sites showed high levels of iron, sulfur, and TOC, the three necessary ingredients for sedimentary pyrite formation. Two Mississippi sites (BH and PACB) contained no or far fewer of pyrite-like sulfides. Thus, those sites were not examined. Only two of the sites hosting large amounts of framboidal sulfides (BD and BJN) were analyzed for their trace metal contents associated with pyrite. SEM and EDAX analysis

were first conducted in order to discern the grain size, texture, and chemical content of framboidal pyrites. SEM images demonstrate the occurrence of aggregates of equi-dimensional spheroids of about 10 – 30 μm (Figures 45-47). EDAX spectrum of these spheroids consistently results in peaks for Fe and S, with minor amounts of Si, O, and Al (Table 11). Other elements are much less abundant and thus cannot be quantitatively measured using EDAX. These iron sulfides have been interpreted as the pyritized corpses of nannobacterial cells embedded in decaying organic matter (Folk, 2005). Wilkin and Barnes (1996) presented formation mechanisms responsible for the unique pyrite framboid texture involving nucleation transform and aggregation of tiny microcrystals. The precipitation of framboidal pyrite was likely performed by sulfate-reducing bacteria fueled by inflow of organic matter.

Influx of oil may affect the fate and transformation of trace metals in marsh sediments. A question to be addressed in this research is whether the toxic metals (e.g., As and Hg) remain in solution or are largely sequestered in sulfide solids. Elevated levels of trace metals have been documented in oiled marsh sediments (see Sediment Geochemistry section). However, the pore-water analysis showed very low metal concentrations in porewaters (Keimowitz, personal communication). It is hypothesized that many trace metals are sequestered in pyrite-like monosulfides formed in marsh sediments; those authigenic and biogenic pyrites have a large capacity for retaining chalcophile metals, thereby serving as "sinks" for trace metals (Berner, 1970; Huerta-Diaz and Morse, 1992; Orberger et al., 2003) in strongly-reducing conditions.

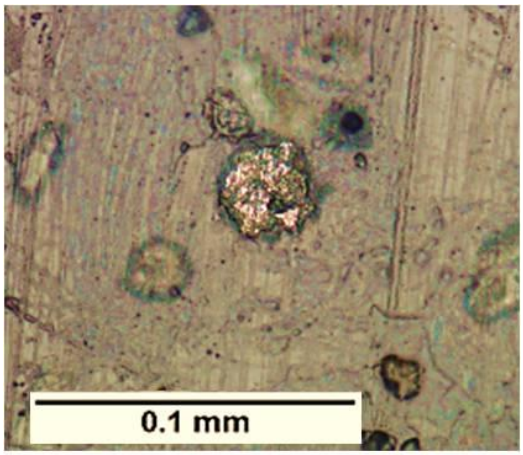

20x Reflected Light BD

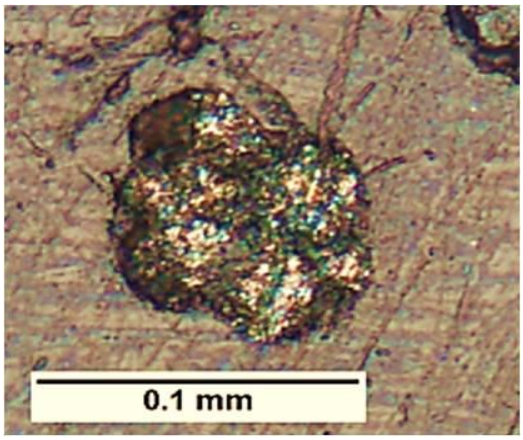

20x Reflected Light BD

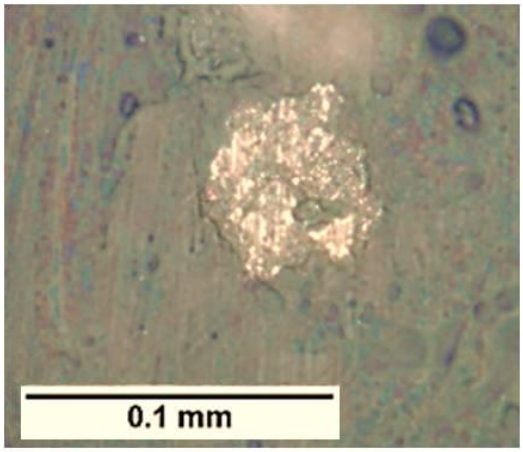

20x Reflected Light BD

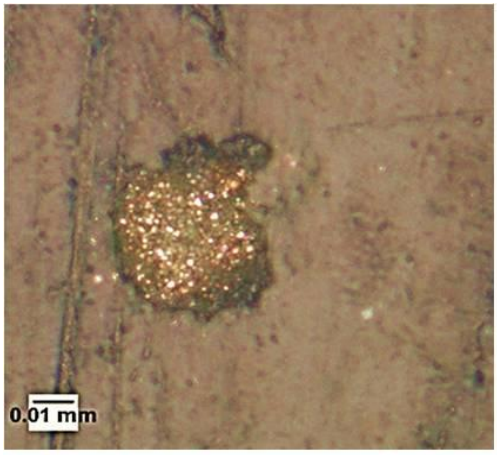

40x Reflected Light BJN

Figure 44. Photomicrographs in reflected light showing variations of the framboidal texture of biogenic pyrites formed in oiled Louisiana marshes.

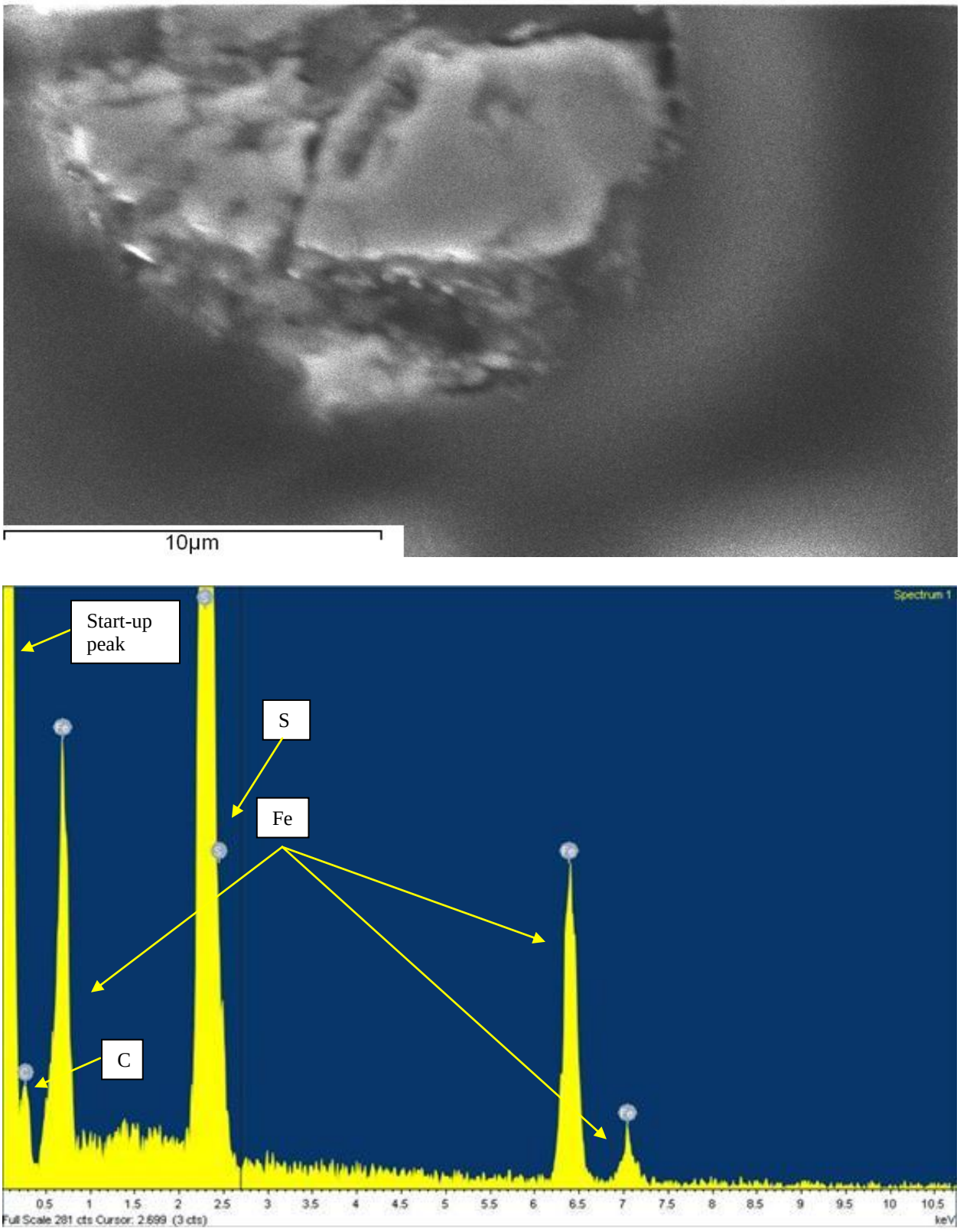

Figure 45. SEM photo and EDAX spectrum of framboidal pyrite (from BD S-2 Spectrum 2) showing iron and sulfur as primary constituents, with carbon being a lesser component.

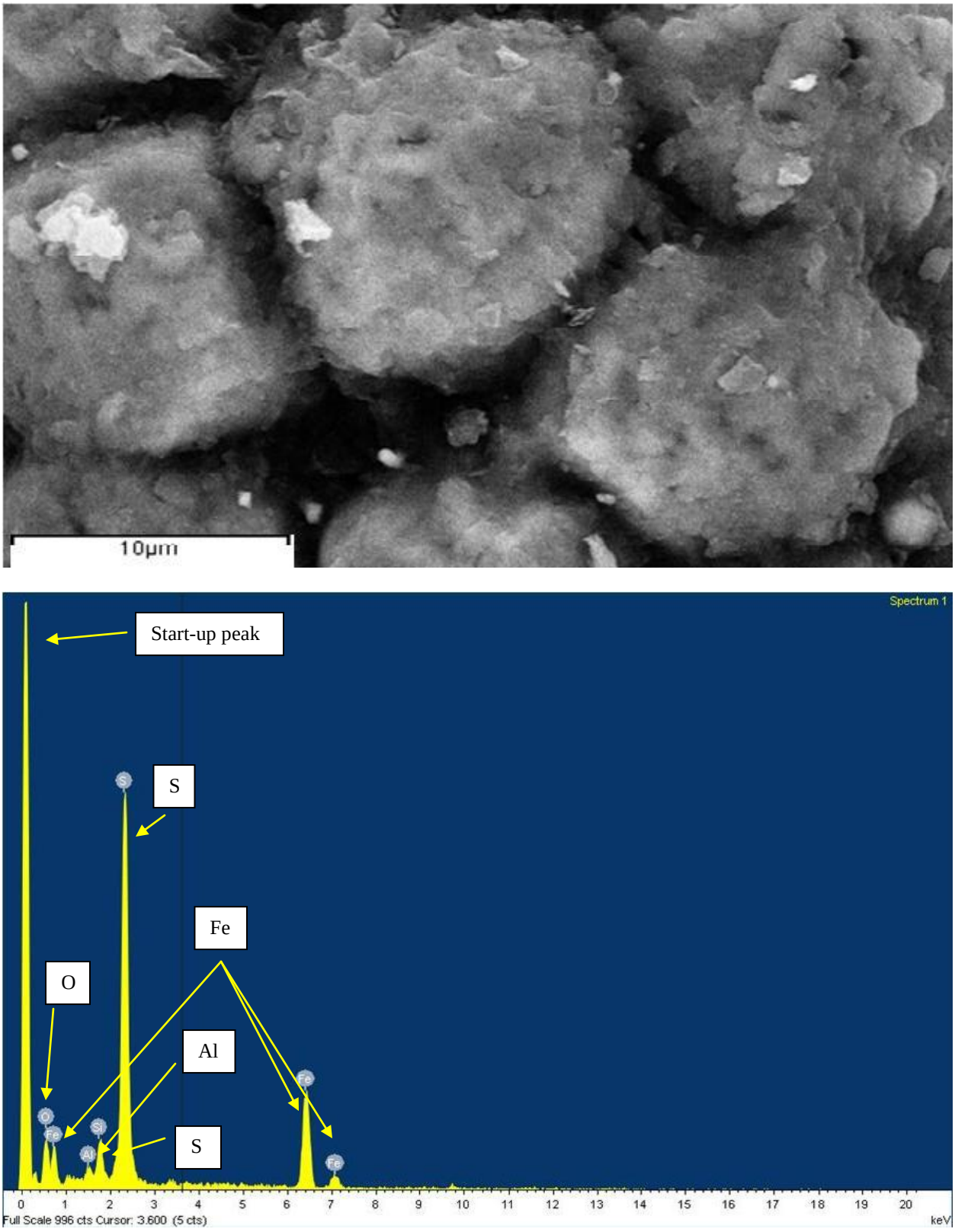

Figure 46. SEM photo and EDAX spectrum of framboidal pyrite (from BD P-1 Spectrum 1) showing iron and sulfur as primary constituents, with O, Si, and Al being lesser components.

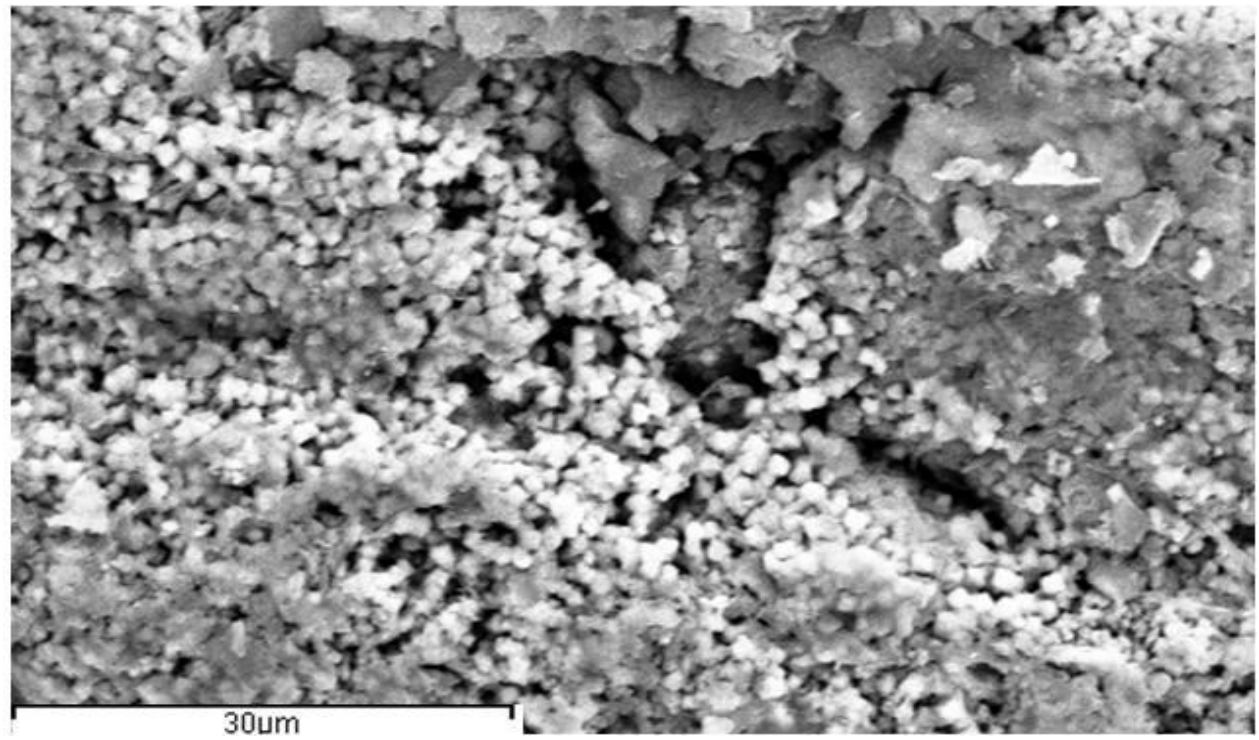

.

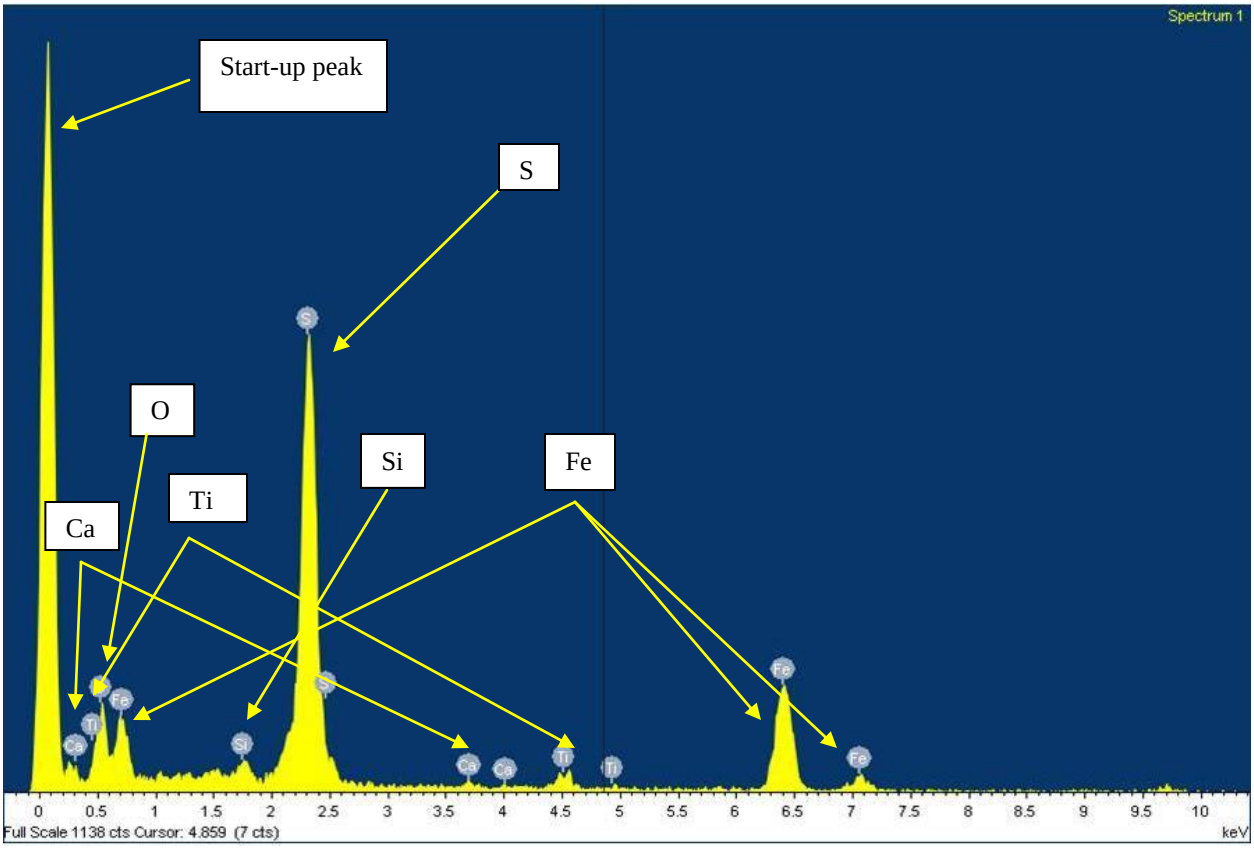

Figure 47. SEM photo and EDAX spectrum of framboidal pyrite (BJN P-1 Spectrum 1) showing iron and sulfur as primary constituents, with calcium and titanium being lesser components.

Table 11. Elemental composition by percentage of various slide-mounted and puck-mounted grains analyzed via SEM w/ EDAX.

Sample ID	Fe %	S %	Si %	Al %	Total %
Slide-Mounted					
BD S-2 Spectrum 2	62.51	37.49	-	-	100.00
BD S-2 Spectrum 7	64.11	35.89	-	-	100.00
WB S-1 Spectrum 5	65.11	34.89	-	-	100.00
WB S-3 Spectrum 2	63.35	36.65	-	-	100.00
Puck-Mounted					
BD P-1 Spectrum 1	53.90	46.10	-	-	100.00
WB P-1 Spectrum 1	67.97	32.03	-	-	100.00
BJN P-1 Spectrum 1	32.64	55.10	8.80	3.46	100.00
BJS P-1 Spectrum 1	50.61	48.24	1.15	-	100.00

Trace metals, such as arsenic and mercury, however, were not detected by EDAX analyses. The sensitivity of the EDAX system appears to be insufficient for detecting minute quantities of trace metals that typically exist in sulfides. In order to quantify trace metal concentrations, laser ablation, coupled with high-resolution ICP-MS was used to measure the trace elements contents of sulfide solids. A petrographic microscope was utilized first to identify and locate crystals of framboidal pyrites. The selected crystals were ablated by the laser, and plasma containing the ablated particles was transported to the mass detector of ICP/MS system. The ablating spot size ranged from 15-25 µm. Intensity (cps) of ionized metals associated with

the plasma cloud was recorded by a computer. The intensities give a relative abundance of the ions of interest. Intensities were then converted to concentrations using relative sensitivity factors determined on NIST SRM 610 (Gaboardi and Humayun, 2009). This process has the capability of quantifying concentrations of trace metals with sensitivities that are orders of magnitude better than SEM/ EDAX.

Several framboidal pyrites from BD and BJN sites were analyzed by LA-ICP-MS. A suite of metals of interest (S, V, Mn, Fe, Co, Ni, Cu, Zn, As, Se, Mo, Cd, Te, Hg, Pb) was decided ahead of time, and only those particular metals were measured for this study. Figures 48-51 show the relative intensity of various metals with respect to time as the laser ablates deeper into crystals. Concentrations of metals have been normalized to iron and listed for each site studied (Tables 12-14).

Average S and Fe concentrations in framboid pyrites recovered from BD sites are 40.0 % and 53.7 %, respectively. Among the three BJN samples, S averaged 33.7 % and Fe averaged 59.3 %, respectively. These results confirmed that Fe and S are the main constituents in the samples. Analyzed pyrites also show high concentration of Mn, Pb, Zn, and As (average concentrations > 1,000 mg/kg) and minor amounts of Ni, Co, V, Hg, Se, and Cd. Metals Hg and Te are also present, but their concentrations are not calculated due to the lack of standard references. In five samples (BD-4, BD-5, BD-6, BJN-1, BJN-2), some trace metals show very high concentrations. Over time, framboidal pyrites will stabilize, and their Fe/S ratios will change. As the grains mature and more iron and sulfur is accumulated, it is likely that trace metal sorption is slowed, leading to a decrease in the concentrations of these minor constituents. Samples BD-1, BD-3, BD-8, BD-9, and BJN-3 appeared to have the framboidal shape, but are all likely poorly-crystallized to amorphous Fe/S solids, as their Fe/S ratios are all nearly a 1:1 ratio

versus the framboidal pyrites with different Fe/S ratios (i.e. higher Fe and Lower S concentrations). Trace metals are sufficiently lower in these grains, so it is likely that as they sorbed more sulfur from the sulfur-rich waters, their ability to sorb trace elements declined, ultimately leading to a loss of intensity for trace elements in these grains. With continued sulfur saturation, it is likely that over time the amorphous Fe/S solids will convert into pyrite (FeS_2).

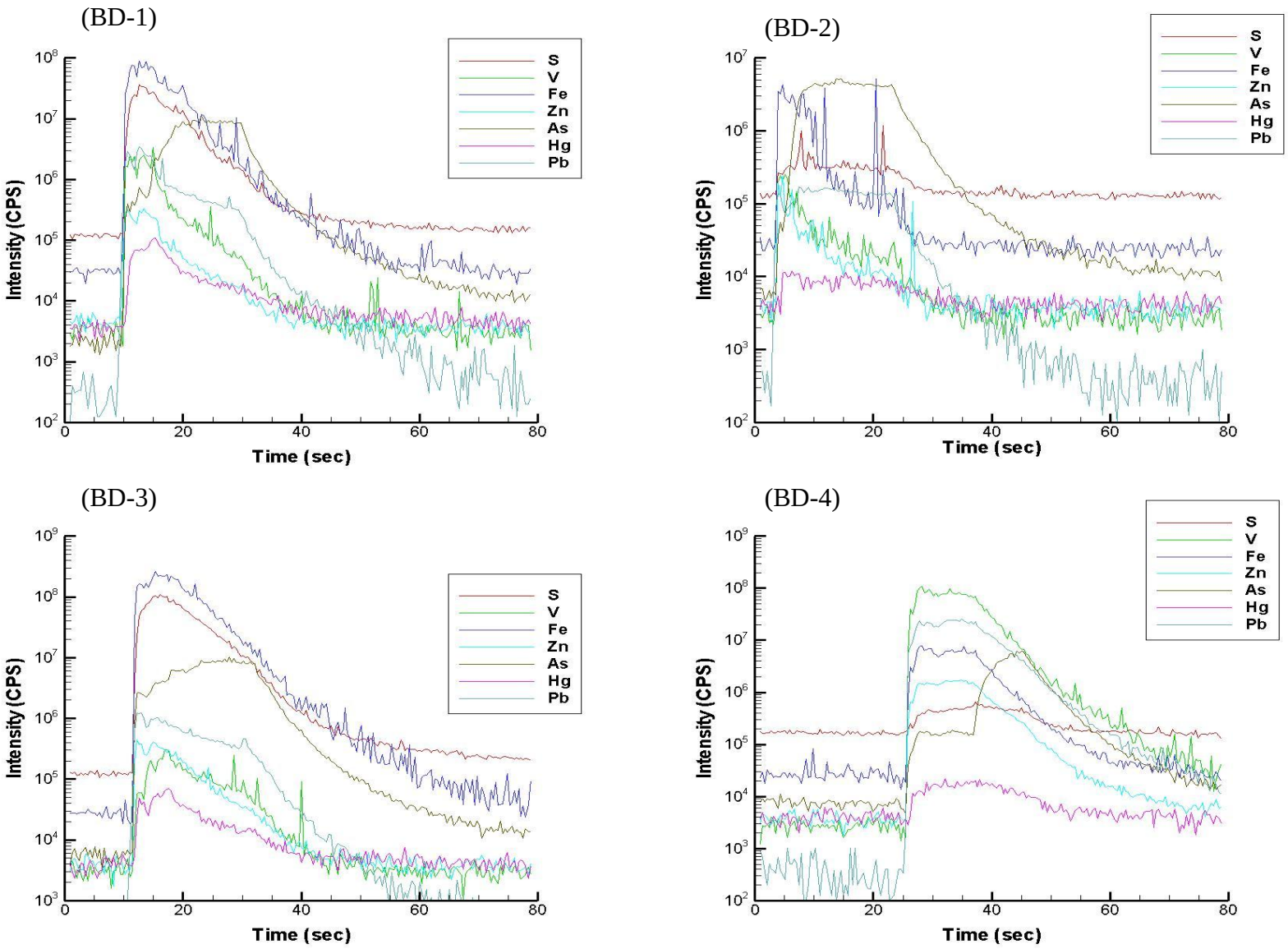

Figure 48. LA-ICP/MS spectrum of pyrites from Bayou Dulac, samples BD-1 through BD-4.

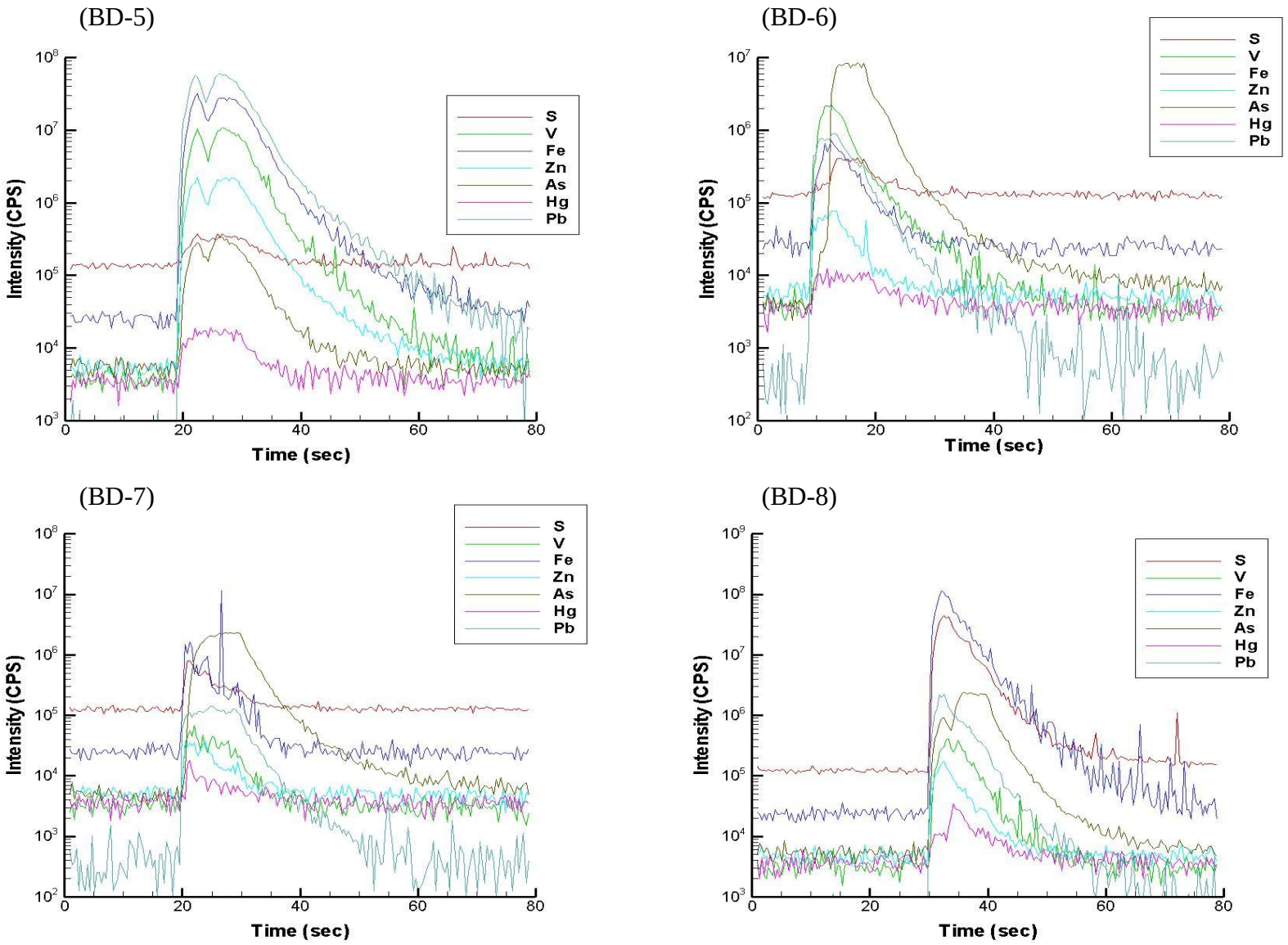

Figure 49. LA-ICP/MS spectrum of pyrites from Bayou Dulac, samples BD-5 through BD-8.

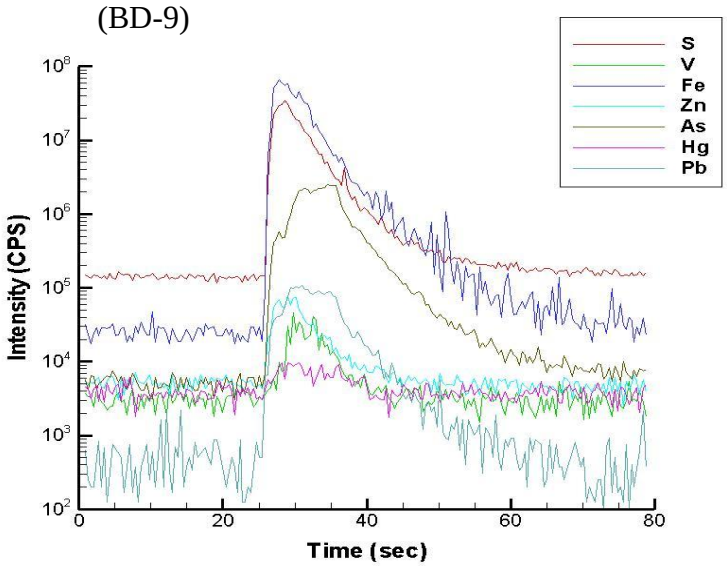

Figure 50. LA-ICP/MS spectrum of pyrites from Bayou Dulac, sample BD-9.

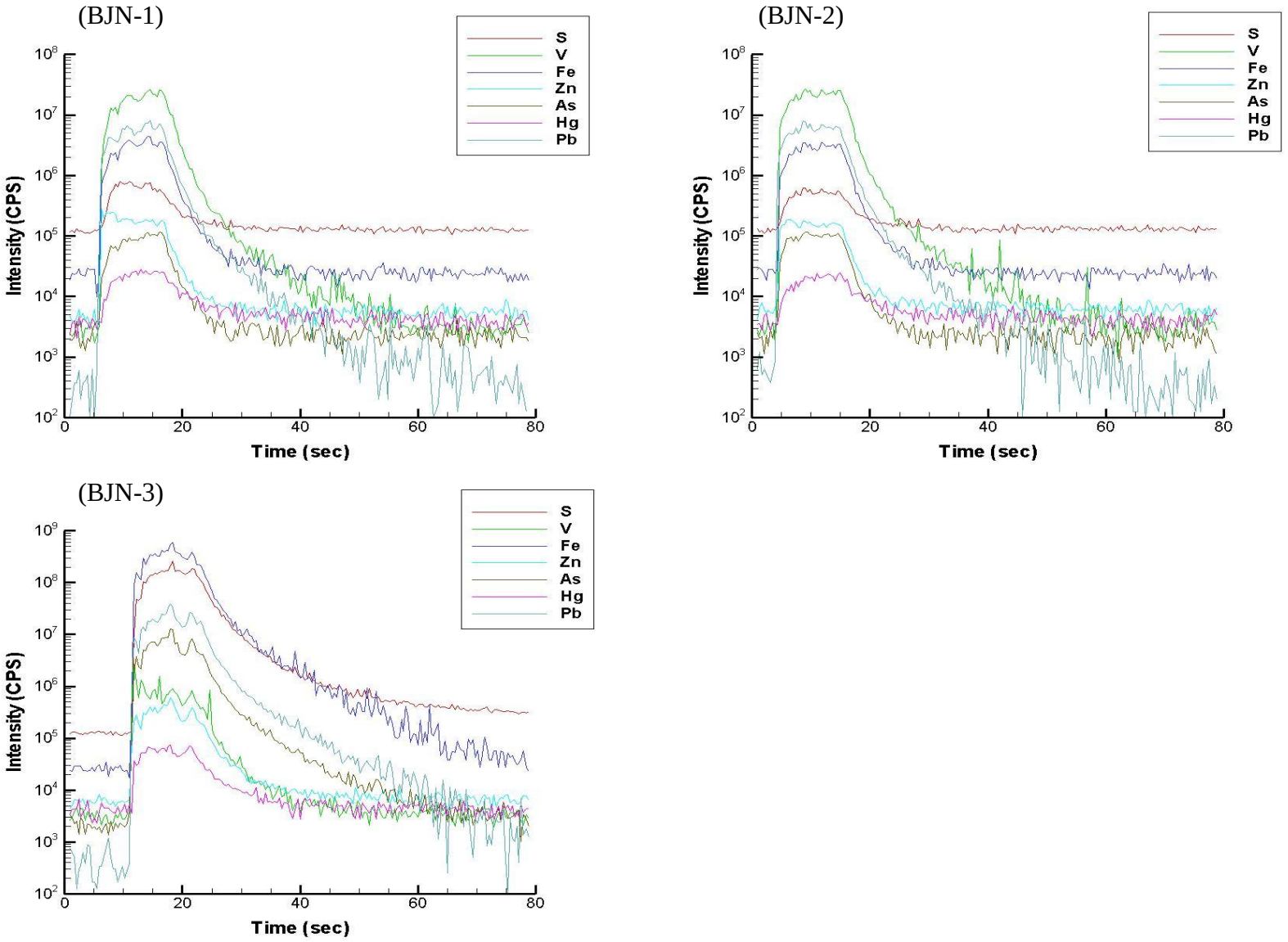

Figure 51. LA-ICP/MS spectrum of pyrites from Bay Jimmy North, samples BJN-1 through BJN-3.

Table 12. Average elemental concentrations measured from LA-ICP/MS analysis of pyrites from BD. Results are normalized to Fe.

Metals	Conc.	BD 1	BD 2	BD 3	BD 4	BD 5
S	**wt. %**	**47.9**	**31.3**	**49.6**	**14.2**	**2.5**
V	mg/kg	208	477	10	134332	5202
Mn	mg/kg	738	4131	1312	14768	13968
Fe	**wt. %**	**51.2**	**54.1**	**50.0**	**62.8**	**91.9**
Co	mg/kg	29	87	209	235	739
Ni	mg/kg	51	0	449	240	1030
Cu	mg/kg	130	1071	38	1191	642
Zn	mg/kg	192	1872	83	18006	7765
As	mg/kg	7591	137509	2238	24137	679
Se	mg/kg	6	7	5	68	27
Mo	mg/kg	16	32	48	1096	274
Cd	mg/kg	3	9	4	394	32
Te125(LR)*	mg/kg	-	-	-	-	-
Hg202(LR)*	mg/kg	-	-	-	-	-
Pb	mg/kg	280	1128	43	36000	26024

* not calculated due to lack of calibration standards

Table 13. Average elemental concentrations measured from LA-ICP/MS analysis of pyrites from BD. Results are normalized to Fe.

Metal	Conc.	BD 6	BD 7	BD 8	BD 9
S	**wt. %**	**43.4**	**40.7**	**50.7**	**52.5**
V	mg/kg	14569	312	39	4
Mn	mg/kg	6824	4718	1216	72
Fe	**wt. %**	**25.6**	**51.6**	**48.9**	**47.3**
Co	mg/kg	74	59	137	27
Ni	mg/kg	0	0	237	0
Cu	mg/kg	1814	1402	230	98
Zn	mg/kg	3859	1127	84	65
As	mg/kg	285240	75952	1295	2033
Se	mg/kg	0	0	3	0
Mo	mg/kg	14	243	44	2
Cd	mg/kg	138	50	6	4
Te125(LR)	mg/kg	-	-	-	-
Hg202(LR)	mg/kg	-	-	-	-
Pb	mg/kg	6367	1063	149	20

Table 14. Average elemental concentrations measured from LA-ICP/MS analysis of pyrites from BJN. Results are normalized to Fe.

Metal	Conc.	BJN 1	BJN 2	BJN 3
S	**wt. %**	**26.2**	**23.8**	**51.0**
V	mg/kg	65984	83702	21
Mn	mg/kg	1901	1994	1068
Fe	**wt. %**	**64.5**	**65.0**	**48.4**
Co	mg/kg	135	130	1484
Ni	mg/kg	0	0	1671
Cu	mg/kg	1558	1390	312
Zn	mg/kg	4543	4211	56
As	mg/kg	1200	1500	652
Se	mg/kg	141	191	18
Mo	mg/kg	748	773	74
Cd	mg/kg	532	497	10
Te125(LR)	mg/kg	-	-	-
Hg202(LR)	mg/kg	-	-	-
Pb	mg/kg	17011	20068	445

Microbial Communities in Affected Wetlands

The most probable number (MPN) technique was utilized to quantify iron- and sulfate-reducing bacteria in samples taken from the top (0-3 cm), middle (12-15 cm), and bottom (27-30 cm) portion of sediment cores from each site. It was anticipated that anaerobic microbial populations would increase with depth in sediments, in response to more reducing conditions. Results show that, at many sites, the bacteria were more abundant in the upper portions of the sediments and that the bacterial populations varied inversely with depth (Appendices 6-7). In Mississippi, BH sediments contain significantly lower amounts of SRB than those at PACB. Perhaps levels of SRB activity increased in PACB in response to small inflow of oil from the Macondo-1 spill. In Louisiana, RG actually contained some of the highest numbers of SRB

(1600 MPN/g in the 0-3 cm section, and >1600 MPN/g in the 12-15 cm and 27-30 cm section) despite containing lower DOC and TOC concentrations than the other Louisiana sites. BD and BB show similarly high numbers in the upper sediments, with decreasing numbers deeper in the sediments. BJN had relatively high numbers in the upper section, but overall averaged only 104.5 MPN/g, despite being heavily contaminated. The majority of sites sampled showed >1600 MPN/g of FeRB, which plays a key role in iron reduction and subsequent formation of iron sulfide.

Sulfate-reducing bacteria were expected to be more active in deeper layers due to more favorable reducing conditions. The SRB MPN results showed an opposite trend: the anaerobic bacterial communities decreased in number with depth. A likely explanation for this is that there is not enough organic carbon to sustain larger communities beneath the sediment surface. Moreover, most of the oil that washed onshore likely settled at the of water-sediment interface and enhanced the microbial activities there. Many sites show high values of SRB through the sampled intervals at depth, supporting active SRB biomineralization processes (i.e., sulfide formation) that retain most trace metals in sediments. The Mississippi PACB site was slightly contaminated with oil and contains higher bacteria populations than BH (which was unaffected), largely due to more organic carbon (electron donors) in the environment. It is not clear why RG contains higher numbers of bacteria than the contaminated sites; a possible reason is that the RG site is more restricted to wave flushing than the Barataria Bay sites, meaning that the Barataria Bay sites would become more oxidized. It is possible that those sites in the more open Barataria Bay could be subjected to other, not yet understood conditions which negatively affect microbial communities.

GC-MS Analysis of Bulk Oil and Petroleum Biomarkers

Organic compounds were extracted from oiled sediments and contaminated plant samples using a modified EPA 3570 method. In addition, initial source crude from the Macondo-1 well acquired from BP was prepared. All extracted samples were diluted with hexane using a 200:1 ratio. Most of the solutions produced from unaffected sites were clear, while samples extracted from oiled sites exhibited yellowish hues or were dark brown to black. GC-MS analysis of these extracted organic compounds was conducted to define the source and the extent of degradation of spilled oil in affected salt marshes.

Samples were first analyzed via CG-MS-TOF. GC-MS full-scan spectra allow the entire range of compounds comprising the hydrocarbon to be shown. Full-scan spectra alone are not very useful for hydrocarbon fingerprinting. Hence, in order to fingerprint the source of oil, the GC-MS was also run in high-sensitivity selected ion mode (SIM) to provide an analysis of specific compounds known as biomarkers. GC-MS-SIM analysis produces fragmentograms that show unique spectra for ions with specific mass-to-charge ratios (m/z) of 191, 217, and 218.

The samples analyzed by GC-MS analysis include: (1) a sample of crude oil from the Macondo-1 well; (2) samples of degraded oil scrapped off plants collected at BJN site; (3) PAHs extracted from surface oiled sediments at BJN; and (4) PAHs extracted from sediments located in the middle (12-15 cm) of the sediment columns at BD sites.

A GC-MS full spectrum of the BP Macondo-1 crude oil is shown in Figure 52. In GC-MS analysis, lighter organic components are vaporized during early stages at lower temperatures and heavier ones are vaporized later at higher temperatures. The GC-MS spectrum clearly shows that the BP crude sample is much more plentiful in lighter components, as indicated by the occurrence of highest peaks in the first 14 minutes. Figure 55 shows a full-scan chromatogram of

BJS oiled sediment, indicating the presence of various hydrocarbons. Though not part of the areas analyzed for this study, BJS is in very close proximity to BJN, and likely resembles what a full-scan would look like for degraded oil in BJN. Heavier components persist (over the 14 – 26 minute range), while lighter compounds are largely absent from the graph. Fragmentograms of degraded oils extracted from a depth of 12 – 15 cm from oiled BJS and BD sites also show a relative lack of light compounds but exhibit multiple high-intensity peaks over the 16-21 minute range for heavy compounds (Figure 56). This pattern indicates that the degraded oils are more enriched in heavier compounds than the initial BP source oils. This large contrast demonstrates that, whereas most light compounds are biodegraded or vaporized quickly (within months), the residues of heavier fractions of oil remain in sediments, and even as the oil seeps deeper into sediments, bacteria are not necessarily degrading the heavier fractions. Oudot and Chaillan (2010) have shown that the heavier saturated components of oil (e.g., asphaltenes, resins, and polycyclic aromatics) can remain in the environment for at least decades after contamination, and this pattern can be seen in the spectra for the degraded oils extracted from marsh plants and sediments at heavily contaminated Louisiana sites. In addition to typical oil degradation (evaporation, dispersion, etc.), it seems likely that microbial communities are preferentially utilizing the lighter carbon compounds as their carbon source, leading to a residual oil, rich in heavy components.

Petroleum biomarkers with specific mass-to-charge (m/z) ratios (i.e. m/z 191, 217, 218, etc.) are made up of terpanes (m/z 191) and steranes (m/z 271, 218) from a particular source and reservoir. These specific biomarkers are resistent to biodegradation and environment alteration compared to most organic compounds, thus providing a reliable way to correlate the spilled oils with their initial sources. Biomarkers of the hydrocarbon have also been analyzed by GC-MS-

SIM in an attempt to correlate the degraded oils from marsh sediments and plants to the Macondo-1 well oil. Steranes and terpanes are great biomarkers to use because they tend to remain unchanged through various degradation processes; they are often used in oil-oil and oil-source correlations (Barakat et al., 2002). Ratios of different compounds analyzed in the m/z 191 peaks of oil from sediments and plants (Table 15) match well with ratios found in the initial crude oil sample from the BP well, despite differences in the fragmentograms from the oil found in the sediments and plants is quite different from the BP sample. Ts/Tm (18α-22,29,30-trisnorneohopane/17α-22,29,30-trisnorhopane) ratios, which are routinely used in oil-spill forensics due to their general lack of degradation, show a narrow window of ratios among the various samples analyzed (0.900-1.078), suggesting a common origin for them all. Tricyclic terpanes are also very good fingerprinting compounds; 24Tri/23Tri (C24 tricyclic terpane/C23 tricyclic terpane) ratios also show a very narrow range (0.909-1.040) among the various contaminated sample sites and Macondo-1 source crude. C29/C30 (17α,21β(H)-30-norhopane/17α, 21β(H)-hopane) ratios among plant and surface sediment samples and the BP crude sample fall within a narrow range (0.531-0.592). However, sediments collected from the middle of the sediment columns in Bayou Dulac have slightly different signatures (0.691). Ratios of 29D/29H (18α(H)-30-norneohopane/17α,21β(H)-30-norhopane) in the Bay Jimmy North and BP samples are very similar (0.557 and 0.564, respectively).

In summary, the results suggest that microbes are degrading the lighter compounds, as evidenced in the weathering patterns of the full GC-MS spectrum and fragmentograms from the various oiled sediments and degraded oil samples. Biomarkers, due to their resistance to biodegradation over long periods of time in the environment, show an affinity between BP crude oil and the oils from contaminated sediments and plants. Our GC-MS spectrum confirms that

heavier components are not degraded (microbially or otherwise) or vaporized, as evidenced by the enrichment of heavier compounds in the fragmentograms.

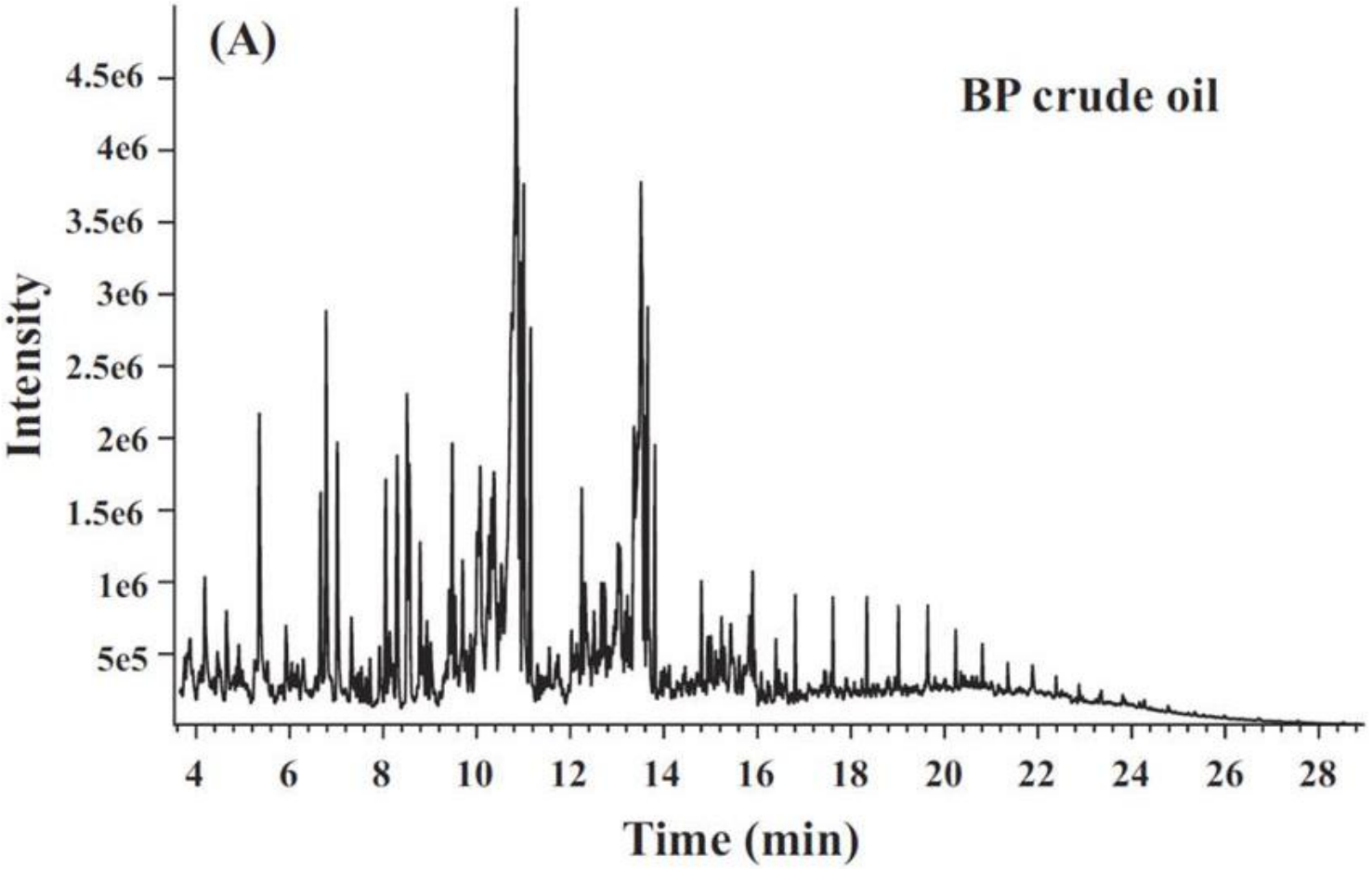

Figure 52. Gas chromatogram of BP Macondo-1 crude oil showing much higher quantities of lighter compounds (up to the 14 minute mark) than heavier ones (later times).

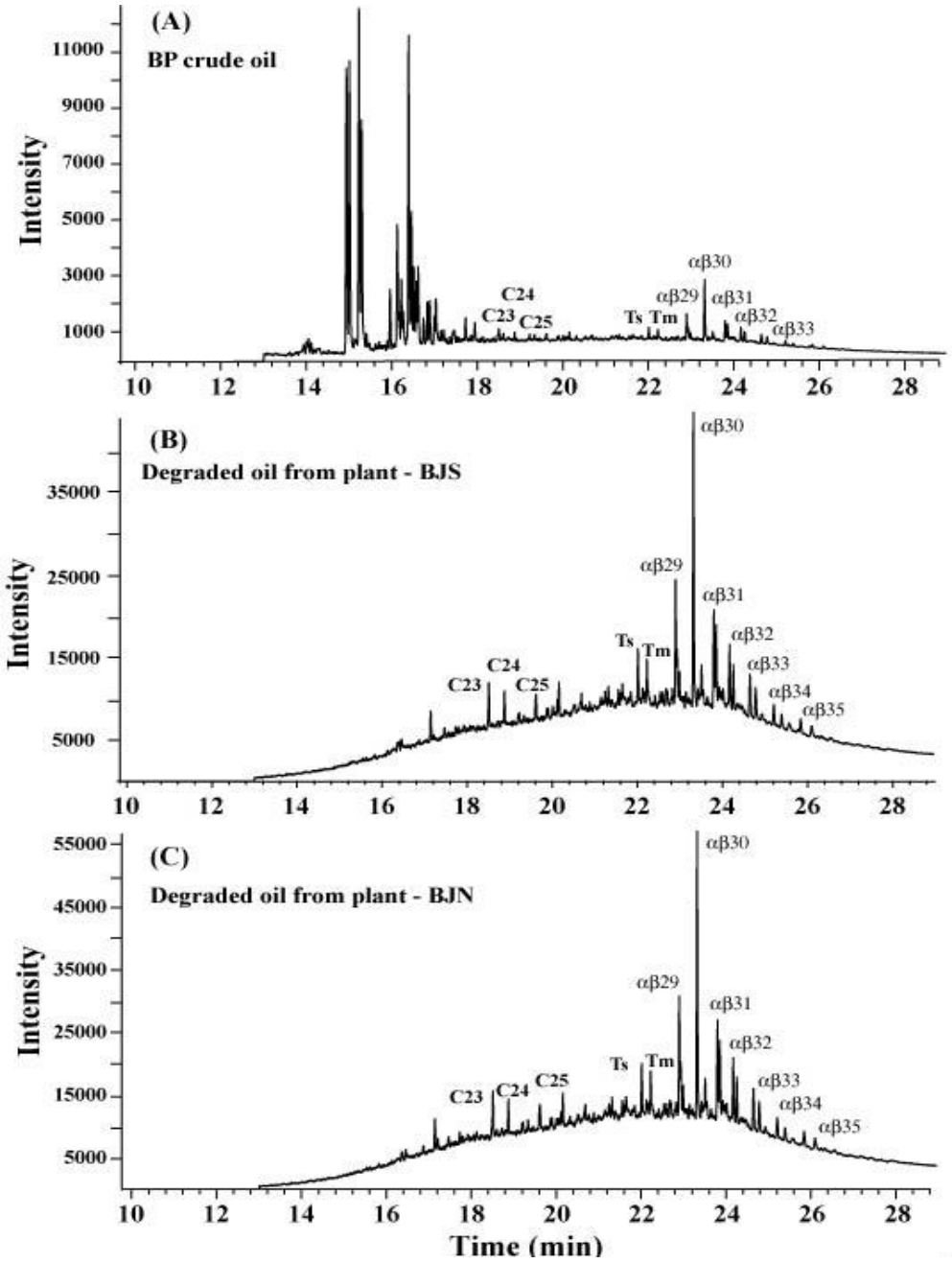

Figure 53. Fragmentograms produced by GC/MS-SIM analysis showing the enrichment of heavier carbon components in (A) BP crude oil from the Macondo-1 well, (B) degraded oil from plants in Bay Jimmy South, and (C) degraded oil from plants in Bay Jimmy North.

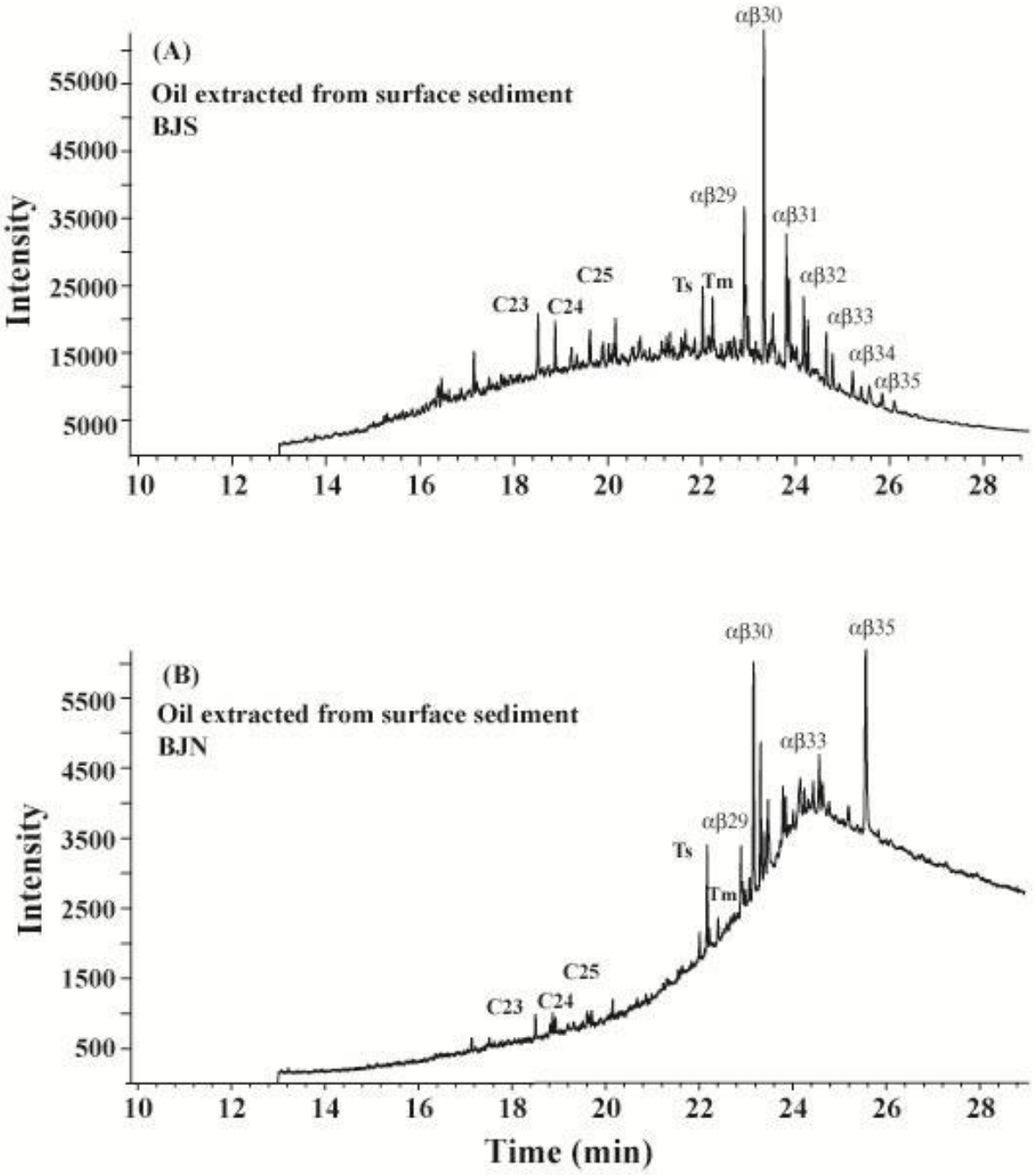

Figure 54. Fragmentograms produced by GC/MS-SIM analysis showing the enrichment of heavier carbon components in (A) oil from surficial sediment samples in Bay Jimmy South, and (B) oil from surficial sediment samples in Bay Jimmy North.

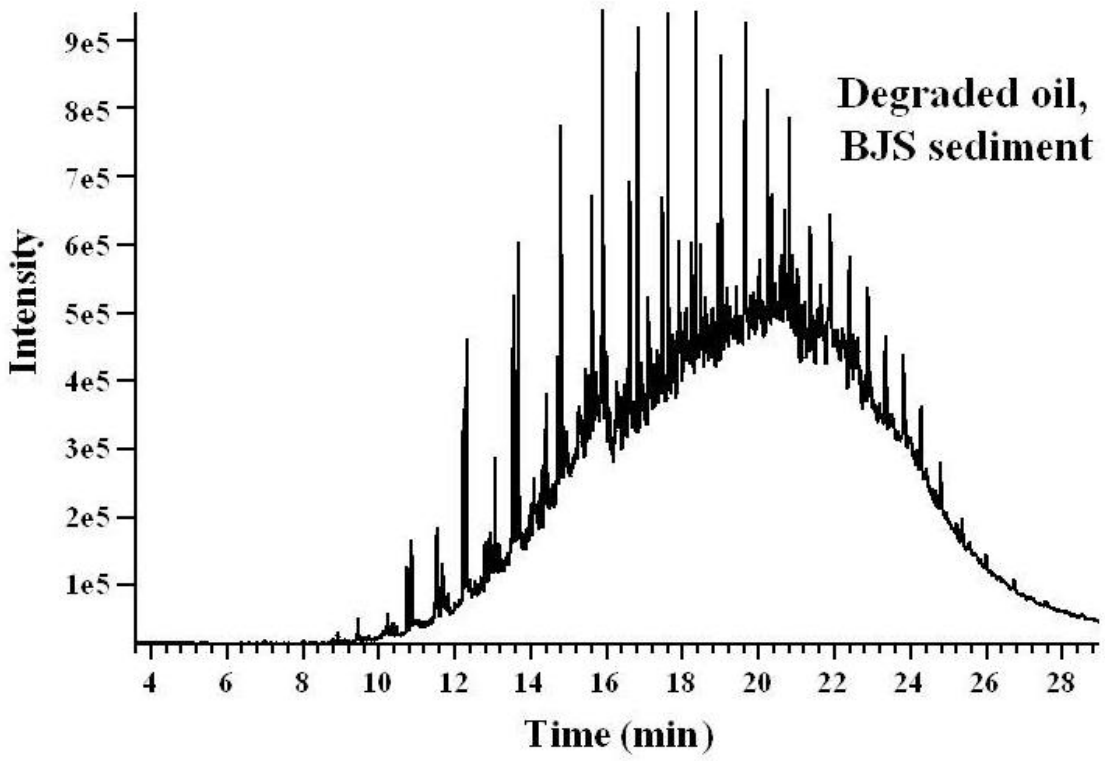

Figure 55. Gas chromatogram of oiled BJS sediment (0-3 cm) showing much higher quantities of heavier components, implying that microbes are preferentially utilizing the lighter components of oil as a carbon source.

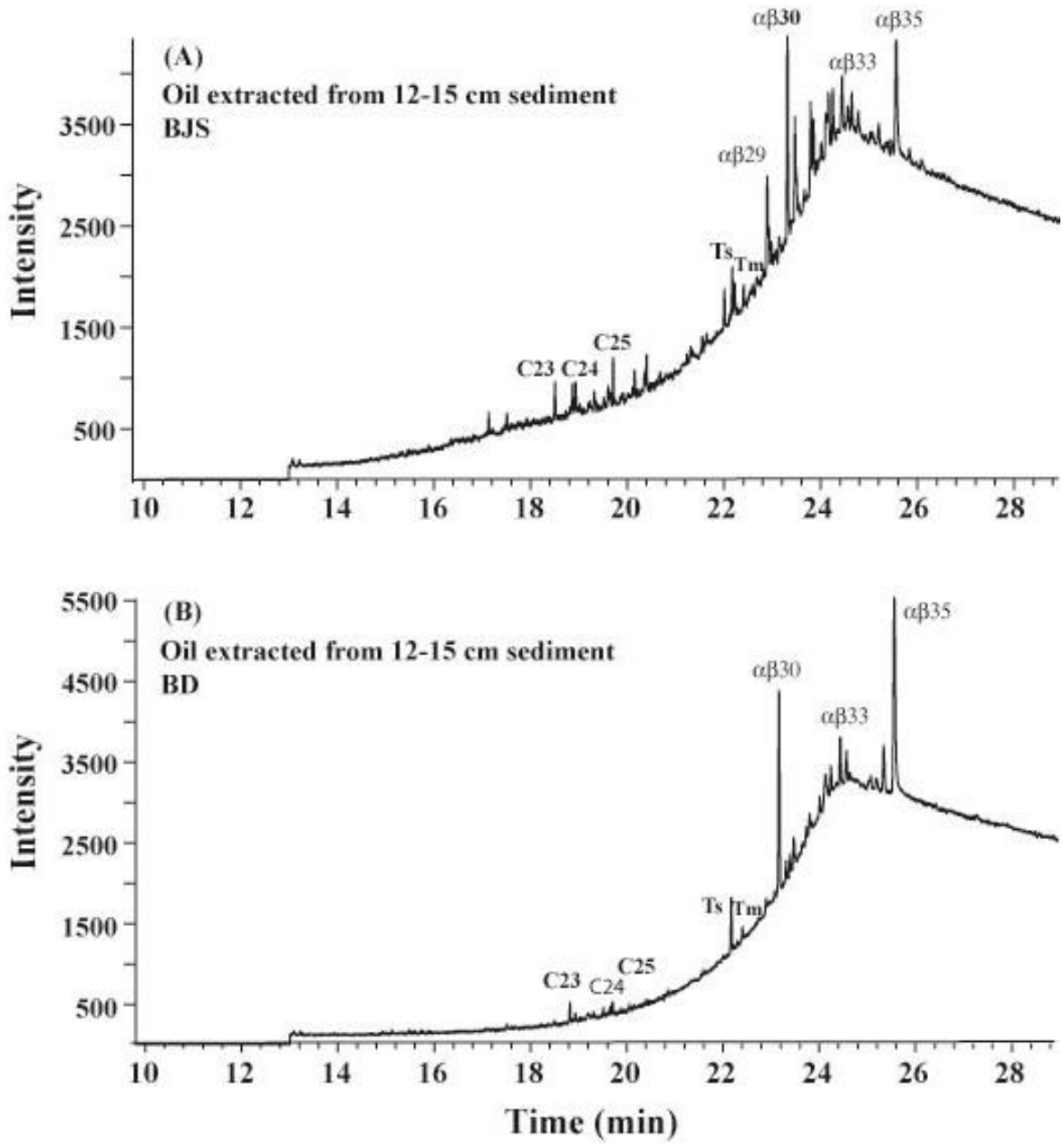

Figure 56. Fragmentograms produced by GC/MS-SIM analysis showing the enrichment of heavier carbon components in (A) oil from 12-15 cm deep sediment samples in Bay Jimmy South, and (B) oil from 12-15 cm sediment sample in Bay Jimmy North.

Table 15. Calculated ratios of selected biomarkers associated with BP crude oil and various oil samples extracted from marsh sediments and plants.

Oil samples	Ts/Tm[1]	24Tri/23Tri[2]	C29/C30[3]	29D/29H[4]
BP crude oil	1.070	0.914	0.586	0.564
Weathered oil/BJS	1.078	0.909	0.537	0.564
Weathered oil/BJN	1.057	0.912	0.531	0.557
Surface sediment/BJS	1.074	0.940	0.587	0.559
Surface sediment/BJN	0.965	1.001	0.592	-
Sediment (15 cm)/BJS	0.900	1.040	0.771	-
Sediment (15 cm)/BD	0.962	0.960	0.691	-

[1]Ts/Tm = 18α-22,29,30-trisnorneohopane/17α-22,29,30-trisnorhopane
[2]24Tri/23Tri = C24 tricyclic terpane/C23 tricyclic terpane
[3]C29/C30 = 17α,21β(H)-30-norhopane/17α,21β(H)-hopane
[4]29D/29H = 18α(H)-30-norneohopane/17α,21β(H)-30-norhopane

Carbon Isotopic Compositions

The stable carbon-isotopic compositions of wetland sediments are determined primarily by the type of vegetation growing in the area. These isotopic values can be skewed when oil is introduced into the environment. For example, crude oil may have much different carbon isotopic signatures (more negative) than the vegetation, resulting in a substantial shift in $^{13}C/^{12}C$ ratios of bulk sediments. Carbon isotopic signatures of plants reflect the preferential use of ^{12}C during photosynthesis (Park and Epstein, 1961). The $^{12}C/^{13}C$ ratios vary among various types of plants, because different plants have separate pathways for carbon fixation (O'Leary, 1988). Fossil fuels, such as petroleum formed from the bacterial oxidation of organic compounds are typically depleted in ^{13}C (< -15‰, PDB) relative to an inorganic carbon source such as marine carbonate rocks (≈ 0 ‰).

Carbon isotopic analyses were performed on initial crude oil collected from the Macondo-1 well, sediment cores from different depths, and plants collected from each marsh site. Crude oils originating from the Gulf of Mexico region typically have $\delta^{13}C$ values ranging from -26.6 to -33.0‰ (Stahl, 1977; Macko and Parker, 1983). The initial BP crude oil from the Macondo-1 well falls precisely within this range with an average $\delta^{13}C$ value of -27.0‰. Isotopic analysis of the oil scraped off of plant samples (i.e. weathered oil) at BJN site yielded a very similar $\delta^{13}C$ value of -26.7 ‰. This result indicates that the isotopic signatures are conservative and not affected by oil degradation, an observation made previously in *Spartina* plants in a study by Benner et al. (1987). Thus, stable carbon isotopic analysis can provide a reliable way to trace the spilled oil in coastal marshes. Marsh plants and their residues constitute the main sources of organic matter in marsh sediments. As long as the marsh plants carry a $\delta^{13}C$ signature distinguishable from spilled oil, contaminated sediments will exhibit large variation in $\delta^{13}C$ values compared to those of plants. $\delta^{13}C$ values of plants and sediments at all sites are listed in Appendix 5. Both C_3-type *Juncus* and C_4-type *Spartina* plants are found at BH sites. Only *Spartina* plants are found at PACB site. Three Louisiana marsh sites (RG, BD, and BB) are dominated by the C_4 plant *Spartina sp.*, which has $\delta^{13}C$ values ranging from -14.4 to -17.7‰ (Chmura et al., 1987), higher than those of BP crude oil. The BJN site contains both *Juncus* (-27.1‰) and *Spartina* (-14.7‰), although likely *Juncus* comparatively minor.

Carbon isotopic compositions of BP oil, marsh sediments, and marsh plants were plotted on a histogram (Figure 57) and a box plot (Figure 58). At the Mississippi sites, BH sediments are more depleted in ^{13}C (mean $\delta^{13}C$ = -24.5‰) than PACB sediments (mean $\delta^{13}C$ = -21.7‰). This may be related to the type of plants at these sites, as PACB is dominated solely by *Spartina* with an average $\delta^{13}C$ value of -14.1‰. In contrast, BH contains both *Spartina* ($\delta^{13}C$ value of -14.2‰)

and *Juncus* plants with much lower $\delta^{13}C$ value of -25.2‰. $\delta^{13}C$ values of sediments are significantly lower than those of the dominant marsh plants at the PACB site, indicating some degree of contamination from isotopically light oil. At the Louisiana sites, RG held an average $\delta^{13}C$ signature of -21.5‰. At the three Barataria sites, BD, BB, and BJN, average $\delta^{13}C$ values for sediments are -19.6‰, -18.9‰, and -18.3‰, respectively, significantly lower than those of their C_4-dominated vegetation (-14.8±0.6 ‰). This reflects the influence of isotopically light crude oil. As expected, contaminated sediments show strong depletion in ^{13}C due to the incursion of oil. In summary, stable carbon isotopic signatures can serve as a conservative tracer to investigate the source of spilled oil in coastal marshes, provided that the marsh site is dominated by C_4 plants and organic matter with distinctly different $\delta^{13}C$ values than those of spilled oils.

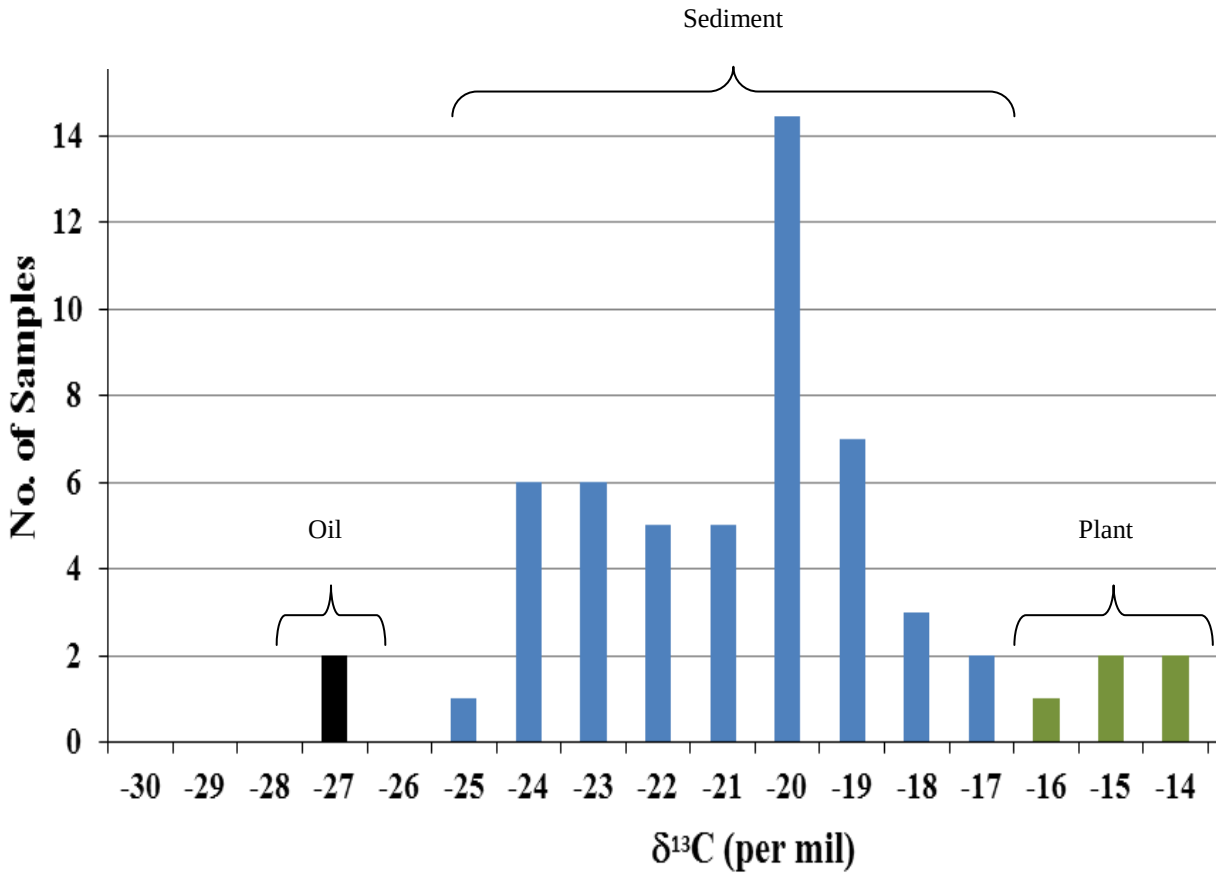

Figure 57. Histogram showing variations between the three types of material subjected to carbon isotopic analysis (plants, sediments, oil). The histogram shows an influence of oil on the sediments, as the wetland sediments are more depleted in ^{13}C than the plants.

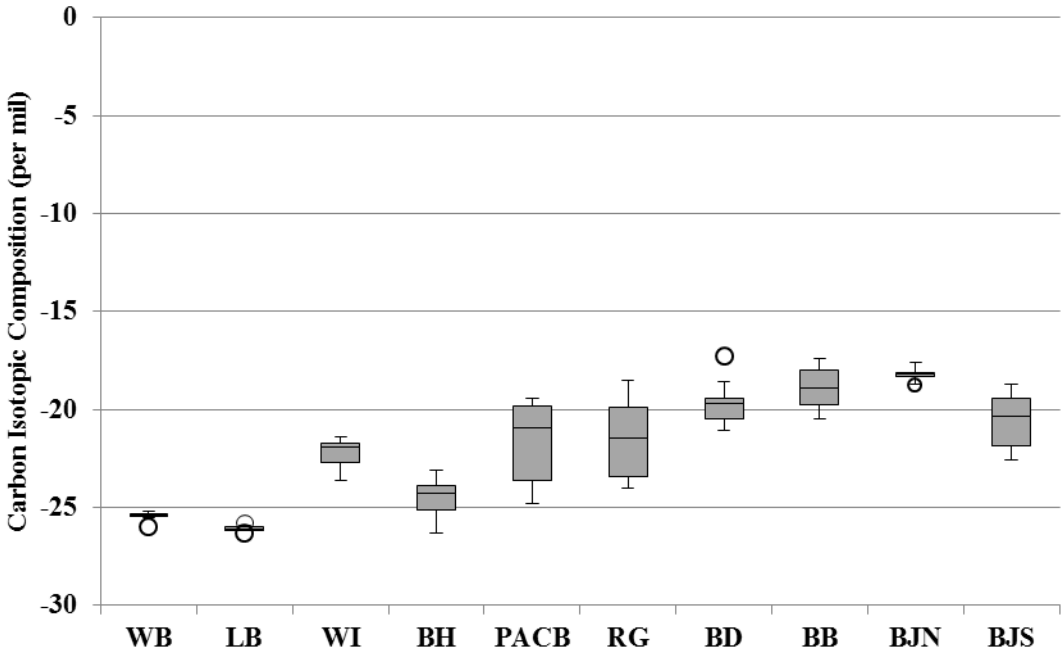

Figure 58. Box plot showing the range of $\delta^{13}C$ signatures within and among sites.

CONCLUSIONS

The 2010 Gulf oil spill had significant impacts on affected Mississippi and Louisiana coastal wetland sites (PACB, BD, BB, BJN). Comparison with non-contaminated or less-affected sites (BH, RG), provides a picture of the impact the oil spill has had within the first 6 to 9 months after the Deepwater Horizon explosion. Results indicate that the sediment and pore-water geochemistry in these contaminated estuarine settings have been greatly affected. Total digestion analysis of wetland sediments shows higher concentrations of certain trace metals/metalloids (e.g., Ni, Cu, Pb, Zn, Co, V, Ba, Hg, As) in heavily-oiled Louisiana wetlands compared to less-affected and pristine sites in Mississippi. In addition, average normalized enrichment factor calculations indicate that metals are enriched beyond terrestrial levels, supporting a marine/oil source for metal contamination. Levels of certain metals/metalloids (e.g., arsenic) in sediments correlate well with ($r = 0.47$) the abundance of clay size particles, confirming that the fine-grained sediments in salt marshes have high capacity to adsorb metals derived from terrestrial or marine sources. Higher metal concentrations in oiled sediments also can be positively correlated to higher TOC contents, indicating that organic carbon and metal contaminants are likely derived from the same source. At heavily-oiled Louisiana sites (e.g., BD, BB, BJN), elevated levels of metals and total organic carbon (TOC) have been found in sediments down to depths of 30 cm. Contamination is not limited to shallow sediments; oil and various associated metals have invaded into deeper (pre-industrial) portions of the marsh sediments.

Porewaters extracted from contaminated Louisiana sediments are characterized by very high levels of DOC (up to hundreds of mg/kg) and reduced sulfur concentrations (up to 80 mg/kg). In general, pristine sites exhibit much lower concentrations in DOC (generally < 30 mg/kg) and reduced sulfur contents (< 1 mg/kg). The influx of oil into the wetlands may have provided the initial substrate and carbon source for stimulating sulfate-reducing bacteria. Moreover, pore-water pH values show a general increasing trend (ranging from 6.6 to 8.0) with depth, possibly reflecting the combined effects of bacterial sulfate reduction and saltwater intrusion at depth. Despite high levels of trace metals in bulk sediments, concentrations of trace metals dissolved in porewaters are generally low. This result is unexpected, as inflow of oil and bacterial reduction of metal-sorbed sediments would typically lead to higher dissolved metal concentrations in contaminated water. Geochemical analyses indicate that most metals are sequestered in sulfides and other solids in sediments via adsorption or co-precipitation processes. SEM analysis identified pyrite-like sulfides with distinct framboidal form in oiled sediments. EDAX analysis further confirmed the presence of Fe and S as the main constituents in these framboids. LA-ICP-MS analyses show that sulfide framboids contain various levels of trace metals. Some analyzed pyrite grain show high concentrations of Mn, Pb, Zn, and As (average concentrations > 1,000 mg/kg) and minor amounts of Ni, Co, V, Hg, Se, and Cd. Sulfide solids likely serve as local sinks for chalcophile ("sulfur-loving") trace metals under sulfate-reducing conditions. Increased bacterial populations were found primarily in oiled wetlands (PACB, BD, BB, and BJN) and have likely greatly affected the fate and transformation of metals within these environments. Abundance of SRB and elevated sulfide concentrations in porewaters extracted from heavily oiled Louisiana sites suggest that microbial sulfate reduction may be enhanced by the influx of oil and organic matter. It appears that high organic matter content and bacterially-

mediated sulfate reduction facilitate metal retention via sulfide formation in the oiled marsh sediments.

GC-MS full-scan analysis shows significant degradation of lighter compounds while heavier oils persist in sediments. This result suggests that natural microbes have initially utilized oil as a metabolic carbon source; microbes appear to preferentially break the lighter compounds of the oil to gain energy. This implies that the impacted wetlands likely will become enriched in heavier components of the oil, which can remain in environments up to decades after an oil spill (Oudot and Chaillain, 2010). High sensitivity GC-MS-SIM biomarker analysis clearly correlates M-252 crude oil to organic compounds extracted from marsh sediments down to 15 cm. The extraction protocol and biomarker correlation can be potentially applied to monitor long-term transformation of persistent oil compounds in heavily contaminated wetlands. Carbon isotopic measurements show that the spilled BP oil has a unique $\delta^{13}C$ signature that is significantly different from those of the C4 plants that dominate Louisiana salt marshes (*Spartina sp.*). The Barataria sites (BD, BB, and BJN) appear to have received the most severe contamination based on $\delta^{13}C$ signatures that are significantly more depleted than those of local living plant mass or decomposed plant parts. Such a large carbon isotopic difference between the marsh vegetation and the oil provides an excellent opportunity to examine the source and movement of spilled oils in coastal marshes.

Recent studies have shown that isolated giant plumes of the spilled BP spilled oil still exist under the Gulf of Mexico (New York Times, 2012), and it is probable that these oil plumes will continue to wash into these coastal wetlands over time with the aid of storm surge and hurricane activities. This study shows that microbial degradation of oil and formation of framboidal sulfides serve to reduce the levels of oil and immobilize trace metals in coastal

wetlands. A chief concern is that, in Fe-limited salt-marsh environments, formation of iron sulfides may not keep pace with oil-related metal contamination. Moreover, re-oxidation in tidally-influenced marshes has the potential to oxidize and subsequently disaggregate the sulfides, thereby releasing sorbed metals from the sulfides and into the water column.

REFERENCES

Acha', D., and Hintelmann, H., 2011, Importance of sulfate reducing bacteria in mercury methylation and demethylationin periphyton from Boloivian Amazon region: Chemosphere, v. 82, p. 911-916.

Ball, J. S., Wegner, W. J., Hyden, H. J., Horr, C. A., and Myers, A. T., 1960, Metal content of twenty-four petroleums: Journal of Chemical Engineering, v. 5, p. 553-557.

Barakat, A. O., Mostafa, A. R., Qian, Y., and Kennicutt II, M. C., 2002, Application of petroleum hydrocarbon chemical fingerprinting in oil spill inevestigations – Gulf of Suez, Egypt: Spill Science & Technology Bulletin, v. 7, p. 229-239.

Barwise, A. J. G., 1990, Role of nickel and vanadium in petroleum classification: Energy and Fuels, v. 4, p. 647-652.

Beauchemin, S. and Kwong, Y. T. J., 2006, Impact of redox conditions on arsenic mobilization from tailings in a wetland with neutral drainage: Environmental Science & Technology, v. 40, p. 6297-6303.

Benner, R., Fogel, M. L., Sprague, E. K., and Hodson, R. E., 1987, Depletion of ^{13}C in lignin and its implications for stable carbon isotope studies: Nature, v. 329, p. 708-710.

Berner, R. A., 1969, The synthesis of framboidal pyrite: Economic Geology, v. 64, p. 383-384.

Berner, R. A., 1970, Sedimentary pyrite formation: American Journal of Science, v. 268, p. l-23.

Berner, R. A., 1983, Sedimentary pyrite formation: An update: Geochemica et Cosmochimica, v. 48, p. 605-615.

Bianchi, T. S., Wysocki, L. A., Schreiner, K. M., Filley, T. R., Corbett, D. R., and Kolker, A. S., 2010, Sources of terrestrial organic carbon in the Mississippi plume region: Evidence for the importance of coastal marsh inputs: Aquatic Geochemistry, v. 17, p. 431-456.

Bicker, A. R., 1969, Geologic map of Mississippi: U.S. Geological Survey, scale 1:500,000.

Bose, P. and Sharma, A., 2002, Role of iron in controlling speciation and mobilization of arsenic in subsurface environment: Water Research, v. 36, p. 4916-4926.

Burnol, A. and Charlet, L., 2010, Fe(II)-Fe(III)-bearing phases as a mineralogical control on the heterogeneity of arsenic in Southeast Asian groundwater: Environmental Science & Technology, v. 44, p. 7541-7547.

Brown, T. L., LeMay Jr., H. E., and Bursten, B. E., 2006, Chemistry: The Central Science, 10th ed., Pearson Education, Inc., Upper Saddle River, NJ, 1128 pp.

Canfield, D. E., Raiswell, R., and Bottrell, S., 1992, The reactivity of sedimentary iron minerals toward sulfide: American Journal of Science, v. 292, p. 659-683.

Champine, J. E., Goodwin, S., 1991, Acetate catabolism in the dissimilatory iron-reducing isolate GS-15: Journal of Bacteriology, v. 173, p. 2704-2706.

Chapelle, F., 1993, Groundwater Microbiology and Geochemistry: John Wiley and Sons, Inc. New York, NY, p. 48-274.

Chmura, G., Socki, R., and Abernethy, R., 1987, An inventory of ^{13}C abundances in coastal wetlands of Louisiana, USA: Vegetation and sediments: Oecologia, v. 74, p. 264-271.

Ciccioli, P.W., Cooper, T., Hammer, P.M., and Hayes, J.M., 1980, Organic solute-mineral surface interaction: A new method for the determination of groundwater velocities: Water Resources, v. 16, p. 217-223.

Cleveland, C.J., Hogan, C.M., and Saundry, P., 2010, Deepwater Horizon oil spill, Encyclopedia of the Earth, http://www.eoearth.org/article/Deepwater_Horizon_oil_spill (accessed August 2011).

Compeau, G., and Bartha, R., 1984, Methylation and demethylation of mercury under controlled redox, pH, and salinity conditions: Applied Environmental Microbiology, v. 48, p. 1203-1207.

Corbett, D. R., McKee, B., and Duncan, D., 2004, An evaluation of mobile mud dynamics in the Mississippi River deltaic region: Marine Geology, v. 209, p. 91-112.

Crone, T. J., and Tolstoy, M., 2010, Magnitude of the 2010 Gulf of Mexico oil leak: Science, v. 330, p. 634.

Davaranche, M., Grybos, M., Gruau, G., Pedrot, M., Dia, A., and Marsac, R., 2011, Rare earth elements: A tool for identifying trace metal sources during wetland soil reduction: Chemical Geology, v. 284, p. 127-137.

DeLaune, R. D., A. Jugsujinda, Devai, I., and Patrick Jr., W.H., 2004, Relationship of sediment redox conditions to methylmercury in surface sediment of Louisiana Lakes: Journal of Environmental Science and Health, v. 39, p. 1925-1935.

Donald, R., and Southam, G., 1999, Low temperature anaerobic bacterial diagenesis of ferrous monosulfide to pyrite: Geochimica et Cosmochimica Acta, v. 63, p. 2019-2023.

Drever, J. I., 1997, The Geochemistry of Natural Water, 3rd ed., Prentice Hall, Upper Saddle River, NJ, 436 pp.

Dzombak, D. A., and Luthy, R. G., 1984, Estimating adsorption of polycyclic aromatic hydrocarbons on soils: Soil Science, v. 137, p. 5-12.

Fitzgerald, D. M., Kulp, M., Penland, S., Flocks, J., and Kindinger, J., 2004, Morphologic and stratigraphic evolution of muddy ebb-tidal deltas along a subsiding coast: Barataria Bay, Mississippi River delta: Sedimentology, v. 51, p. 1157-1178.

Flocks, J., Kindinger, J., Marot, M., and Holmes, C., 2009, Sediment characterization and dynamics in Lake Pontchartrain, Louisiana: Journal of Coastal Research, v. 54, p. 113-126.

Folk, R. L., 2005, Nannobacteria and the formation of framboidal pyrite; Textual evidence: Journal of Earth Systems Science, v. 114, p. 369-374.

Freeze, R. A., and Cherry, J. A., 1978, Groundwater: Prentice-Hall, Englewood Cliffs, NJ, 604 pp.

Gaboardi, M., and Humayun, M., 2009, Elemental fractionation during LA-ICP-MS analysis of silicate glasses: Implications for matrix-independent standardization, Journal of Analytical Atomic Spectrometry, v. 24, p. 1188-1197.

Guo, T. Z., DeLaune, R. D., and Patrick Jr., W. H., 1997, The influence of sediment redox chemistry on chemically active forms of arsenic, cadmium, chromium, and zinc in estuarine sediment: Environment International, v. 23, p. 305-316.

Greene Jr., D. L., Rodriguez, A. B., and Anderson, J. B., 2007, Seaward-branching coastal-plain and Piedmont incised-valley systems through multiple sea-level cycles; Late Quaternary examples from Mobile Bay and Mississippi Sound, U.S.A.: Journal of Sedimentary Research, v. 77, p. 139-158.

Hammerschmidt, C. R. and Fitzgerald, W. F., 2004, Geochemical controls on the production and distribution of methylmercury in near-shore marine sediments: Environmental Science & Technology, v. 38, p. 1487-1495.

Horowitz, A. J., and Elrick, K. A., 1987, The relation of stream sediment surface area, grain size and composition to trace element chemistry: Applied Geochemistry, v. 2, p. 437-451.

Huerta-Diaz, M., and Morse, J., 1992, Pyritization of trace metals in anoxic marine sediments: Geochimica et Cosmochimica Acta, v.56, p. 2681-2702.

Islam, F., Gault, A., Boothman, C., Polya, D., Charnock, J, Chatterjee, D., and Lloyd, J, 2004. Role of metal-reducing bacteria in arsenic release from Bengal delta sediments: Nature, v. 430, p. 68-71.

Karchmer, J. H., and Gunn, E. L., 1952, Determination of trace metals in petroleum fractions: Analytical Geochemistry, v. 24, p. 1733-1741.

Kennicut II, M. C., McDonald, T. J., Comet P. A., and Brooks, J. M., 1991, The origins of petroleum in the northern Gulf of Mexico: Geochimica et Cosmochimica Acta, v.56, p. 1259-1280.

Keimowitz, A. R, Simpson, H. J., Stute, M., Datta, S., Chillrud, S. N., Ross, J., and Tsang, M., 2005, Naturally occurring arsenic: Mobilization at a landfill in Maine and implications for remediation: Applied Geochemistry, v. 20, p. 1985-2002.

Keimowitz, A., Lee, M., and Saunders, J., 2010, Assessing the effects of the Gulf oil spill on mobility of toxic metals and microbial activities in Alabama Coastal Wetlands: NSF Rapid Grant Narrative.

Kujawinski, E. B., Kido Soule M. C., Valentine, D. L., Boysen, A. K., Longnecker, K., and Redmond, M. C., 2011, Fate of dispersants associated with the Deepwater Horizon oil Spill: Environmental Science and Technology, v. 45, p. 1298-1306.

Lee, M.-K., Saunders, J., and Wilkin, R., 2005, Geochemical modeling of arsenic speciation and mobilization: Implications for bioremediation: Advances in Arsenic Research, v. 915, p. 398-413.

Lee, M.-K., Griffin, J., Saunders, J. A., Wang, Y., and Jean, J., 2007, Reactive transport of trace elements and isotopes in Alabama coastal plain aquifers: Journal of Geophysical Research, v. 112, G02026.

Lee, M.-K., 2011, Quarterly Interim Report of MESC BPGRI Grant : Assessing the Effects of Oil/Dispersant on Mobility and Biotransformation of Toxic Metals in Gulf Coastal Wetlands: Department of Geology and Geography, Auburn University.

Liermann, L. J., Hausrath, E. M., Anbar, E. D., Brantley, S. L., 2007, Assimilatory and dissimilatory processes of microorganisms affecting metals in the environment: Journal of Analytical Atomic Spectrometry, v. 22, p. 867-877.

Lloyd, J. R., and Mabbett, A. N., 2011, Metal reduction by sulfate –reducing bacteria: Physiological diversity and metal specificity: Hydrometallurgy, v. 59, p. 327-337.

Lonergan, D. J., Jenter, H. L., Coates, J. D., Phillips, E. J. P., Schmidt, T. M., and Lovley, D.R., 1996, Phylogenetic analysis of dissimilatory Fe (III)-reducing bacteria: Journal of Bacteriology, v. 178, p. 2402- 2408.

Lovley, D. R., and Chapelle, F. H., 1995, Deep subsurface microbial processes: Reviews of Geophysics, v. 33, p. 365-381.

Macko, S., and Parker, P., 1983, Stable nitrogen and carbon isotope ratios of beach tars on south Texas barrier island: Marine Environmental Resources, v.10, p. 93-103.

Madigan, M., Martinko, J., and Parker, J., 1997, Brock Biology of Microorganisms: Eighth Ed. Prentice Hall, Upper Saddle River, NJ, 986 pp.

Mason, R. P., Abbott, M. L., Bodaly, R. A., Bullock Jr., O. R., Dricoll, C. T., Evers, D., Lindberg, S. E., Murray, M., and Swain, E. B., 2005, Monitoring the response to changing mercury deposition: Environmental Science and Technology, v. 39, p. 14-22.

Merritt, K. A. and Amirbahman, A., 2009, Mercury methylation dynamics in estuarine and coastal marine environments — A critical review: Earth Science Reviews, v. 96, p. 54-66.

Monrreal, R. H., 2007, Hydrology and Water Chemistry in Weeks Bay, Alabama: Implications of Mercury Bioaccumalation [M.S. Thesis]: Auburn University, 65 pp.

Morrison, R. and Murphy, B., 2006, Environmental Forensics: Elsevier Publishing, Boston, MA, p. 340-429.

Morse, J. W., 1999, Sulfides in sandy sediments: New insights on the reactions responsible for sedimentary pyrite formation: Aquatic Geochemistry, v. 5, p. 75-85.

Natter, M. G., 2012, Fate and transformation of oils and trace metals in Alabama and Louisiana coastal marsh sediments associated with the British Petroleum Gulf oil spill [M.S. Thesis]: Auburn University, 169 pp.

New York Times, Giant plumes of oil forming under the Gulf. http://www.nytimes.com/2010/05/16/us/16oil.html, (accessed April, 2012).

O'Leary, M. H., 1988, Carbon isotopes in photosynthesis: Bioscience, v. 38, p. 328 -335.

Olivie-Lauquet, G., Gruau, G., Dia, A., Riou, C., Jaffrezic, A., and Henin, O., 2000, Release of trace elements in wetlands: Role of seasonal variability: Water Resources, v. 35, p. 943-952.

Orberger, B., Pasava, J., Gallien, J. P., Daudin, L., and Pinti, D. L., 2003, Biogenic and abiogenic hydrothermal sulfides: Controls of rare metal distribution in black shales (Yukon Territories, Canada): Journal of Geochemical Exploration, v. 78-79, p. 559-563.

Oudot, J. and Chaillan, F., 2010, Pyrolysis of asphaltenes and biomarkers for the fingerprinting of the *Amoco Cadiz* oil spill after 23 years: Comptes Rendus Chimie, v. 13, p. 548-552.

Overton, E. B., Ashton, B. M., and Miles, M. S., 2004, Historical polycyclic aromatic and petrinic hydrocarbon loading in northern central Gulf of Mexico shelf sediments: Marine Pollution Bulletin, v. 49, p. 557-563.

Park, R., and Epstein, S., 1961, Metabolic fractionation of $^{13}C/^{12}C$ in plants: Plant Physiology, v. 36, p. 133-138.

Rickard, D., and Luther III, G. W., 2006, Metal sulfide complexes and clusters: Reviews in Mineralogy and Geochemistry, v. 61, p. 421-504.

Rogers, R. D., McFarlane, J. C., and Cross, A. J., 1980, Adsorption and desorption of benzene in two soils and montmorillonite clay: Environmental Science and Technology, v. 14, p. 457-460.

Rosenbauer, R. J., Cambell, P. L., Lam, A., Lorenson, T. D., Hostettler, F. D., Thomas, B., and Wong, F. L., 2010, Reconnaissance of Macondo-1 Well Oil in Sediment and Tarballs from the Northern Gulf of Mexico Shoreline, Texas to Florida: USGS Open-File report 2010-1290, 22 pp.

Saunders, J. A., Lee, M.-K., Shamsudduha, M., Dhakal, P., Uddin, A., Chowdury, M. T., and Ahmed K. M., 2008, Geochemistry and mineralogy of arsenic in (natural) anaerobic Groundwaters: Applied Geochemistry, v. 23, p. 3205-3214.

Stahl, W., 1977, Carbon and nitrogen isotopes in hydrocarbon research and exploration: Chemical Geology, v. 20, p. 121-149.

Straub, K. L., Benz, M., and Schink, B., 2000, Iron metabolism in anoxic environments at near neutral pH: FEMS Microbiology Ecology, v. 34, p. 181-186.

USA Today, Oil cleanup not over in Louisiana's Bay Jimmy, http://www.usatoday.com/news/nation/environment/2010-10-19-oil19_ST_N.htm, (accessed April, 2012).

Ventura, G. T., Raghuraman, B., Nelson R. K., Mullins, O. C., and Reddy, C. M., 2010, Compound class oil fingerprinting techniques using comprehensive two-dimensional gas chromatography (GC X GC): Organic Geochemistry, v. 41, p. 1026-1035.

Wang, Z., Fingas, M., Owens, E. H., Sigouin, L., and Brown, C. E., 2001, Long-term fate and persistence of the spilled Metula oil in a marine salt marsh environment: Degradation of petroleum biomarkers: Journal of Chromatography A., v. 926, p. 275-290.

Wang, Z., and Fingas, M. F., 2003, Development of oil hydrocarbon fingerprinting and identification techniques: Marine Pollution Bulletin, v. 47, p. 423-452.

Wang, Z., and Stout, S., 2007, Oil Spill Environmental Forensics Fingerprinting and Source Identification: Elsevier Publishing, Boston, MA, p. 1-146.

Wedepohl, K. H., 1995, The composition of the continental crust: Geochimica et Cosmochimica Acta, v. 59, p. 1217-1232.

Wilkin, R. T., and Barnes, H. L., 1996, Formation processes of framboidal pyrite: Geochimica et Cosmochimica Acta, v. 61, p. 323-339.

Wilkin, R. T., Barnes, H. L., and Brantley, S. L., 1996, The size distribution of framboidal pyrite in modern sediments: An indicator of redox conditions: Geochimica et Cosmochimica Acta, v. 60, p. 3897–3912.

Wright D. A., and Welbourn, P., 2002, Environmental Toxicity, Cambridge University Press, Cambridge, UK, 630 pp.

Appendix 1. Dissolved organic carbon, dissolved reduced Fe and sulfide contents of porewaters.

Sample ID	Sediment depth (cm)	Pore-water DOC (mg/kg)	Pore-water Fe (mg/kg)	Pore-water sulfide (mg/kg)
WB	0-3	38.19	-	-
WB	3-6	30.80	-	.002
WB	6-9	70.80	-	-
WB	9-12	64.88	0.09	.100
WB	12-15	46.77	-	-
WB	15-18	35.54	0.05	-
WB	18-21	38.80	0.07	-
WB	21-24	37.12	0.03	-
WB	24-27	32.62	-	-
WB	27-30	36.80	0.13	-
LB	0-3	19.88	-	-
LB	3-6	0.60	0.25	.080
LB	6-9	0.55	-	-
LB	9-12	26.30	0.36	.690
LB	12-15	12.90	-	-
LB	15-18	14.45	-	-
LB	18-21	1.92	-	-
LB	21-24	14.63	-	-
LB	24-27	0.16	-	-
LB	27-30	13.40	-	-
WI	0-3	0.21	-	-
WI	3-6	31.54	0.61	.003
WI	6-9	54.62	-	-
WI	9-12	25.83	0.62	.787
WI	12-15	26.91	-	-
WI	15-18	18.94	-	-
WI	18-21	-	-	-
WI	21-24	-	-	-
WI	24-27	-	-	-
WI	27-30	-	-	-
BH	0-3	16.19	0.03	-
BH	3-6	19.56	0.03	-
BH	6-9	12.06	0.01	-
BH	9-12	18.27	0.02	-
BH	12-15	13.08	0.01	-
BH	15-18	24.98	0.02	-
BH	18-21	19.65	0.01	-
BH	21-24	20.20	0.02	-
BH	24-27	22.86	0.01	-
BH	27-30	-	0.03	-

PACB	0-3	37.86	0.02	-
PACB	3-6	31.60	0.02	-
PACB	6-9	27.62	0.01	-
PACB	9-12	15.66	0.03	-
PACB	12-15	26.19	0.01	-
PACB	15-18	0.25	0.02	-
PACB	18-21	0.53	0.01	-
PACB	21-24	11.22	0.04	-
PACB	24-27	10.24	0.01	-
PACB	27-30	0.35	-	-
RG	0-3	35.74	-	.030
RG	3-6	48.67	0.01	-
RG	6-9	61.06	0.02	-
RG	9-12	56.56	0.02	-
RG	12-15	96.19	0.02	-
RG	15-18	112.60	-	-
RG	18-21	122.90	-	-
RG	21-24	142.90	-	-
RG	24-27	162.50	-	-
RG	27-30	173.00	0.01	8.86
BD	0-3	79.03	0.02	.003
BD	3-6	185.80	0.01	4.40
BD	6-9	234.00	0.01	-
BD	9-12	231.70	0.02	23.52
BD	12-15	224.40	0.01	28.96
BD	15-18	225.40	0.01	41.84
BD	18-21	229.80	0.02	58.68
BD	21-24	234.70	0.01	53.60
BD	24-27	227.30	0.01	46.00
BD	27-30	225.80	0.02	-
BB	0-3	69.40	0.03	41.50
BB	3-6	134.10	0.03	19.48
BB	6-9	148.40	0.01	26.92
BB	9-12	50.03	0.02	33.08
BB	12-15	213.80	0.01	32.96
BB	15-18	334.20	0.02	41.28
BB	18-21	361.10	0.01	44.64
BB	21-24	253.70	0.02	48.00
BB	24-27	226.00	0.01	49.20
BB	27-30	102.80	0.03	30.80
BJN	0-3	85.07	0.02	.270
BJN	3-6	182.40	0.01	4.82
BJN	6-9	239.50	0.01	20.12

BJN	9-12	137.90	0.02	35.34
BJN	12-15	234.40	0.01	54.24
BJN	15-18	269.40	0.01	50.80
BJN	18-21	108.20	0.02	69.10
BJN	21-24	75.42	0.01	65.10
BJN	24-27	308.00	0.01	70.40
BJN	27-30	391.10	0.02	82.80
BJS	0-3	69.63	0.03	.010
BJS	3-6	109.30	0.03	.240
BJS	6-9	142.20	0.01	4.62
BJS	9-12	188.70	0.02	6.32
BJS	12-15	231.40	0.01	9.12
BJS	15-18	274.00	0.02	7.52
BJS	18-21	308.40	0.01	8.32
BJS	21-24	334.20	0.02	6.64
BJS	24-27	279.90	0.01	4.06
BJS	27-30	346.90	0.03	2.78

Appendix 2a. Grain distribution by weight percent in 0-3 cm sediments.

Phi Size 0-3 cm	WB %	LB %	WI %	BH %	PACB %	RG %	BD %	BB %	BJN %	BJS %
<-1 phi	0.00	0.00	0.20	0.00	0.00	0.00	0.00	0.00	0.00	0.00
-1 to 0 phi	0.00	0.00	0.23	2.26	0.00	0.00	0.00	0.00	0.00	0.00
0 to 1 phi	0.00	0.15	4.96	0.55	0.05	0.00	0.00	0.00	0.00	0.00
1 to 2 phi	0.00	1.13	47.68	2.48	10.67	0.06	0.00	0.00	0.00	0.00
2 to 3 phi	0.00	23.41	29.06	14.75	33.60	23.51	0.00	0.00	0.00	0.00
3 to 4 phi	0.00	49.90	5.79	15.71	18.83	33.11	0.00	0.00	0.00	0.00
4 to 5 phi	3.32	5.95	1.14	9.56	8.32	22.44	7.29	19.77	22.56	30.81
5 to 6 phi	13.74	2.93	0.97	13.98	5.95	3.17	15.63	18.22	15.15	18.02
6 to 7 phi	22.75	3.21	2.11	8.22	4.50	6.05	30.21	21.71	13.47	13.95
7 to 8 phi	7.58	1.70	2.47	7.36	3.51	1.58	12.50	11.24	13.80	9.88
8 to 9 phi	6.64	2.08	1.23	6.01	1.60	1.58	4.69	5.04	2.36	4.65
9 to 10 phi	9.48	1.42	1.23	2.82	1.37	2.70	7.29	8.53	10.10	7.85
> 10 phi	36.49	7.46	2.38	16.19	11.06	5.77	22.40	15.50	22.56	14.83

Appendix 2b. Grain distribution by weight percent in 12-15 cm sediments.

Phi Size 12-15 cm	WB %	LB %	WI %	BH %	PACB %	RG %	BD %	BB %	BJN %	BJS %
<-1 phi	0.00	0.00	0.00	0.00	0.00	0.00	0.00	0.00	0.00	0.00
-1 to 0 phi	0.00	0.02	0.09	0.00	0.00	0.00	0.00	0.00	0.00	0.00
0 to 1 phi	0.00	0.51	5.88	0.24	0.35	0.12	0.00	0.00	0.00	0.00
1 to 2 phi	0.00	1.11	56.28	3.30	11.76	0.41	0.00	0.00	0.00	0.00
2 to 3 phi	0.00	37.90	26.54	22.24	34.79	16.54	0.00	0.00	0.00	0.00
3 to 4 phi	0.00	43.63	3.92	21.89	9.02	30.46	0.00	0.00	0.00	0.00
4 to 5 phi	10.64	8.32	0.70	13.90	9.05	18.98	1.68	0.00	5.82	9.69
5 to 6 phi	14.01	1.00	0.70	10.25	8.28	9.24	7.56	3.79	9.84	23.35
6 to 7 phi	14.57	0.42	1.57	7.66	6.49	4.41	26.89	27.96	6.22	18.50
7 to 8 phi	11.48	1.16	0.52	4.54	3.93	3.25	20.17	23.22	12.45	13.22
8 to 9 phi	10.08	0.58	0.52	0.71	1.88	1.33	9.24	7.11	7.03	8.81
9 to 10 phi	4.76	0.83	1.30	1.96	3.59	4.08	9.24	9.00	11.65	7.05
> 10 phi	34.45	4.24	1.39	10.34	10.76	11.24	25.21	28.91	46.99	19.38

Appendix 2c. Grain distribution by weight percent in 27-30 cm sediments.

Phi Size 27-30 cm	WB %	LB %	WI %	BH %	PACB %	RG %	BD %	BB %	BJN %	BJS %
<-1 phi	0.00	0.00	0.27	0.00	0.00	0.00	0.00	0.00	0.00	0.00
-1 to 0 phi	0.00	0.15	0.62	0.52	0.05	0.00	0.00	0.00	0.00	0.00
0 to 1 phi	0.00	0.76	6.92	1.08	0.66	0.00	0.00	0.00	0.00	0.00
1 to 2 phi	0.00	2.30	65.92	2.52	17.25	0.00	0.00	0.00	0.00	0.00
2 to 3 phi	0.00	34.56	16.30	11.49	45.64	0.00	0.00	0.00	0.00	0.00
3 to 4 phi	0.00	31.10	2.54	13.43	10.46	0.00	0.00	0.00	0.00	0.00
4 to 5 phi	3.91	4.88	2.87	19.19	6.91	3.75	4.51	1.64	4.05	21.86
5 to 6 phi	12.85	2.62	0.38	16.44	7.78	12.62	12.78	14.25	32.43	23.72
6 to 7 phi	15.92	4.25	0.38	10.46	4.07	24.46	11.65	16.71	45.27	13.26
7 to 8 phi	14.53	3.71	0.70	6.09	1.36	19.72	19.55	13.15	4.73	9.30
8 to 9 phi	14.53	2.35	0.32	7.31	1.73	7.50	9.02	10.96	0.68	5.35
9 to 10 phi	7.54	2.89	0.26	3.25	0.37	16.57	9.02	9.32	2.03	6.98
> 10 phi	30.73	10.22	2.43	8.22	3.70	15.38	33.46	33.97	10.81	19.53

Appendix 3. Bulk major ion compositions of coastal wetland sediments.

Sample ID	Sample depth (cm)	Fe %	K %	P %	Al %	S %	Ca %	Mg %	Na %
WB	0-3	3.400	0.25	0.043	2.090	1.670	0.160	0.450	0.791
WB	3-6	3.390	0.24	0.039	2.150	1.850	0.180	0.460	0.714
WB	6-9	3.270	0.26	0.034	2.170	1.860	0.180	0.530	1.007
WB	9-12	2.900	0.22	0.030	1.830	1.690	0.190	0.420	0.778
WB	12-15	2.930	0.20	0.027	1.970	1.860	0.200	0.400	0.502
WB	15-18	3.120	0.21	0.028	2.190	1.950	0.160	0.410	0.393
WB	18-21	2.940	0.19	0.024	1.930	1.870	0.140	0.370	0.275
WB	21-24	2.420	0.15	0.019	1.580	1.480	0.130	0.290	0.184
WB	24-27	2.570	0.17	0.020	1.600	1.440	0.130	0.340	0.190
WB	27-30	2.330	0.15	0.016	1.180	1.430	0.110	0.320	0.168
LB	0-3	0.250	0.04	0.003	0.310	0.290	0.600	0.100	0.428
LB	3-6	0.220	0.04	0.001	0.320	0.250	0.050	0.090	0.348
LB	6-9	0.240	0.03	0.002	0.300	0.300	0.050	0.070	0.247
LB	9-12	0.280	0.04	0.001	0.340	0.320	0.040	0.070	0.271
LB	12-15	0.430	0.04	0.001	0.370	0.510	0.040	0.080	0.283
LB	15-18	0.310	0.02	0.001	0.210	0.420	0.030	0.050	0.196
LB	18-21	0.460	0.04	0.001	0.370	0.590	0.040	0.080	0.212
LB	21-24	0.420	0.03	0.001	0.310	0.540	0.030	0.080	0.220
LB	24-27	0.430	0.03	0.001	0.250	0.550	0.030	0.060	0.187
LB	27-30	0.620	0.03	0.001	0.300	0.690	0.050	0.070	0.187
WI	0-3	0.450	0.09	0.019	0.360	0.500	0.130	0.260	0.917
WI	3-6	0.970	0.14	0.020	0.720	0.880	0.200	0.430	1.348
WI	6-9	1.260	0.16	0.022	1.010	1.080	0.230	0.560	1.337
WI	9-12	1.150	0.14	0.018	0.870	0.960	0.190	0.440	1.004
WI	12-15	1.030	0.13	0.014	0.740	0.870	0.340	0.400	1.006
WI	15-18	0.750	0.10	0.009	0.590	0.650	0.090	0.290	0.689
WI	18-21	0.750	0.11	0.008	0.630	0.650	0.100	0.310	0.847
WI	21-24	0.410	0.06	0.005	0.340	0.340	0.050	0.170	0.549
WI	24-27	0.370	0.06	0.004	0.340	0.330	0.060	0.160	0.500
WI	27-30	0.520	0.08	0.005	0.400	0.510	0.080	0.240	0.739
BH	0-3	0.700	0.12	0.004	0.550	0.640	0.180	0.190	0.745
BH	3-6	0.740	0.13	0.003	0.640	0.680	0.110	0.200	0.602
BH	6-9	0.890	0.14	0.002	0.640	0.870	0.110	0.200	0.496
BH	9-12	0.990	0.10	0.001	0.490	1.140	0.100	0.160	0.451
BH	12-15	1.120	0.06	0.001	0.330	1.320	0.060	0.110	0.320
BH	15-18	0.650	0.05	0.001	0.280	0.840	0.050	0.090	0.287
BH	18-21	0.310	0.05	0.001	0.220	0.430	0.050	0.080	0.266
BH	21-24	0.210	0.04	0.001	0.200	0.280	0.040	0.070	0.244

BH	24-27	0.190	0.04	0.001	0.200	0.270	0.040	0.070	0.252
BH	27-30	0.140	0.04	0.001	0.180	0.220	0.030	0.060	0.216
PACB	0-3	0.260	0.05	0.014	0.160	0.150	0.060	0.080	0.383
PACB	3-6	0.560	0.08	0.012	0.290	0.530	0.100	0.120	0.418
PACB	6-9	1.450	0.18	0.013	0.740	1.320	0.160	0.260	0.588
PACB	9-12	1.000	0.13	0.010	0.540	0.900	0.080	0.190	0.419
PACB	12-15	1.340	0.16	0.012	0.660	1.130	0.100	0.220	0.459
PACB	15-18	1.420	0.18	0.012	0.680	1.130	0.080	0.220	0.423
PACB	18-21	1.190	0.18	0.010	0.650	0.920	0.090	0.220	0.412
PACB	21-24	0.950	0.16	0.008	0.600	0.740	0.080	0.190	0.369
PACB	24-27	1.050	0.16	0.008	0.620	0.850	0.080	0.190	0.398
PACB	27-30	0.750	0.11	0.005	0.440	0.650	0.050	0.140	0.323
RG	0-3	1.010	0.15	0.050	0.580	0.340	0.200	0.300	0.512
RG	3-6	1.130	0.15	0.040	0.610	0.720	0.220	0.270	0.305
RG	6-9	1.400	0.16	0.038	0.680	0.960	0.140	0.300	0.296
RG	9-12	1.300	0.15	0.041	0.640	0.910	0.160	0.290	0.254
RG	12-15	1.420	0.17	0.040	0.730	0.960	0.180	0.340	0.258
RG	15-18	1.810	0.20	0.033	0.970	1.400	0.160	0.380	0.388
RG	18-21	1.460	0.24	0.031	1.190	0.940	0.160	0.450	0.494
RG	21-24	1.410	0.25	0.027	1.130	1.060	0.160	0.460	0.609
RG	24-27	1.140	0.25	0.027	1.110	0.640	0.150	0.440	0.507
RG	27-30	1.540	0.26	0.028	1.250	1.030	0.150	0.470	0.509
BD	0-3	1.390	0.33	0.043	1.010	1.320	0.530	0.620	1.336
BD	3-6	1.460	0.36	0.037	1.190	1.370	0.280	0.680	1.367
BD	6-9	1.680	0.38	0.031	1.190	1.570	0.270	0.680	1.256
BD	9-12	1.880	0.38	0.030	1.180	2.020	0.300	0.700	1.384
BD	12-15	1.810	0.33	0.035	1.020	2.440	0.370	0.700	1.617
BD	15-18	1.870	0.34	0.040	1.160	2.470	0.400	0.770	1.639
BD	18-21	1.480	0.26	0.042	0.760	2.890	0.500	0.790	2.159
BD	21-24	1.360	0.36	0.039	1.150	1.790	0.410	0.790	1.733
BD	24-27	1.150	0.31	0.036	1.000	1.570	0.410	0.740	1.617
BD	27-30	1.260	0.27	0.035	0.860	1.700	0.360	0.650	1.301
BB	0-3	1.760	0.30	0.049	0.860	1.780	0.510	0.590	1.402
BB	3-6	1.980	0.34	0.030	0.970	2.070	0.260	0.620	1.351
BB	6-9	1.430	0.36	0.028	1.060	1.310	0.240	0.640	1.180
BB	9-12	1.370	0.36	0.033	1.130	1.380	0.300	0.700	1.299
BB	12-15	1.900	0.28	0.047	0.930	2.990	0.490	0.740	1.946
BB	15-18	1.900	0.33	0.039	1.020	2.420	0.420	0.730	1.647
BB	18-21	1.410	0.25	0.031	0.790	1.300	0.210	0.470	0.744
BB	21-24	1.370	0.25	0.041	0.700	2.610	0.550	0.810	2.467
BB	24-27	1.600	0.36	0.030	1.250	1.110	0.230	0.660	0.850
BB	27-30	1.260	0.35	0.033	1.210	0.800	0.300	0.660	1.023

BJN	0-3	1.380	0.32	0.037	0.820	1.700	0.470	0.650	1.847
BJN	3-6	1.600	0.31	0.034	0.750	2.120	0.670	0.680	2.063
BJN	6-9	1.320	0.31	0.035	0.820	1.650	0.350	0.650	1.781
BJN	9-12	0.980	0.31	0.032	0.850	1.130	0.330	0.620	1.394
BJN	12-15	1.280	0.31	0.027	0.770	1.560	0.330	0.590	1.460
BJN	15-18	1.480	0.29	0.033	0.770	2.120	0.400	0.650	1.828
BJN	18-21	1.180	0.26	0.029	0.750	1.550	0.320	0.550	1.418
BJN	21-24	1.150	0.23	0.041	0.700	2.040	0.450	0.640	1.990
BJN	24-27	0.880	0.17	0.022	0.460	0.800	0.130	0.280	0.433
BJN	27-30	1.150	0.27	0.037	0.860	1.410	0.300	0.550	1.190
BJS	0-3	1.390	0.29	0.047	0.810	1.580	0.450	0.600	1.356
BJS	3-6	1.380	0.30	0.035	0.900	1.290	0.220	0.550	0.953
BJS	6-9	1.770	0.28	0.037	0.820	2.080	0.300	0.590	1.223
BJS	9-12	1.590	0.29	0.039	0.780	2.210	0.370	0.700	1.791
BJS	12-15	1.270	0.30	0.036	0.860	1.610	0.310	0.640	1.460
BJS	15-18	1.220	0.33	0.032	0.950	1.300	0.280	0.630	1.395
BJS	18-21	1.230	0.29	0.029	0.750	1.380	0.280	0.570	1.263
BJS	21-24	0.710	0.24	0.024	0.620	0.700	0.230	0.440	0.871
BJS	24-27	0.580	0.22	0.019	0.550	0.780	0.240	0.450	1.025
BJS	27-30	0.550	0.20	0.018	0.490	0.510	0.150	0.330	0.572

Appendix 4a. Trace metal compositions (in mg/kg) of coastal wetland sediments.

Sample ID	Sample depth (cm)	Cu mg/kg	Pb mg/kg	Zn mg/kg	Ni mg/kg	Co mg/kg	Mn mg/kg
WB	0-3	20.40	21.50	76.00	13.60	8.60	381.00
WB	3-6	21.00	20.80	78.00	13.30	8.40	384.00
WB	6-9	15.10	20.20	73.00	13.10	8.30	350.00
WB	9-12	13.30	16.90	63.00	11.20	7.00	308.00
WB	12-15	13.70	18.80	65.00	11.40	6.80	314.00
WB	15-18	14.80	21.20	68.00	12.70	7.40	296.00
WB	18-21	24.90	19.30	59.00	11.90	6.40	230.00
WB	21-24	10.80	15.90	46.00	8.80	5.20	167.00
WB	24-27	10.60	15.80	45.00	9.90	6.10	174.00
WB	27-30	8.70	13.90	39.00	8.20	5.80	149.00
LB	0-3	3.10	4.40	3.00	1.40	0.50	12.00
LB	3-6	2.30	4.90	3.00	1.30	0.60	7.00
LB	6-9	1.30	4.40	2.00	1.60	0.60	5.00
LB	9-12	2.90	4.50	2.00	1.20	0.70	5.00
LB	12-15	3.50	5.20	2.00	1.70	1.10	6.00
LB	15-18	3.20	3.50	2.00	0.90	0.60	4.00
LB	18-21	2.70	4.50	3.00	1.10	0.80	8.00
LB	21-24	2.30	3.90	3.00	1.40	0.70	8.00
LB	24-27	2.50	3.20	3.00	1.40	0.70	7.00
LB	27-30	3.60	3.90	4.00	1.70	1.20	8.00
WI	0-3	17.30	5.20	24.00	3.70	0.80	23.00
WI	3-6	21.20	10.00	33.00	7.90	1.90	53.00
WI	6-9	24.10	14.20	45.00	9.00	2.40	71.00
WI	9-12	21.00	12.60	50.00	7.90	2.20	61.00
WI	12-15	24.20	11.70	43.00	6.80	2.10	57.00
WI	15-18	14.80	8.30	23.00	4.20	1.40	39.00
WI	18-21	11.30	7.50	25.00	5.00	1.50	34.00
WI	21-24	15.50	4.00	14.00	3.20	0.80	17.00
WI	24-27	42.60	3.80	13.00	2.90	0.90	15.00
WI	27-30	13.00	4.40	10.00	4.20	1.60	17.00
BH	0-3	8.50	7.10	9.00	2.60	1.00	23.00
BH	3-6	3.00	8.10	7.00	3.00	1.00	18.00
BH	6-9	4.60	10.40	6.00	2.70	1.50	17.00
BH	9-12	6.90	9.70	5.00	2.60	1.40	15.00
BH	12-15	2.70	7.60	2.00	1.90	1.80	13.00
BH	15-18	2.20	5.60	1.00	0.80	0.50	10.00
BH	18-21	1.20	4.90	1.00	0.70	0.30	7.00
BH	21-24	2.10	4.40	1.00	0.60	0.30	6.00

BH	24-27	1.30	4.60	1.00	0.70	0.20	6.00
BH	27-30	4.50	4.30	1.00	0.40	0.10	5.00
PACB	0-3	3.40	3.20	6.00	1.00	0.80	52.00
PACB	3-6	4.60	4.20	11.00	2.10	1.30	71.00
PACB	6-9	7.00	8.50	22.00	5.10	3.30	240.00
PACB	9-12	5.60	6.40	17.00	4.10	2.40	156.00
PACB	12-15	10.80	8.10	19.00	4.80	2.80	205.00
PACB	15-18	4.30	8.20	18.00	4.40	3.00	224.00
PACB	18-21	5.70	7.60	13.00	4.60	2.70	141.00
PACB	21-24	2.90	6.50	12.00	4.00	2.10	78.00
PACB	24-27	3.40	7.10	11.00	4.10	2.30	61.00
PACB	27-30	2.70	5.60	7.00	3.00	2.30	32.00
RG	0-3	66.00	13.30	45.00	8.80	4.60	410.00
RG	3-6	22.80	10.90	39.00	9.50	5.50	176.00
RG	6-9	17.70	11.20	41.00	10.20	5.70	169.00
RG	9-12	28.40	10.40	43.00	9.90	5.40	164.00
RG	12-15	23.80	13.10	45.00	10.60	5.80	200.00
RG	15-18	19.80	17.70	48.00	12.10	5.80	236.00
RG	18-21	24.00	17.80	44.00	11.50	4.20	200.00
RG	21-24	45.10	17.10	46.00	10.60	4.30	205.00
RG	24-27	29.90	14.80	41.00	10.40	4.40	178.00
RG	27-30	25.30	17.30	51.00	14.50	7.30	180.00
BD	0-3	22.90	11.50	44.00	12.60	5.40	211.00
BD	3-6	28.20	11.40	61.00	14.80	5.20	206.00
BD	6-9	20.50	10.20	62.00	15.30	5.70	219.00
BD	9-12	21.20	11.10	41.00	12.30	5.40	258.00
BD	12-15	34.10	15.70	44.00	17.20	7.90	262.00
BD	15-18	30.70	14.00	61.00	19.40	6.80	264.00
BD	18-21	35.00	13.00	48.00	18.70	8.30	298.00
BD	21-24	36.30	12.50	73.00	17.80	7.30	247.00
BD	24-27	37.40	11.50	46.00	13.70	4.00	228.00
BD	27-30	25.40	10.70	53.00	13.50	5.70	217.00
BB	0-3	126.20	32.00	67.00	16.70	8.30	283.00
BB	3-6	40.80	11.00	62.00	16.50	7.80	229.00
BB	6-9	32.20	11.00	47.00	12.40	5.50	192.00
BB	9-12	25.70	14.50	47.00	14.20	5.30	198.00
BB	12-15	50.20	21.60	74.00	26.40	11.70	259.00
BB	15-18	36.40	14.70	60.00	20.10	8.00	252.00
BB	18-21	16.00	10.50	41.00	12.40	4.50	163.00
BB	21-24	42.50	12.70	51.00	17.30	6.40	251.00
BB	24-27	22.60	16.10	61.00	16.00	6.10	192.00
BB	27-30	35.10	17.00	50.00	14.60	4.60	198.00

BJN	0-3	24.70	13.20	52.00	15.40	4.40	173.00
BJN	3-6	28.10	12.60	50.00	14.90	6.10	195.00
BJN	6-9	25.00	11.80	40.00	13.30	4.40	170.00
BJN	9-12	27.10	11.00	42.00	11.70	5.30	160.00
BJN	12-15	20.60	10.30	39.00	10.60	6.40	191.00
BJN	15-18	26.70	12.80	35.00	11.30	5.20	220.00
BJN	18-21	23.90	10.20	30.00	11.50	3.80	127.00
BJN	21-24	25.70	13.80	27.00	12.60	3.90	151.00
BJN	24-27	9.00	5.60	19.00	6.60	3.00	72.00
BJN	27-30	18.00	9.80	31.00	12.50	3.70	119.00
BJS	0-3	31.80	12.80	43.00	13.40	5.60	219.00
BJS	3-6	45.60	12.40	48.00	14.40	5.60	241.00
BJS	6-9	26.00	12.40	46.00	14.60	6.20	271.00
BJS	9-12	27.30	12.60	42.00	14.00	5.30	279.00
BJS	12-15	38.00	11.80	44.00	13.60	4.90	204.00
BJS	15-18	22.70	10.80	37.00	11.20	3.50	181.00
BJS	18-21	21.90	9.90	32.00	10.30	3.20	172.00
BJS	21-24	20.00	7.20	24.00	8.00	1.90	123.00
BJS	24-27	15.80	8.00	21.00	6.80	1.80	111.00
BJS	27-30	12.50	6.20	18.00	6.30	2.20	79.00

Appendix 4b. Trace metal compositions (in mg/kg) of coastal wetland sediments.

Sample ID	Sample depth (cm)	As mg/kg	Th mg/kg	Sr mg/kg	V mg/kg	Ba mg/kg	Cr mg/kg	Hg mg/kg
WB	0-3	10.70	7.10	33.00	35.00	32.00	32.00	0.08
WB	3-6	10.50	7.20	32.00	35.00	32.00	31.00	0.08
WB	6-9	10.30	7.30	39.00	35.00	31.00	30.00	0.08
WB	9-12	9.60	6.30	33.00	29.00	25.00	26.00	0.07
WB	12-15	9.80	6.70	32.00	34.00	26.00	27.00	0.06
WB	15-18	10.90	7.20	29.00	38.00	28.00	29.00	0.07
WB	18-21	10.50	6.80	27.00	35.00	25.00	27.00	0.06
WB	21-24	8.30	5.70	21.00	29.00	20.00	21.00	0.05
WB	24-27	9.00	6.10	24.00	30.00	23.00	25.00	0.05
WB	27-30	9.30	5.40	22.00	25.00	19.00	19.00	0.04
LB	0-3	1.70	1.70	37.00	10.00	4.00	4.00	0.00
LB	3-6	1.50	1.90	8.00	11.00	3.00	4.00	0.00
LB	6-9	1.90	2.10	7.00	11.00	3.00	4.00	0.01
LB	9-12	2.10	2.10	7.00	10.00	5.00	3.00	0.00
LB	12-15	3.20	2.30	8.00	12.00	3.00	5.00	0.00
LB	15-18	1.90	1.50	5.00	8.00	2.00	3.00	0.00
LB	18-21	1.80	2.20	8.00	11.00	4.00	7.00	0.01
LB	21-24	1.30	1.80	7.00	8.00	4.00	6.00	0.00
LB	24-27	1.30	1.60	6.00	8.00	3.00	5.00	0.00
LB	27-30	1.80	1.80	8.00	10.00	4.00	6.00	0.02
WI	0-3	2.20	1.20	19.00	6.00	7.00	11.00	0.05
WI	3-6	4.80	2.20	28.00	19.00	9.00	22.00	0.05
WI	6-9	5.20	2.70	32.00	26.00	13.00	28.00	0.06
WI	9-12	4.50	2.40	26.00	22.00	10.00	12.00	0.07
WI	12-15	4.10	2.00	26.00	18.00	8.00	20.00	0.06
WI	15-18	2.80	1.90	15.00	13.00	7.00	15.00	0.04
WI	18-21	3.50	1.90	17.00	14.00	7.00	15.00	0.04
WI	21-24	2.40	1.00	10.00	9.00	5.00	9.00	0.04
WI	24-27	2.10	1.20	10.00	8.00	5.00	10.00	0.03
WI	27-30	3.70	1.70	14.00	13.00	5.00	12.00	0.01
BH	0-3	2.40	2.70	21.00	13.00	9.00	7.00	0.00
BH	3-6	1.90	3.20	18.00	14.00	8.00	7.00	0.00
BH	6-9	2.00	3.10	19.00	13.00	7.00	7.00	0.01
BH	9-12	2.70	2.70	17.00	10.00	6.00	5.00	0.01
BH	12-15	2.20	1.80	12.00	6.00	4.00	3.00	0.01
BH	15-18	0.70	1.70	10.00	4.00	3.00	2.00	0.00
BH	18-21	0.50	1.50	9.00	3.00	3.00	2.00	0.01
BH	21-24	0.50	1.40	7.00	3.00	3.00	2.00	0.00

BH	24-27	0.50	1.40	8.00	3.00	6.00	2.00	0.00
BH	27-30	0.50	1.40	7.00	2.00	4.00	2.00	0.00
PACB	0-3	1.70	0.90	7.00	9.00	4.00	2.00	0.00
PACB	3-6	3.10	1.50	10.00	12.00	5.00	5.00	0.00
PACB	6-9	6.50	3.40	19.00	20.00	9.00	12.00	0.02
PACB	9-12	4.20	2.60	13.00	14.00	7.00	1.00	0.00
PACB	12-15	6.10	3.20	15.00	18.00	9.00	11.00	0.00
PACB	15-18	6.30	3.40	15.00	18.00	9.00	11.00	0.00
PACB	18-21	6.10	3.50	15.00	17.00	9.00	10.00	0.00
PACB	21-24	4.90	3.20	13.00	16.00	8.00	9.00	0.02
PACB	24-27	5.30	3.40	14.00	17.00	8.00	9.00	0.00
PACB	27-30	3.80	2.40	10.00	12.00	6.00	6.00	0.01
RG	0-3	4.30	3.80	26.00	14.00	123.00	11.00	0.02
RG	3-6	4.60	4.00	26.00	15.00	71.00	11.00	0.03
RG	6-9	5.60	4.50	20.00	16.00	52.00	11.00	0.03
RG	9-12	6.60	4.20	21.00	15.00	105.00	11.00	0.03
RG	12-15	6.50	4.70	24.00	18.00	134.00	12.00	0.05
RG	15-18	8.00	5.20	33.00	23.00	82.00	15.00	0.06
RG	18-21	5.30	5.90	37.00	27.00	72.00	17.00	0.06
RG	21-24	6.90	5.50	41.00	29.00	65.00	17.00	0.06
RG	24-27	4.70	5.80	40.00	26.00	60.00	17.00	0.06
RG	27-30	7.70	6.40	36.00	29.00	52.00	18.00	0.07
BD	0-3	3.00	3.80	65.00	23.00	97.00	16.00	0.02
BD	3-6	2.60	4.20	58.00	22.00	58.00	17.00	0.02
BD	6-9	3.30	5.00	55.00	23.00	62.00	18.00	0.03
BD	9-12	5.20	5.00	59.00	25.00	63.00	18.00	0.04
BD	12-15	10.40	3.90	69.00	24.00	61.00	16.00	0.05
BD	15-18	5.00	3.80	71.00	22.00	66.00	16.00	0.04
BD	18-21	6.00	2.20	81.00	21.00	54.00	12.00	0.05
BD	21-24	3.60	3.70	71.00	26.00	71.00	17.00	0.04
BD	24-27	2.70	3.20	73.00	24.00	72.00	15.00	0.02
BD	27-30	2.70	3.30	63.00	21.00	60.00	14.00	0.03
BB	0-3	5.40	3.70	64.00	21.00	78.00	14.00	0.05
BB	3-6	4.80	4.50	56.00	21.00	57.00	16.00	0.04
BB	6-9	3.10	4.50	57.00	23.00	63.00	17.00	0.04
BB	9-12	3.20	4.20	60.00	25.00	65.00	18.00	0.04
BB	12-15	7.10	2.10	85.00	22.00	58.00	14.00	0.05
BB	15-18	4.50	3.40	73.00	23.00	72.00	16.00	0.05
BB	18-21	2.70	3.70	42.00	16.00	62.00	12.00	0.02
BB	21-24	4.80	2.30	94.00	24.00	65.00	13.00	0.06
BB	24-27	2.80	6.00	49.00	24.00	77.00	19.00	0.04
BB	27-30	2.20	5.30	59.00	27.00	86.00	19.00	0.04

BJN	0-3	4.60	3.60	63.00	21.00	67.00	13.00	0.05
BJN	3-6	4.60	3.40	86.00	20.00	71.00	12.00	0.07
BJN	6-9	3.00	3.30	64.00	20.00	65.00	13.00	0.05
BJN	9-12	2.50	3.40	59.00	21.00	64.00	14.00	0.05
BJN	12-15	3.50	3.90	59.00	23.00	59.00	13.00	0.06
BJN	15-18	4.20	3.70	69.00	24.00	56.00	7.00	0.07
BJN	18-21	2.70	3.50	59.00	20.00	55.00	12.00	0.04
BJN	21-24	3.30	2.60	78.00	21.00	59.00	12.00	0.03
BJN	24-27	1.60	2.60	28.00	12.00	41.00	7.00	0.02
BJN	27-30	2.30	3.30	55.00	20.00	66.00	13.00	0.02
BJS	0-3	6.70	3.50	60.00	21.00	69.00	14.00	0.05
BJS	3-6	6.70	4.30	42.00	20.00	50.00	14.00	0.05
BJS	6-9	9.40	3.60	52.00	20.00	52.00	13.00	0.06
BJS	9-12	9.00	3.10	64.00	20.00	54.00	5.00	0.06
BJS	12-15	4.60	3.60	58.00	21.00	56.00	14.00	0.05
BJS	15-18	3.10	4.10	55.00	22.00	62.00	15.00	0.02
BJS	18-21	3.20	4.10	49.00	20.00	56.00	13.00	0.04
BJS	21-24	1.70	3.70	41.00	16.00	51.00	10.00	0.03
BJS	24-27	1.70	3.50	45.00	18.00	49.00	10.00	0.03
BJS	27-30	1.40	3.30	30.00	14.00	41.00	9.00	0.02

Appendix 5. Sediment total organic carbon contents (TOC) and carbon isotopic compositions of bulk sediments, marsh plants, oil sample scrapped off the oiled plants, and BP MC-252 oil.

Sample ID	Sample depth(cm)	TOC sed(%)	$\delta^{13}C$ $sed_{(PDB)}$	$\delta^{13}C$ $Juncus_{(PDB)}$	$\delta^{13}C$ $Spartina_{(PDB)}$	$\delta^{13}C$ $oil_{(PDB)}$
WB	plant	-	-	-27.6		
WB	0-3	2.230	-25.9			
WB	3-6	2.290	-25.5			
WB	6-9	1.830	-25.3			
WB	9-12	2.240	-25.4			
WB	12-15	2.190	-25.4			
WB	15-18	1.970	-25.3			
WB	18-21	1.770	-25.3			
WB	21-24	2.330	-25.2			
WB	24-27	1.770	-25.4			
WB	27-30	1.770	-25.4			
LB	plant	-	-	-24.1		
LB	0-3	1.980	-26.1			
LB	3-6	2.220	-26.3			
LB	6-9	2.060	-26.0			
LB	9-12	1.930	-25.9			
LB	12-15	1.850	-26.1			
LB	15-18	1.720	-25.8			
LB	18-21	1.100	-26.3			
LB	21-24	1.320	-26.0			
LB	24-27	1.390	-26.1			
LB	27-30	2.000	-26.1			
WI	plant	-	-		-15.0	
WI	0-3	2.720	-23.6			
WI	3-6	2.990	-22.6			
WI	6-9	3.030	-21.7			
WI	9-12	2.660	-21.9			
WI	12-15	1.910	-21.4			
WI	15-18	2.220	-21.6			
WI	18-21	1.390	-21.9			
WI	21-24	1.470	-22.7			
WI	24-27	1.760	-22.0			
WI	27-30	2.500	-23.4			
BH	plant	-	-	-25.2	-14.5	
BH	0-3	1.730	-24.0			
BH	3-6	2.040	-23.9			
BH	6-9	1.940	-23.5			
BH	9-12	2.120	-23.1			
BH	12-15	2.180	-23.9			

BH	15-18	1.710	-24.6	
BH	18-21	1.460	-25.0	
BH	21-24	1.490	-25.2	
BH	24-27	1.460	-25.8	
BH	27-30	1.420	-26.3	
PACB	plant	-	-	-14.1
PACB	0-3	0.323	-21.1	
PACB	3-6	0.697	-20.1	
PACB	6-9	0.598	-19.4	
PACB	9-12	0.811	-19.6	
PACB	12-15	0.909	-19.7	
PACB	15-18	0.985	-20.8	
PACB	18-21	0.835	-23.3	
PACB	21-24	1.120	-23.7	
PACB	24-27	0.831	-24.2	
PACB	27-30	0.818	-24.8	
RG	plant	-	-	-14.4
RG	0-3	1.010	-22.7	
RG	3-6	1.110	-23.1	
RG	6-9	1.200	-24.0	
RG	9-12	1.050	-23.6	
RG	12-15	1.940	-23.5	
RG	15-18	2.190	-20.2	
RG	18-21	1.690	-19.9	
RG	21-24	1.400	-18.5	
RG	24-27	1.580	-19.9	
RG	27-30	1.680	-19.9	
BD	plant	-	-	-15.1
BD	0-3	4.530	-19.4	
BD	3-6	21.500	-20.3	
BD	6-9	28.900	-21.1	
BD	9-12	19.800	-20.6	
BD	12-15	24.400	-19.7	
BD	15-18	19.200	-20.5	
BD	18-21	19.000	-19.6	
BD	21-24	18.600	-19.2	
BD	24-27	20.280	-18.6	
BD	27-30	22.350	-17.3	
BB	plant	-	-	-15.6
BB	0-3	6.790	-18.9	
BB	3-6	11.100	-20.3	
BB	6-9	10.700	-20.5	
BB	9-12	11.700	-19.8	
BB	12-15	13.600	-19.7	

BB	15-18	9.370	-18.2			
BB	18-21	4.270	-18.9			
BB	21-24	8.840	-17.4			
BB	24-27	9.160	-17.9			
BB	27-30	9.350	-17.8			
BJN	plant	-	-	-27.1	-14.7	-26.7
BJN	0-3	7.810	-18.2			
BJN	3-6	5.090	-18.0			
BJN	6-9	10.100	-18.1			
BJN	9-12	7.720	-18.7			
BJN	12-15	6.820	-18.2			
BJN	15-18	6.780	-18.3			
BJN	18-21	4.120	-18.4			
BJN	21-24	4.370	-18.8			
BJN	24-27	4.010	-17.6			
BJN	27-30	14.090	-18.3			
BJS	plant	-	-	-24.2	-14.3	-26.7
BJS	0-3	6.270	-22.2			
BJS	3-6	9.720	-22.6			
BJS	6-9	5.330	-22.1			
BJS	9-12	16.200	-21.2			
BJS	12-15	14.700	-20.7			
BJS	15-18	10.300	-20.0			
BJS	18-21	9.720	-19.3			
BJS	21-24	7.010	-19.7			
BJS	24-27	6.820	-18.7			
BJS	27-30	4.500	-18.9			
MC 252	Crude					27.1

Appendix 6a. Summary of number of positive tubes in the SRB MPN cultures inoculated with sediment core samples from heavily contamination sites.

Sample	Depth (cm)	10 fold	100 fold	1000 fold	MPN
Bay Jimmy South (BJ) 1	0 - 3	5	2	0	150
Bay Jimmy South (BJ) 2	0 - 3	5	2	0	150
Bay Jimmy South (BJ) 1	12 - 15	5	3	1	79
Bay Jimmy South (BJ) 2	12 - 15	5	3	0	110
Bay Jimmy South (BJ) 1	27 - 30	5	2	0	150
Bay Jimmy South (BJ) 2	27 - 30	5	0	1	31
Bay Jimmy North (BN) 1	0 - 3	5	2	0	150
Bay Jimmy North (BN) 2	0 - 3	5	5	2	540
Bay Jimmy North (BN) 1	12 - 15	5	5	1	350
Bay Jimmy North (BN) 2	12 - 15	5	4	3	280
Bay Jimmy North (BN) 1	27 - 30	5	3	0	79
Bay Jimmy North (BN) 2	27 - 30	5	4	0	130
Bayou Batiste Core C (BB) 1	0 - 3	5	4	5	1600
Bayou Batiste Core C (BB) 2	0 - 3	5	5	5	1600
Bayou Batiste Core C (BB) 1	12 - 15	5	5	3	920
Bayou Batiste Core C (BB) 2	12 - 15	5	5	3	920
Bayou Batiste Core C (BB) 1	27 - 30	5	1	5	220
Bayou Batiste Core C (BB) 2	27 - 30	5	5	0	240
Bayou Dulac Core C (BD) 1	0 - 3	5	5	3	920
Bayou Dulac Core C (BD) 2	0 - 3	5	5	3	920
Bayou Dulac Core C (BD) 1	12 - 15	5	5	0	240
Bayou Dulac Core C (BD) 2	12 - 15	5	4	0	130
Bayou Dulac Core C (BD) 1	27 - 30	5	1	0	33
Bayou Dulac Core C (BD) 2	27 - 30	5	1	0	33

Appendix 6b. Summary of number of positive tubes in the SRB MPN cultures inoculated with sediment core samples from intermediate contaminated sites.

Sample	Depth (cm)	10 fold	100 fold	1000 fold	MPN
Rigolets (RG) 1	0 - 3	5	5	4	1600
Rigolets (RG) 2	0 - 3	5	5	5	1600
Rigolets (RG) 1	12 - 15	5	5	5	1600
Rigolets (RG) 2	12 - 15	5	5	5	1600
Rigolets (RG) 1	27 - 30	5	5	5	1600
Rigolets (RG) 2	27 - 30	5	5	5	1600
Point Aux Chenes Bay (PA) 1	0 - 3	5	5	1	350
Point Aux Chenes Bay (PA) 2	0 - 3	5	5	1	350
Point Aux Chenes Bay (PA) 1	12 - 15	3	2	0	14
Point Aux Chenes Bay (PA) 2	12 - 15	5	5	1	350
Point Aux Chenes Bay (PA) 1	27 - 30	5	2	1	70
Point Aux Chenes Bay (PA) 2	27 - 30	3	2	0	14
Walker Island (W) 1	0 - 3	5	5	1	350
Walker Island (W) 2	0 - 3	5	5	1	350
Walker Island (W) 1	9-12	5	1	0	33
Walker Island (W) 2	9-12	5	0	0	23
Walker Island (W) 1	15-18	5	1	0	33
Walker Island (W) 2	15-18	5	2	1	70

Appendix 6c. Summary of number of positive tubes in the SRB MPN cultures inoculated with sediment core samples from pristine sites.

Sample	Depth (cm)	10 fold	100 fold	1000 fold	MPN
Long's Bayou (LB) 1	0 - 3	5	5	3	920
Long's Bayou (LB) 2	0 - 3	5	5	2	540
Long's Bayou (LB) 1	12 - 15	5	1	0	33
Long's Bayou (LB) 2	12 - 15	5	0	0	23
Long's Bayou (LB) 1	27 - 30	0	1	1	1.8
Long's Bayou (LB) 2	27 - 30	1	1	0	1.9
Weeks Bay Force F Core (WF) 1	0 - 3	5	5	1	350
Weeks Bay Force F Core (WF) 2	0 - 3	5	5	2	540
Weeks Bay Force F Core (WF) 1	12 - 15	5	4	1	170
Weeks Bay Force F Core (WF) 2	12 - 15	5	5	2	540
Weeks Bay Force F Core (WF) 1	27 - 30	5	5	2	540
Weeks Bay Force F Core (WF) 2	27 - 30	5	5	3	920
Weeks Bay Force E Core (WE) 1	0 - 3	5	5	3	920
Weeks Bay Force E Core (WE) 2	0 - 3	5	5	1	350
Weeks Bay Force E Core (WE) 1	15-18	5	4	0	130
Weeks Bay Force E Core (WE) 2	15-18	5	4	0	130
Weeks Bay Force E Core (WE) 1	27 - 30	5	5	4	1600
Weeks Bay Force E Core (WE) 2	27 - 30	5	5	1	350
Bayou Heron (BH) 1	0 - 3	5	5	2	540
Bayou Heron (BH) 2	0 - 3	5	5	3	920
Bayou Heron (BH) 1	12 - 15	5	2	0	49
Bayou Heron (BH) 2	12 - 15	5	0	0	23
Bayou Heron (BH) 1	27 - 30	3	1	0	11
Bayou Heron (BH) 2	27 - 30	2	0	0	4.5

Appendix 7a. Summary of number of positive tubes in the IRB MPN cultures inoculated with sediment core samples from heavily contamination sites.

Sample	Depth	10 fold	100 fold	1000 fold	MPN
Bay Jimmy South (BJ) 1	0 - 3	5	5	5	>1600
Bay Jimmy South (BJ) 2	0 - 3	5	5	5	>1600
Bay Jimmy South (BJ) 1	12 - 15	5	5	5	>1600
Bay Jimmy South (BJ) 2	12 - 15	5	5	5	>1600
Bay Jimmy South (BJ) 1	27 - 30	5	5	5	>1600
Bay Jimmy South (BJ) 2	27 - 30	5	5	5	>1600
Bay Jimmy North (BN) 1	0 - 3	5	5	5	>1600
Bay Jimmy North (BN) 2	0 - 3	5	5	5	>1600
Bay Jimmy North (BN) 1	12 - 15	5	5	5	>1600
Bay Jimmy North (BN) 2	12 - 15	5	5	5	>1600
Bay Jimmy North (BN) 1	27 - 30	5	5	5	>1600
Bay Jimmy North (BN) 2	27 - 30	5	5	5	>1600
Bayou Batiste Core C (BB) 1	0 - 3	5	5	5	>1600
Bayou Batiste Core C (BB) 2	0 - 3	5	5	5	>1600
Bayou Batiste Core C (BB) 1	12 - 15	5	5	5	>1600
Bayou Batiste Core C (BB) 2	12 - 15	5	5	5	>1600
Bayou Batiste Core C (BB) 1	27 - 30	5	5	5	>1600
Bayou Batiste Core C (BB) 2	27 - 30	5	5	5	>1600
Bayou Dulac Core C (BD) 1	0 - 3	5	5	5	>1600
Bayou Dulac Core C (BD) 2	0 - 3	5	5	5	>1600
Bayou Dulac Core C (BD) 1	12 - 15	5	5	5	>1600
Bayou Dulac Core C (BD) 2	12 - 15	5	5	5	>1600
Bayou Dulac Core C (BD) 1	27 - 30	5	5	5	>1600
Bayou Dulac Core C (BD) 2	27 - 30	5	5	5	>1600

Appendix 7b. Summary of number of positive tubes in the IRB MPN cultures inoculated with sediment core samples from pristine sites.

Sample	Depth (cm)	10 fold	100 fold	1000 fold	MPN
Long's Bayou (LB) 1	0 - 3	5	5	5	>1600
Long's Bayou (LB) 2	0 - 3	5	5	5	>1600
Long's Bayou (LB) 1	12 - 15	5	5	5	>1600
Long's Bayou (LB) 2	12 - 15	5	5	5	>1600
Long's Bayou (LB) 1	27 - 30	5	5	5	>1600
Long's Bayou (LB) 2	27 - 30	5	5	5	>1600
Weeks Bay Force F Core (WF) 1	0 - 3	5	5	5	>1600
Weeks Bay Force F Core (WF) 2	0 - 3	5	5	5	>1600
Weeks Bay Force F Core (WF) 1	12 - 15	5	5	5	>1600
Weeks Bay Force F Core (WF) 2	12 - 15	5	5	5	>1600
Weeks Bay Force F Core (WF) 1	27 - 30	5	5	5	>1600
Weeks Bay Force F Core (WF) 2	27 - 30	5	5	5	>1600
Weeks Bay Force E Core (WE) 1	0 - 3	5	5	5	>1600
Weeks Bay Force E Core (WE) 2	0 - 3	5	5	5	>1600
Weeks Bay Force E Core (WE) 1	15-18	5	5	5	>1600
Weeks Bay Force E Core (WE) 2	15-18	5	5	5	>1600
Weeks Bay Force E Core (WE) 1	27 - 30	5	5	5	>1600
Weeks Bay Force E Core (WE) 2	27 - 30	5	5	5	>1600
Bayou Heron (BH) 1	0 - 3	5	5	5	>1600
Bayou Heron (BH) 2	0 - 3	5	5	5	>1600
Bayou Heron (BH) 1	12 - 15	5	5	5	>1600
Bayou Heron (BH) 2	12 - 15	5	5	5	>1600
Bayou Heron (BH) 1	27 - 30	5	5	5	>1600
Bayou Heron (BH) 2	27 - 30	5	5	5	>1600